

Joint mAsTer of Mediterranean Initiatives on renewabLe and sustainAble energy

Palestine Polytechnic University  
Deanship of Graduate Studies and Scientific Research  
Master Program of Renewable Energy and Sustainability

---

A Simulation Study to Evaluate the Vapor Jet Refrigeration Cycle  
Driven by Solar Thermal Energy for Air Conditioning Application at  
Two Different Areas in Palestine

---

By  
Khaled Ayoub Sider

---

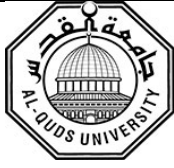
Supervisor  
Dr. Ishaq Sider

---

*Thesis submitted in partial fulfillment of requirements of the degree  
Master of Science in Renewable Energy & Sustainability*

---

February, 2019



**Joint mAsTer of Mediterranean Initiatives on renewabLe and sustainAble energy**

The undersigned hereby certify that they have read, examined and recommended to the Deanship of Graduate Studies and Scientific Research at Palestine Polytechnic University and the Faculty of Science at Al-Quds University the approval of a thesis entitled:

**A Simulation Study to Evaluate the Vapor Jet Refrigeration Cycle Driven by Solar Thermal Energy for Air Conditioning Application at Two Different Areas in Palestine.**

Submitted by

**Khaled Ayoub Sider**

In partial fulfillment of the requirements for the degree of Master in Renewable Energy & Sustainability.

**Graduate Advisory Committee:**

Dr. Ishaq Sider  
(Supervisor), Palestine Polytechnic University

Signature: \_\_\_\_\_

Date: \_\_\_\_\_

Dr. Maher AL-Maghalseh  
(Internal committee member), Palestine Polytechnic University

Signature: \_\_\_\_\_

Date: \_\_\_\_\_

Dr. Abdelrahim Abusafa  
(External committee member), An-Najah National University.

Signature: \_\_\_\_\_

Date: \_\_\_\_\_

Thesis Approved by:

Name: Dr. Murad Abu Sbeih

Name: Dr. Wadie Sultan

Dean of Graduate Studies & Scientific Research  
Palestine Polytechnic University

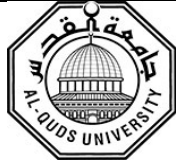
Dean of Faculty of Graduate Studies  
Al-Quds University

Signature:.....

Signature:.....

Date:.....

Date:.....



## **A Simulation Study to Evaluate the Vapor Jet Refrigeration Cycle Driven by Solar Thermal Energy for Air Conditioning Application at Two Different Areas in Palestine**

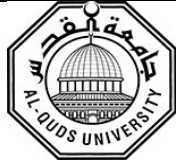
**By Khaled Ayoub Sider**

### **ABSTRACT**

The need for air conditioning in rural areas in which there is no source of traditional electrical power leads to look for an alternative solutions. Usually the population of these areas use typical movable houses (TMH's) as residence. Solar thermal system drive vapor jet refrigeration cycle (VJRC) is a valid solution for this kind of situation, which replaces the traditional vapor compression refrigeration cycle that used the electricity.

Mathematical model was carried out for (VJRC) using Engineering equation solver (EES) software at various design conditions (generator, evaporator and condenser temperature), characteristic curves and tables for the (VJRC) were found at 10°C evaporator temperature. Hourly simulation of cooling load demand for specific construction TMH was calculated using TRNBuild subsystem in TRNSYS software with the standard design conditions in Hebron and Jericho cities. Furthermore hourly simulation of the overall solar thermal cooling system was carried out over the study period (May-September), while considering climatic data for the two cities using TRANSYS software compiled with Excel software which contained the characteristic tables of the VJRC that obtained from the EES. The instantaneous performance of the system, Cooling load demand and evaporator cooling load available were calculated. Effect of climate according to the location, solar collector area, storage tank volume were studied to produce the maximum suitable evaporator cooling load to meet the requirement of the human comfort.

EES Mathematical model for the VJRC demonstrated that the performance of the cycle is increased with increasing the generator and evaporator temperature, but decreases with increasing condensing temperatures. Cooling load simulation for Hebron and Jericho TMH demonstrated that the maximum cooling load demand during the study period were: 5.35 kW and 7.02 kW respectively; and the seasonal cooling energy demands were: 5749 kWh/year and



**Joint mAsTer of Mediterranean Initiatives on renewabLe and sustainAble energy**

14864 kWh/year respectively according to the climate conditions. Simulation for the overall system demonstrated that the proposed system was efficient for Hebron city in contrast to Jericho city where the proposed system showed lack of cooling energy produced. Also the optimal sizes and options of the overall system were determined for Hebron city. An economical study was done on the proposed system where the results demonstrated that the proposed system in Hebron city is more economical than Jericho where the simple payback period of Hebron city reached to 12.9 year while in Jericho city is 15 year at the same system size.



## دراسة محاكاة لتقييم دورة تبريد نفائثة بخارية تعمل بالطاقة الحرارية الشمسية لأغراض التكييف في منطقتين مختلفتين في فلسطين

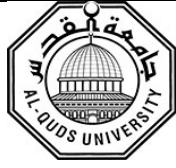
اعداد: خالد ايوب سدر

### ملخص

تدفع الحاجة الى تكييف الهواء في المناطق الريفية التي لا تتوفر فيها الكهرباء الى البحث عن حلول بديلة, حيث عادة ما يستخدم السكان في هذه المناطق وحدات سكنية متماثلة متنقلة للعيش. تعتبر دورة التبريد النفائثة البخارية التي تعمل بالطاقة الشمسية حلا فعالا في هذه الحالات بدلا من دائرة التبريد الانضغاطية التي تعمل بالكهرباء.

تم عمل نموذج رياضي لدورة التبريد النفائثة باستخدام برنامج حل المعادلات الهندسية (EES) تحت ظروف تصميمية مختلفة مثل درجة حرارة المولد و المبخر والمكثف, كما وتم ايجات منحنيات وجداول الخواص للدورة عند درجة حرارة  $10^{\circ}\text{C}$  للمبخر. تم عمل محاكاة لحمل التبريد الخاص بالوحدة السكنية النموذجية ذات المواصفات المحددة باستخدام برنامج TRNBuild التابع لبرنامج TRNSYS وذلك تحت الظروف التصميمية لمدينتي الخليل واريحا. علاوة على ذلك, أجريت محاكاة على مدار الساعة لنظام التبريد الحراري الشمسي المتكامل خلال فترة الدراسة (مايو- سبتمبر), مع الأخذ بعين الاعتبار البيانات المناخية للمدينتين وذلك باستخدام برنامج TRANSYS بالتوافق مع برنامج Excel الذي يحتوي على جداول الخواص لدائرة التبريد والتي تم الحصول عليها من برنامج EES. تم حساب معامل الأداء اللحظي للنظام, وحساب حمل التبريد المطلوب في الوحدة السكنية بالإضافة الى حمل تبريد المبخر في دائرة التبريد. تمت دراسة تأثير المناخ حسب الموقع الجغرافي ومساحة سطح المجمعات الشمسية الحرارية وحجم خزان التخزين لإنتاج أقصى حمل تبريد للدورة من أجل تلبية متطلبات الراحة البشرية.

أظهرت نتائج النموذج الرياضي باستخدام برنامج EES بان أداء دورة التبريد النفائثة يزداد بإزيد درجة حرارة المولد ودرجة حرارة المبخر, لكنه يتناقص مع ازدياد درجة حرارة المكثف. كما وظهرت نتائج محاكاة حمل التبريد للوحدة السكنية بان أقصى حمل تبريد كانت قيمته  $5.35 \text{ kW}$  و  $7.02 \text{ kW}$  لمدينتي الخليل واريحا على التوالي. وان قيمة الطاقة التبريدية الموسمية المطلوبة للوحدة السكنية هي  $5749 \text{ kWh/year}$  و  $14864 \text{ kWh/year}$  لمدينتي الخليل واريحا على التوالي. كما وظهرت نتائج النظام الكلي بان النظام المقترح ذو فعالية عالية في حال استخدامة في مدينة الخليل ولكنه غير فعال في مدينة اريحا حيث ان طاقة التبريد المنتجة غير كافية. كما وتم تحديد حجم وخيارات النظام الكلي المثلى في مدينة الخليل, تم عمل دراسة اقتصادية للنظام المقترح وقد اظهرت النتائج بان هذا النظام في مدينة الخليل اكثر اقتصادية من مدينة اريحا حيث ان معدل استرجاع راس المال بلغ  $12.9$  سنة في مدينة الخليل بينما وصل الى  $15$  سنة في مدينة اريحا بنفس حجم النظام.



Joint mAsTer of Mediterranean Initiatives on renewabLe and sustainAble energy

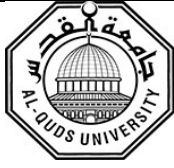
## DECLARATION

I declare that the Master Thesis entitled” **A Simulation Study to Evaluate the Vapor Jet Refrigeration Cycle Driven by Solar Thermal Energy for Air Conditioning Application at Two Different Areas in Palestine**” is my own original work, and herby certify that unless stated, all work contained within this thesis is my own independent research and has not been submitted for the award of any other degree at any institution, except where due acknowledgement is made in the text.

Student Name: **Khaled Ayoub Sider**

Signature: \_\_\_\_\_

Date: \_\_\_\_\_



Joint mAsTer of Mediterranean Initiatives on renewabLe and sustainAble energy

## STATEMENT OF PERMISSION TO USE

In presenting this thesis in partial fulfillment of the requirements for the joint Master's degree in Renewable Energy & Sustainability at Palestine Polytechnic University and Al-Quds University, I agree that the library shall make it available to borrowers under rules of the library.

Brief quotations from this thesis are allowable without special permission, provided that accurate acknowledgement of the source is made.

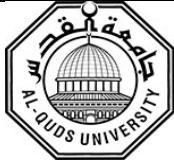
Permission for extensive quotation from, reproduction, or publication of this thesis may be granted by my main supervisor, or in his absence, by the Dean of Graduate Studies and Scientific Research when, in the opinion of either, the proposed use of the material is for scholarly purposes.

Any copying or use of the material in this thesis for financial gain shall not be allowed without my written permission.

Student Name: **Khaled Ayoub Sider**

Signature: \_\_\_\_\_

Date: \_\_\_\_\_



Joint mAsTer of Mediterranean Initiatives on renewabLe and sustainAble energy

## DEDICATION

To my mother and father

To my wife

To my brothers and sisters

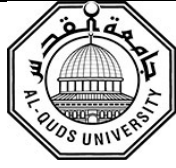
To my real friends

Thank you for your love and support

To the martyrs souls

To our great Palestine





Joint mAsTer of Mediterranean Initiatives on renewabLe and sustainAble energy

## ACKNOWLEDGEMENT

First and foremost I would like to thank God. I would like to show my gratitude to my family for their continued support, patience and encouragement over the years of my education. I greatly appreciate the thesis's supervisor Dr. Ishaq Sider for his continuous support and time he spent with me in order to succeed this thesis. Many thanks to Dr. Sameer Khader the coordinator of the Master Program of Renewable Energy and Sustainability for all his guidance's, Many thanks for Eng Younis Badran and Eng Mutaz Jawadeh for their supports and many thanks for all my teachers over the years of my education.

Finally I would like to thank JAMILA Project-544339-TEMPUS-1-2013-1-IT-TEMPUS-JPCR funded by the European Union which was administrated by Sapienza University of Rome and partner Universities for their support in launching this program, provided infrastructure and opportunities for scientific visits.



## TABLE OF CONTENT

ABSTRACT.....	III
ملخص.....	V
DECLARATION .....	VI
STATEMENT OF PERMISSION TO USE.....	VII
DEDICATION.....	VIII
ACKNOWLEDGEMENT .....	IX
TABLE OF CONTENT .....	X
LIST OF FIGURES .....	XII
LIST OF TABLES.....	XIV
LIST OF ABBREVIATIONS.....	XV
LIST OF SYMBOLS .....	XV
CHAPTER 1: Introduction .....	1
1.1 Overview .....	1
1.2 Working principle .....	2
1.3 Literature review .....	4
1.4 Methodology .....	9
1.5 Scope of this study .....	10
1.6 Thesis Structure.....	11
CHAPTER 2: Theory.....	12
2.1 Introduction .....	12
2.2 Ejector theory .....	12
2.3 VJRC theory.....	16
2.4 Solar collector theory .....	18
2.5 Incident solar radiation theory.....	20
CHAPTER 3: Climate and Building Descriptions.....	23
3.1 Introduction .....	23
3.2 Location and Climate .....	23
3.3 Building Description .....	26
CHAPTER 4 : Simulation and Results .....	30



4.1 Introduction .....	30
4.2 VJRC simulation and results .....	30
4.2.1 VJRC simulation .....	30
4.2.2 VJRC results.....	32
4.2.2.1 Effect of the generator temperature on the cycle performance .....	33
4.2.2.2 Effect of the evaporator temperature on the cycle performance .....	33
4.2.2.3 Effect of the condenser temperature on the cycle performance .....	34
4.2.2.4 VJRC characteristic curves and tables .....	35
4.3 Building cooling load simulation and results.....	37
4.3.1 Building cooling load simulation .....	37
4.3.2 Building cooling load results.....	41
4.4 Collector tilt angle estimation .....	43
4.5 Overall system simulation and results.....	45
4.5.1 Overall system simulation .....	45
4.5.2 Overall system results .....	48
4.5.2.1 Solar thermal subsystem results .....	48
4.5.2.2 Overall system performance results .....	49
4.5.2.2 Evaporator cooling load results.....	49
4.5.2.3 Effect of the collector area on the evaporator cooling load and energy.....	51
4.5.2.4 Effect of the storage tank volume on the evaporator cooling load and energy.....	54
4.5.2.5 Effect of the collector area and the storage tank volume on the evaporator cooling energy.....	60
CHAPTER 5 : Economical Study.....	64
CHAPTER 6 : Conclusions and Recomendations .....	68
6.1 Introduction .....	68
6.2 Conclusions .....	68
6.3 Recomendations .....	69
References.....	70
Appendixes .....	73



### LIST OF FIGURES

Figure 1. 1: Schematic diagram of the VJRC ..... 3

Figure 1. 2: Ejector flow regimes ..... 5

Figure 1. 3: Effect of generator temperature on ejector and cycle performance ..... 7

Figure 1. 4: Effect of condenser temperature on ejector and cycle performance . ..... 7

Figure 1. 5: Effect of evaporator temperature on ejector and cycle performance ..... 8

Figure 2. 1: Schematic diagram of the proposed system ..... 12

Figure 2. 2: Pressure and velocity profile along the typical ejector..... 14

Figure 2. 3: T-s and p-h diagrams of VJRC..... 17

Figure 2. 4: Efficiency of the evacuated tube and flat plate collectors ..... 20

Figure 2. 5: Solar radiation striking a collector ..... 20

Figure 2. 6: Solar angels ..... 21

Figure 3. 1: Annual distribution of ambient temperatures for Hebron and Jericho cities..... 24

Figure 3. 2: Annual distribution of global horizontal solar radiation for Hebron and Jericho cities  
W/m<sup>2</sup> ..... 25

Figure 3. 3: Mean monthly distributions for ambient temperatures for Hebron and Jericho cities °C.  
..... 25

Figure 3. 4: Mean monthly solar radiation per day for Hebron and Jericho cities kWh/m<sup>2</sup>.day. .... 26

Figure 3. 5: Architecture design of the TMH..... 27

Figure 3. 6: TMH constructions, a: for walls, roof, door and floor, b: for windows ..... 28

Figure 4. 1: Flowchart for analysis and calculate the VJRC parameters ..... 31

Figure 4. 2: P-h diagram for VJRC at fixed operating conditions 110 °C, 35 °C and 10°C for  
generator, condenser and evaporator temperature respectively. .... 32

Figure 4. 3: Variations of COP with generator temperatures ..... 33

Figure 4. 4: Variations in COP with evaporator temperatures..... 34

Figure 4. 5: Variations in COP with condenser temperatures..... 35

Figure 4. 6: Characteristic curves for VJRC at 10°C evaporator temperature..... 36

Figure 4. 7: Heat Balance on the Cooling Zone..... 38

Figure 4. 8: TRNBuild main window ..... 39

Figure 4. 9: Simulation Studio window components for building cooling load ..... 40

Figure 4. 10: Distribution of the insolation and ambient temperatures for five days (1 to 5 July) in  
Hebron and Jericho cites ..... 41

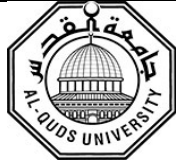


Figure 4. 11: Cooling load demand and ambient temperature for five days (1 to 5 July) in Hebron and Jericho cites..... 42

Figure 4. 12: Monthly mean cooling energy demand for study period for Hebron and Jericho cites .42

Figure 4. 13: Total seasonal cooling energy demand for Hebron and Jericho cites ..... 43

Figure 4. 14: Average daily mean insolation per month at different tilt angles for Hebron city..... 44

Figure 4. 15: Total amount of insolation at different tilt angles during the study period ..... 44

Figure 4. 16: Simulation Studio window components for overall system ..... 45

Figure 4. 17: Characteristics of the solar thermal subsystem for the tested sample period (1 to 5 July) in Hebron city using 20 m<sup>2</sup> collector area and 1 m<sup>3</sup> storage tank ..... 48

Figure 4. 18: Performance of the VJRC, and ETC efficiency according the solar insolation for the tested sample period in Hebron city using 20 m<sup>2</sup> collector area and 1 m<sup>3</sup> storage tank..... 49

Figure 4. 19: Instantaneous cooling load demand and the evaporator cooling load for the tested sample period in Hebron city using 20 m<sup>2</sup> collector area and 1 m<sup>3</sup> storage tank..... 50

Figure 4. 20: Effect of the collector area on the instantaneous evaporator cooling load for the tested sample period in Hebron city using 1 m<sup>3</sup> storage tank ..... 52

Figure 4.21: Effect of the collector area on the instantaneous evaporator cooling load for the tested sample period in Jericho city using 1 m<sup>3</sup> storage tank ..... 53

Figure 4. 22: Effect of the collector area on the seasonal evaporator cooling energy using 1 m<sup>2</sup> storage tank in Hebron city ..... 54

Figure 4. 23: Effect of the storage tank on the evaporator cooling load for the tested sample period in Hebron city using 10 m<sup>2</sup> collector area..... 56

Figure 4. 24: Effect of the storage tank on the evaporator cooling load for the tested sample period in Hebron city using 35 m<sup>2</sup> collector area..... 57

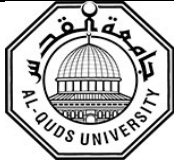
Figure 4.25: Effect of the storage tank on the evaporator cooling load for the tested sample period in Jericho city using 10 m<sup>2</sup> collector area ..... 57

Figure 4.26: Effect of the storage tank on the evaporator cooling load for the tested sample period in Jericho city using 100 m<sup>2</sup> collector area ..... 57

Figure 4. 27: Percentage of seasonal evaporator cooling energy from the cooling energy demand for Hebron city at different collector area and storage tank volume ..... 60

Figure 4. 28: Percentage of seasonal evaporator cooling energy from the cooling energy demand for Jericho city at different collector area and storage tank volume..... 63

Figure 5.1: Cash flow chart for the proposed system in Hebron and Jericho ..... 66



## LIST OF TABLES

Table 2. 1: Typical operating temperature of different solar collectors.....	18
Table 2. 2: Parameters of the evacuated tube and flat plate collectors .....	19
Table 3. 1: The inside and outside Conventional surface resistances .....	28
Table 3. 2: Constructional components of the TMH .....	28
Table 4. 1: VJRC data and results at fixed operating conditions 110 °C, 35 °C and 10°C for generator, condenser and evaporator temperature respectively. ....	32
Table 4. 2: Components of simulation Studio window and descriptions.....	40
Table 4. 3Components of simulation Studio window and descriptions.....	46
Table 5.1 payback period calculations summary of the three cases .....	65



## LIST OF ABBREVIATIONS

ASHRAE	American Society of Heating, Refrigerating and Air-Conditioning Engineers
COP	Coefficient of Performance
$COP_{\text{carnot}}$	Coefficient of Performance of Carnot cycle
CRF	Constant Rate Factor
EES	Engineering Equation Solver
EPW	Energy plus Weather format
ETC	Evacuated Tube Solar Collector
FPC	Flat Plate Collector
HTF	Heat Transfer Fluid
HVAC	Heating Ventilation and Air conditioning
IRR	Internal Rate of Return
NPV	Net Present Value
PAL MET	Palestinian Meteorology
TMH	Typical Movable House Unit
TRANSYS	Transient System Simulation program
TRNBuild	TRANSYS Building input data visual interface
VJRC	Vapor Jet Refrigeration Cycle

## LIST OF SYMBOLS

A:	Area
$a_1$	First order heat loss coefficient
$a_2$	Second order heat loss coefficient
$A_{\text{coll}}$	Collector area
c	Speed of sound at local static temperature
$c_p$	Specific heat at constant pressure
G	Solar radiation
h:	Specific enthalpy
$h_p$	Primary stream enthalpy
$h_s$	Secondary stream enthalpy
IB	Beam portion of the radiation
IBC	Direct solar flux striking a surface
$I_c$	Total insolation on the collector
IDC	Diffuse radiation on the collector
IDH	Diffuse insolation on a horizontal surface
IRC	Reflect insolation striking a collector
k	Specific heat ratio
M	Local Mach number
$M^*$	Critical Mach number
$\dot{m}$ :	Mass flow
$\dot{m}_c$	Condenser mass flow rate
$\dot{m}_p$	Primary fluid flow rate



$\dot{m}_s$	Secondary fluid flow rate
$n$	Day number
$P$ :	Pressure
$P_c$	Condenser pressure
$P_e$	Evaporator pressure
$P_g$	Generator pressure
$q_c$	Condenser energy
$Q_c$	Condenser load
$Q_{coll}$	Collector useful energy
$Q_{conv}$	Convective heat flow
$q_e$	Evaporator energy
$Q_e$	Evaporator load
$q_g$	Generator energy
$Q_g$	Generator load
$Q_{r,wi}$	Radiative heat flow to the walls and windows:
$R$	Universal gas constant
$R_{inside}$	Inside conventional surface resistances
$R_{outside}$	Outside conventional surface resistances
$T$	Temperature
$T_a$	Ambient air temperature
$T_c$	Condenser temperature
$T_e$	Evaporator temperature
$T_g$	Generator temperature
$T_m$	Mean collector fluid temperature
$U$	Over all heat transfer coefficient
$V$ :	Velocity
$V_p$	Primary stream velocity
$V_s$	Secondary stream velocity
$w$	Entrainment ratio
$W_p$	Pump power

### Greek symbols

$\Sigma$	Tilt angle
$\beta$	Altitude angle
$\eta_0$	Maximum efficiency of the collector
$\eta_d$	Isentropic efficiency of the diffuser
$\eta_m$	Mixing chamber efficiency
$\eta_n$	Isentropic efficiency of the primary nozzle
$\eta_{sc}$	Solar collector efficiency
$\rho$ :	Density
$\phi_C$	Collector azimuth
$\phi_S$	Solar azimuth angle



# CHAPTER 1

## Introduction

### 1.1 Overview

The increasing demand for human comfort has led to a rapid increase in the use of the cooling system and, as a result, the demand for electricity due to building air conditioning increased. Where the overall consumption from buildings reach up to 40% in developed countries [1]. Although, the electric power is widely spread but still some rural areas have no electricity coverage due to high initial cost involved. Deployment of thermal energy refrigeration, using low grade heat or solar energy, would provide a reasonable solution for such rural areas with advantage of reduction of energy consumption. Between the numerous technologies for thermal refrigeration techniques, vapor jet refrigeration cycle (VJRC) driven by solar thermal energy appear the most favorable alternative to the traditional vapor compression refrigeration cycle. [2]. VJRC is simple to construct, robust, low operating maintenance and has no mechanical moving segments making it a highly unfailing system which is capable of running low temperature heat from solar energy or other substitute like waste heat , which can create a more cheaper operation of the cooling system.

Ejectors can be classified into two main categories based on the nozzle position and two other more based on the geometry and dimensions; constant pressure mixing ejector, constant area mixing ejector, fixed and variable ejector geometry respectively [3].

VJRC uses water as a refrigerant is completely safe. Such systems were tested with high success in refrigeration in the early years of the last century. At low temperatures the saturation pressures of the water are low (8.129 mbar at 4 °C). When using water as refrigerant, temperature attained is not enough for refrigeration applications but it is more efficient and satisfactory for air-conditioning, cooling, or chilling applications [4]. Water usage in VJRC has many advantages compared with other refrigerants (Halocarbons, hydrocarbon and mixtures refrigerants), water is available and inexpensive, has a high latent heat, and has no environmental impacts such as ozone depletion and global warming.

VJRC can operate at low generator temperature around 100 °C. It can easily be powered by evacuated tube solar collectors (ETC). Since the cooling load is commonly synchronized with the availability of solar energy, this becomes an attractive application of solar energy. Palestine is located within the solar countries and considered as one of the highest solar potential energy in the world, this makes it one of the best countries to utilize the solar thermal energy in the solar thermal air conditioning systems, especially in rural areas where there is no or insufficient electricity and there is a sufficient lands for solar collectors.

Transient system simulation program (TRNSYS) and Engineering Equation Solver (EES) are used to model and analyze the solar thermal refrigeration systems. EES software is used to build a mathematical models of the refrigeration cycles and to simulate the effect of operation conditions. Also, TRNSYS software is used to simulate and analysis the cycle using solar thermal power system under different operation conditions and parameters at various regions and climate, and find the optimum design parameters for the system.

This simulation study is based on a constant pressure mixing ejector with variable geometry using water as working fluid. The source of the heat in the refrigeration cycle is the solar energy collected by ETC in two different cities in West Bank in Palestine. The cooling capacity of the cycle is used to compensate the cooling load demand for a TMH that commonly used in the rural areas in this cities.

## **1.2 Working principle**

The proposed system that studied consist from three subsystems; VJRC subsystem, building cooling load subsystem and solar thermal subsystem. Figure 1.1 shows the Schematic diagram of the VJRC, it can be noticed that the VJRC subsystem is consists of two loops, the power loop and the refrigeration loop. The power loop consists from generator, ejector, condenser and circulation pump, and the refrigeration loop consists from ejector, condenser, expansion device and evaporator.

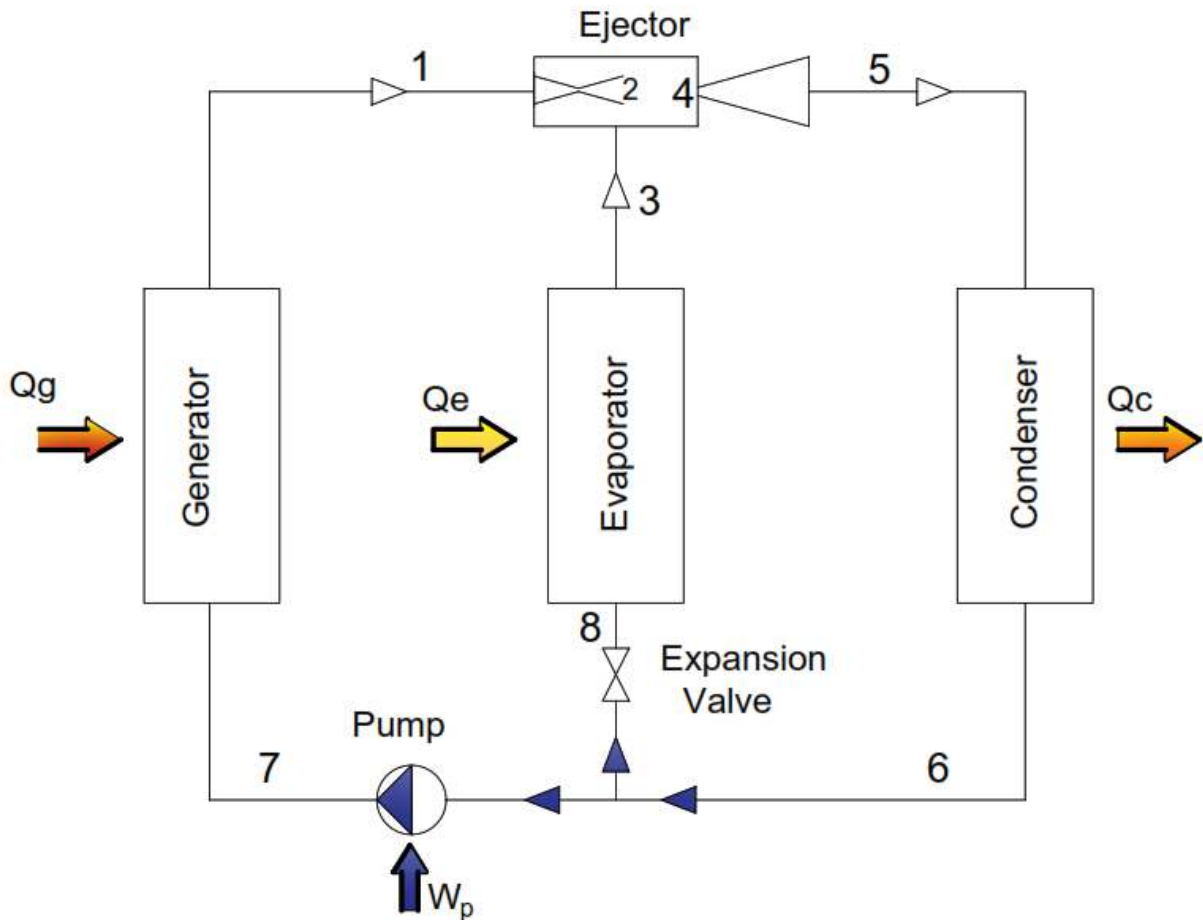


Figure 1. 1: Schematic diagram of the VJRC

In the power loop the primary fluid is vaporized by adding heat in the generator at high pressure, this high pressure fluid then passes through a supersonic ejector. In the ejector the fluid velocity increased more than Mach number through the supersonic nozzle, and the pressure decreased to the evaporator pressure. The decrease in the pressure that occurs in the nozzle entrains the secondary fluid vapor from the evaporator. The primary and secondary fluids then mix completely in the mixing chamber of the ejector and then enter the diffuser section where the mixed fluid velocity back decreased below Mach number and the pressure increased to reach the condenser pressure. The mixed fluid then flows to the condenser where it is condensed to liquid by rejecting heat to the ambient air.

A part of the liquid that leaving the condenser is then goes to a circulation pump and pumped to the generator to complete the power cycle and the remainder part of the liquid enters and

expanded through an expansion device and enters to the evaporator in the refrigeration loop as a mixture. In the evaporator, the refrigerant evaporates producing a refrigeration load, and the resulting vapor is then sucked by the primary fluid into the ejector to complete the refrigeration loop.

In the proposed system, the solar energy that is collected by ETC's was converted into heat in the solar thermal subsystem and used in the generator to operate the power cycle in the VJRC subsystem. The refrigeration load that produced by the VJRC subsystem was used to compensate the cooling load demand in the house unit subsystem to achieve the human comfort.

### **1.3 Literature review**

The (VJRC) was first developed by Le Blanc and Parson in early 1900 and was very popular in early 1930's for air-conditioning systems in large buildings. The system was replaced with the vapor compression refrigeration system. The vapor compression refrigeration system was higher in its coefficient of performance (COP), and flexibility in manufacturing and operation [5]. Although, refrigeration cycle which depends on vapor compression is more efficient than VJRC's but the environmental effect of these cycles is considered much severe. Latter several mathematical models were developed to study 1-D ejector system with analysis and fluid dynamics theories applied to the primary and secondary flow. The 1-D model of constant-pressure mixing ejector was initially developed in 1950 by Keenan et al. [6]. In this model, the pressure of primary and secondary fluid is equal at the outlet of the nozzle. The mixing of the two fluids starts with constant pressure and reaches the inlet of the throat section. These concept is still considered an effective model for constant pressure mixing ejector. Tashtoush et al [3] studied the performance of the ejector cooling cycle at critical mode under superheated primary flow. They studied the model mathematically using EES software. In addition, the ejector type , it was found that constant-pressure mixing ejector generates higher backpressure than constant-area mixing ejector for the same entrainment ratio and COP. and this was the reason behind the use of constant-pressure mixing ejector more than constant-area mixing ejector.

Many theoretical studies was carried out on operation conditions of the cycle such as the generator, condenser and evaporate temperature and pressure. Al-Khalidy[7] and Rani[8], noted

that the performance of the system increased by increasing generator and evaporator temperatures and decreasing condenser temperature.

Eames et al [9], and Chunnanond et al [10], experimented on a fixed geometry ejectors refrigerator. Results showed that, the operation of the ejector can be divided into three regions at each setting of the operating condition of the generator and evaporator as shown in Figure 1.2 double choked flow in the mixing chamber, primary chocking flow and reversed flow.in the double choked flow the performance of the cooling capacity was constant value when the ejector was operate under a certain condenser pressure that called critical condenser pressure. When the condenser pressure increased to the critical value only the primary fluid chocked and the secondary fluid was preventing from reaching to the sonic velocity which reduce the secondary fluid flows and the performance of the system. Finally, when the condenser pressure still increased the secondary fluid flows drop to zero and the ejector loses its function and primary flow will reverse back into the evaporator.

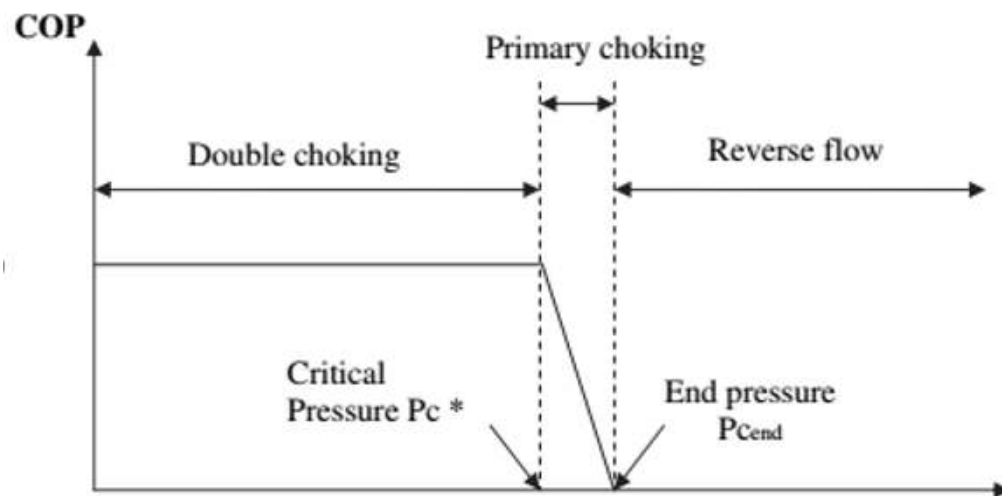


Figure 1. 2: Ejector flow regimes [9]

Eames et al [9], and Chunnanond et al [10] noticed that the mass flow rate of the refrigerant does remain constant in the double choked flow below the critical condenser pressure as shown in figure 1.2. According [9] and [10], operate the ejector at the critical point considered the most economical point that can archived better performance and better cooling capacity . From the results published also, they noted that when the generator temperature increased the performance

of the system decreased. Ruangtrakoon et al. [11] experimental results reported that by decreasing the generator temperature the critical condenser pressure of the ejector decreased and the performance the cycle increased.

Experimental results by Xiaoli Ma [12] using the water as refrigerant, Selvaraju [13] using R134a also conclude the same results. [12] Noted that when the generator temperature increased the performance of the system increased up to maximum value at a certain generator temperature and then the performance goes to decreasing. In the tested generator temperature range of 84 to 96 C, the maximum COP (0.32) were obtained at generator temperature of 90 C. Selvaraju [13] also noted that the COP increases with the generator temperature increasing up to a optimum value and after that the performance return to decreasing. Selvaraju [13] also studied more than one ejector geometry and dimensions, and he noted that every ejector has an optimum and maximum performance at a certain value of generator temperature.

Sun [14] study carried out on the variable geometry ejectors, it was noted that, with the variable geometry ejector. There are no limitations of the performance value of the system, when the generator temperature increased the performance increased without optimum generator temperature Thus, variable geometry ejectors are better than the of fixed geometry ejectors, which variable geometry ejector have a wide range of operation conditions to make it more flexible and reliable more the fixed geometry ejectors and more performance value. variable geometry ejector can be achieved by using more than one ejector in parallel in the same cycle, and only one ejector are used according to the performance of the system in the instant conditions .Figure 1.3 shows the Effect of generator temperature on ejector and cycle performance at condenser and evaporator temperature 35°C and 10°C respectively[14].

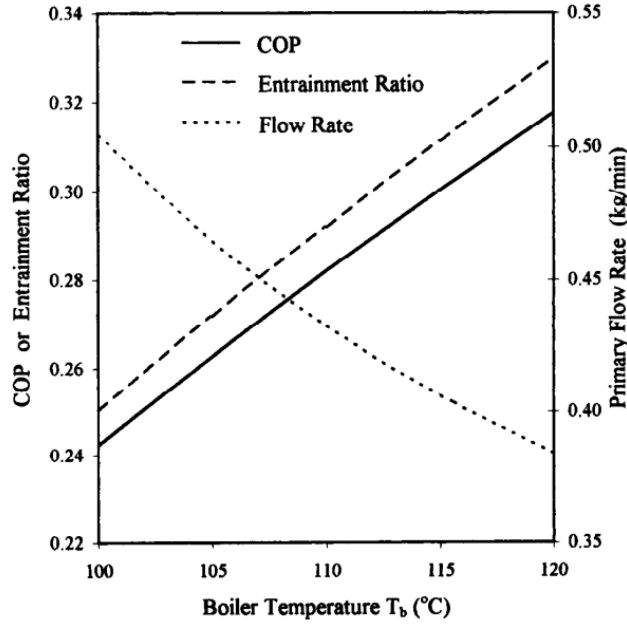


Figure 1. 3: Effect of generator temperature on ejector and cycle performance [14].

All the theoretical and experimental studies [7-14] concluded that the performance of the cycle increased when the evaporator temperature increased and the condenser temperature decreased. Figure 1.4 and figure1.5 show the effect of condenser and evaporator temperatures on the performance of the cycle [14].

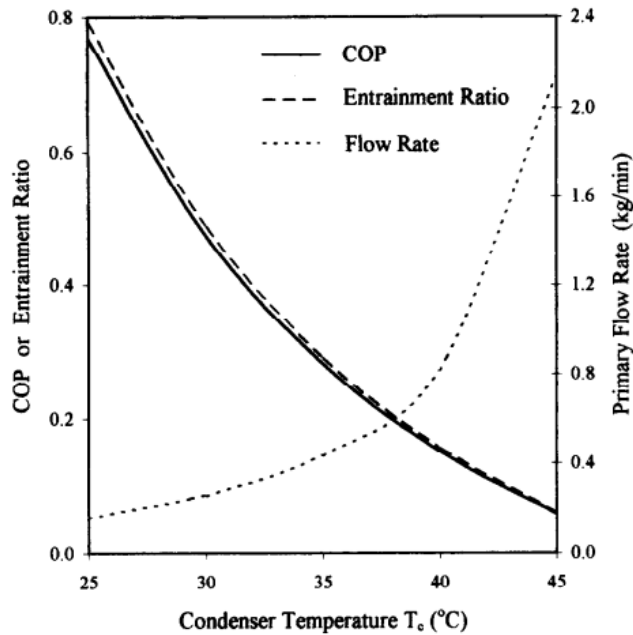


Figure 1. 4 Effect of condenser temperature on ejector and cycle performance [14].

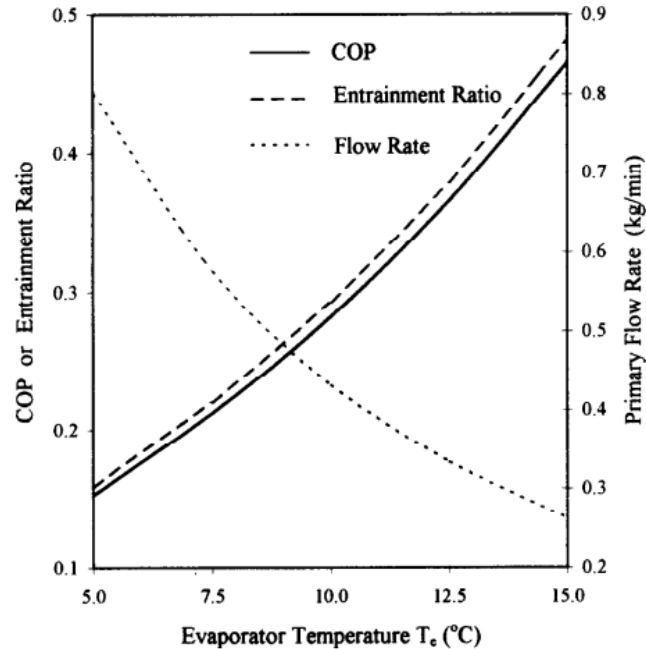


Figure 1. 5 Effect of evaporator temperature on ejector and cycle performance [14].

Alexis and Karayiannis [15] studied the performance of an ejector cooling system driven by solar energy and R134a as working fluid. The system operating in intermediate temperature solar collector in Athens was estimated along the 5 months (May–September). It was found that the COP of ejector cooling system varied from 0.035 to 0.199 when the operation conditions were: generator temperature (82–92°C), condenser temperature (32–40°C) and evaporator temperature (-10–0°C). Where the overall system performance varied from 0.014 to 0.101 with the same operation conditions in July.

Kursad Ersoy et al [16] simulation study using R123 as working fluid and evacuated tube collector in Turkey climates. The performance of the VJRC and the evacuated tube collector were hourly varied by ambient temperature and solar radiation. The maximum performance of the system occurred in the noon time.

Energy storage technology was applied in solar energy driven cooling system to use energy in the peak time or in the time where the sun radiation is absence. Two kinds of thermal storage are used hot storage in the solar collectors side, and cold storage in the evaporator side, Tashtoush et al [17] simulation study using R134a as working fluid and 7 kW cooling load at Jordan climate noted that increasing the hot storage tank size can improve the amount of useful energy gain through the solar collector a little.



Many researchers used TRNSYS software for studying solar thermal cooling systems and refrigeration systems. Pridasawas and Lundqvist [18] studied the effect of solar collector types and operation conditions on the VJRC performance with iso-butane as a refrigerant, Tashtoush et al [17] simulate the solar collector angle and area and study the performance of VJRC for the climatic conditions of Jordan with R134a as a refrigerant, Ahmed et al [19], and Asim et al [20] used TRNSYS to simulate the absorption cooling system under climate of Egypt and Pakistan respectively.

#### **1.4 Methodology**

This simulation study consist from three subsystems as mentioned above; VJRC subsystem, building cooling load subsystem and solar thermal subsystem. The VJRC was simulated by using the water as working fluid by using EES, in this subsystem the various design conditions were studied, and the characteristic curves and tables were found at constant evaporator temperature 10°C, this characteristic tables later were used as input Excel file in the TRNSYS simulation studio to specify the performance of the system at various generator and condenser temperatures and find the cooling load of the cycle.

The building cooling load subsystem was hourly simulated using the TRNBuild subsystem in TRNSYS software to find the cooling load demand of the TMH according to the weather data and conditions in Hebron and Jericho cities, this model for the thermal behavior of the house unit is also was used as input file in the TRNSYS simulation studio. The optimum tilt angle of the solar collector was determined based on the maximum amount of total incident solar radiation for the study period in the two cities.

The overall solar thermal cooling system was hourly simulated by using the TRNSYS simulation studio that consist from VJRC subsystem as TRNSYS / Excel Coupling file and the cooling load of the house by using Multi-zone building file, the overall simulation consider the solar energy collected by ETC at fixed optimum tilt angle and used hot energy storage tank to store the excess thermal energy for peak times or in the times where the sun radiation is absence. This energy delivered to the generator in the VJRC and used to operate the cycle and produce cooling energy in the evaporator, this cooling energy then delivered to a cooling coil to cover the cooling load

demand of the house. Two mainly parameters were studied in the overall system, solar collector area and the storage tank volume in each city, an economical study was done using three methods payback period, net present value and internal rate of return.

### **1.5 Scope of this study**

The importance of this study is that study the use of the VJRC under influence of large operation temperature range and variable cooling load which change every moment, unlike most previous studies in which the system has studied in limited temperature range and constant cooling load. Therefore, this makes the results more realistic and flexible, especially with changing ambient air temperature and solar radiation permanently, which greatly affects the performance and system capacity, this was in Hebron and Jericho cities.

The choice of the cities of Hebron and Jericho in this study is a unique contribution, where the great variation in climate and weather conditions for these areas are reflected largely in the ability and efficiency of the cooling cycles generally and on the solar cooling cycle particularly. The following objectives are the foundations of this research.

- To simulate the performance of the VJRC  
Computer modeling was carried out on single VJRC using water as working fluid. The system was demonstrated on EES software under various operation conditions, the generator temperatures 80-150°C, condenser temperatures 25-40°C and evaporator temperatures 5-15°C. And investigate their effects on the cycle performance and find the characteristic curves and tables of the cycle.
- To simulate the cooling load demand for TMH  
Hourly simulation for cooling load demand for TMH used in rural areas in Hebron city at the south of west bank and Jericho city at the east of west bank in Palestine.
- To find the optimum solar collector tilt angle  
Find the optimum and suitable solar collector tilt angle in the period of study according the clear sky theory and equations to obtain the maximum incident of the solar radiation for the two mentioned cities.

- To simulate the VJRC driven by solar energy

Hourly simulation for VJRC driven by solar energy at different weather and climate of the two cities mentioned above using TRNSYS software, and study the effect of the different parameters (solar collector area and volume of the storage tank) on the performance of the system and the cooling capacity of the cycle also to find the optimum design parameters and system size to supply and cover the cooling load demand in the TMH.

## **1.6 Thesis Structure**

This thesis is structured in five chapters and begins with an introduction in chapter 1, providing an overview of energy consumption in HVAC, ejector configurations, VJRC principals, literature review and finally, scopes and objectives of this study.

Chapter two discusses the theory of the ejector based on constant pressure mixing ejector .In addition the theory of VJRC, solar collector theory, and incident solar radiation calculations according to the clear sky theory and equations.

Chapter three discusses the climate of the selected areas, building constructions and properties, codes and standards and parameters of the cooling load demands.

Chapter four discusses the simulation of the VJRC subsystems and results, Building Cooling load subsystems simulation and results and the overall system simulation and results.

Chapter five discusses the conclusions and future works.

## CHAPTER 2

### Theory

#### 2.1 introduction

As mentioned above the proposed system that studied consist from three subsystems; VJRC subsystem, building cooling load subsystem and solar thermal subsystem. In this chapter all theory's that are needed for VJRC and solar thermal subsystems are illustrated that include the ejector theory, VJRC theory, solar collector and Incident solar radiation theory. Building cooling load subsystem theory will be reviewed later. Figure 2.1 shows the schematic diagram of the proposed system.

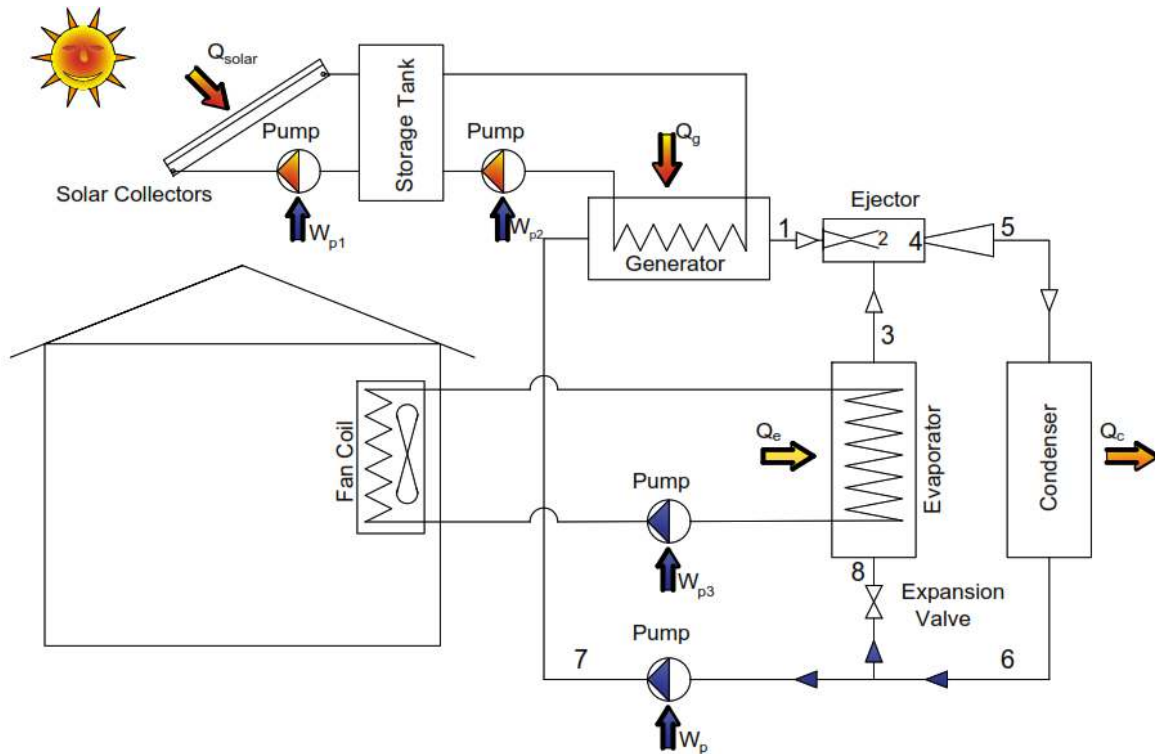


Figure 2. 1: Schematic diagram of the proposed system.

## 2.2 Ejector theory

The ejector is considered the main component in the VJRC. In this study the ejector used was based on the constant pressure mixing ejector that proposed by Eames et al [9] and Sun [14]. Where the theoretical equations of the ejector were based on the well-known steady flow energy equation, momentum and continuity equations as follows.

Energy equation for an adiabatic flow:

$$\sum \dot{m}_i \left( h_i + \frac{V_i^2}{2} \right) = \sum \dot{m}_e \left( h_e + \frac{V_e^2}{2} \right) \dots\dots\dots 2.1$$

Momentum equation:

$$P_i A_i + \sum \dot{m}_i V_i = P_e A_e + \sum \dot{m}_e V_e \dots\dots\dots 2.2$$

Continuity equation:

$$\sum \rho_i A_i V_i = \sum \rho_e A_e V_e \dots\dots\dots 2.3$$

Where:

- $\dot{m}$ : the mass flow
- $h$ : specific enthalpy
- $V$ : velocity
- $P$ : pressure
- $\rho$ : density
- $A$ : area

With reference to Figure 2.2, the following simplified assumptions were made for the one dimensional ejector Analysis by Eames et al [9] and Sun [14].

1. Friction losses were taken in consideration ed by applying isentropic efficiencies to the primary nozzle, diffuser and mixing chamber.
2. The primary and secondary fluids were supplied at zero velocity at P and S respectively.
3. At the outlet of the primary nozzle where the primary and secondary fluids first meet, the static pressure was assumed to be constant.
4. Mixing of the two streams was complete before entering the throat section.

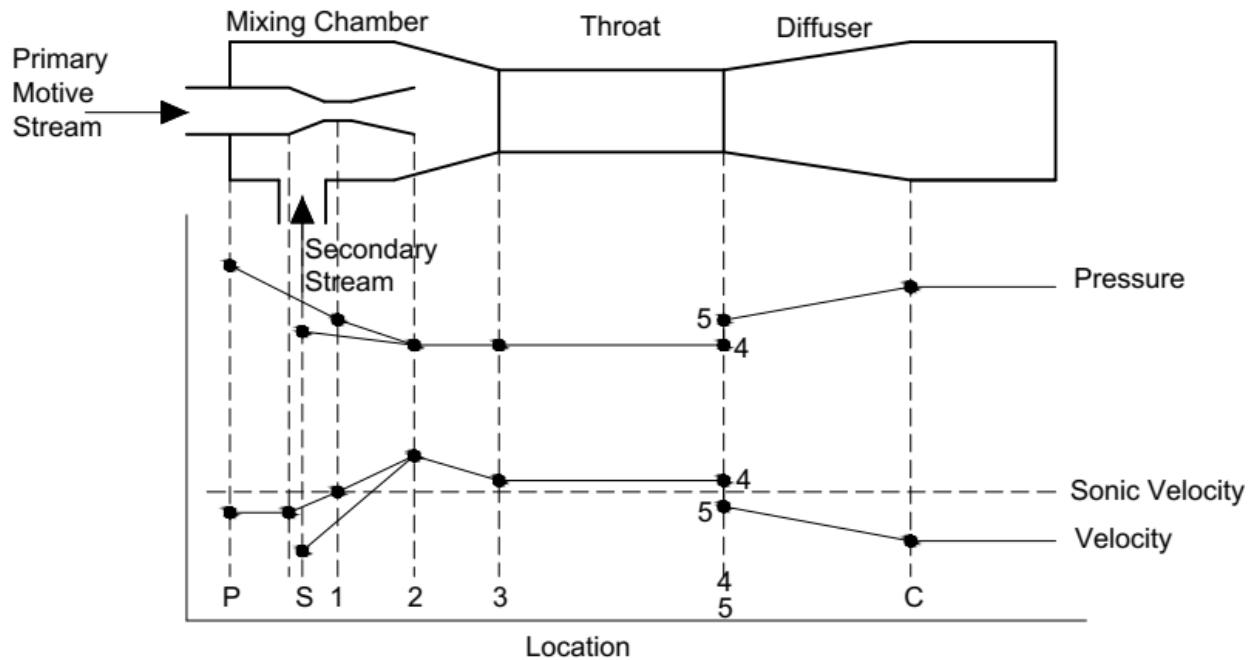


Figure 2. 2: Pressure and velocity profile along the typical ejector

Applying the energy equation (2.1) between points p and 2 to find the velocity of the stream leaving the nozzle, it can be simplified to

$$V_{p2}^2 = 2\eta_n (h_p - h_{p2}) \dots\dots\dots 2.4$$

Where:  $\eta_n$  is an isentropic efficiency of the primary nozzle.

Also the secondary flow velocities at point 2 is

$$V_{s2}^2 = 2 (h_s - h_{s2}) \dots\dots\dots 2.5$$

The specific enthalpy is defined as

$$h = c_p T \dots\dots\dots 2.6$$

Specific heat at constant pressure is defined as

$$c_p = \frac{kR}{k-1} \dots\dots\dots 2.7$$

Where:

R is the universal gas constant

k is the specific heat ratio

The isentropic relationship between pressure and temperature ratios between states 1 and 2 is given by:

$$\left(\frac{T_1}{T_2}\right) = \left(\frac{P_1}{P_2}\right)^{((k-1)/k)} \dots\dots\dots 2.8$$

The speed of sound at local static temperature is

$$c = \sqrt{kRT} \dots\dots\dots 2.9$$

The local Mach number is defined as

$$M = \frac{V}{c} \dots\dots\dots 2.10$$

From the above equations, the relation between the pressure ratio across the nozzle and Mach number at the exit of the nozzle is given as:

$$M_{p2} = \sqrt{\frac{2\eta_n}{k-1} \left[ \left(\frac{P_p}{P_2}\right)^{((k-1)/k)} - 1 \right]} \dots\dots\dots 2.11$$

Similarly to the primary, the Mach number of the secondary fluid at the nozzle exit plane is given as:

$$M_{s2} = \sqrt{\frac{2}{k-1} \left[ \left(\frac{P_s}{P_2}\right)^{((k-1)/k)} - 1 \right]} \dots\dots\dots 2.12$$

By applying the momentum equation on the ejector mixing chamber from 2 to 4. It was assumed that the entire mixing of primary and secondary flows occurs between point's 2 and 4 at constant static pressure. Therefore, equation 2.2 becomes as the following:

$$\eta_m(\dot{m}_p V_{p2} + \dot{m}_s V_{s2}) = (\dot{m}_p + \dot{m}_s) V_4 \dots\dots\dots 2.13$$

Where:  $\eta_m$  is efficiency for the mixing chamber.

Thus the velocity of the mixed fluid at 4 can be written as

$$V_4 = \eta_m \left( \frac{\dot{m}_p V_{p2} + \dot{m}_s V_{s2}}{\dot{m}_p + \dot{m}_s} \right) \dots\dots\dots 2.14$$

Therefore, equation (2.14) can be expressed in terms of Mach number as:

$$M^*_4 = \left( \frac{M^*_2 p_2 + w M^*_2 s_2 \sqrt{T_s/T_p}}{\sqrt{(1+w)(1+w T_s/T_p)}} \right) \dots\dots\dots 2.15$$

Where  $M^*$  is the ratio between the local fluid velocities to the velocity of sound at critical conditions. And the relation between  $M$  and  $M^*$  at any point in the ejector is given by this equation.

$$M^* = \sqrt{\frac{(k+1)M^2/2}{1+(k-1)M^2/2}} \dots\dots\dots 2.16$$

Once the fluids are fully mixed and the mixed flow enters the throat area with a supersonic speed, a normal shock wave occurs at point five which is irreversible leading to a sudden change in the fluid pressure and velocity, where the pressure increased and the Mach number to subsonic. Thus, the Mach number after the shock for the mixed flow is written as:

$$M_5 = \sqrt{\frac{M_4^2 + \frac{2}{(k-1)}}{\frac{2k}{(k-1)} M_4^2 - 1}} \dots\dots\dots 2.17$$

Therefore, the pressure lift ratio across the shock can be found as follows:

$$\frac{P_5}{P_4} = \frac{1+k M_4^2}{1+k M_5^2} \dots\dots\dots 2.18$$

Further compression of the mixing fluid is achieved as it passes through the subsonic diffuser, it is assumed that the flow speed is reduced to zero at the diffuser exit. Thus, the pressure lift across the diffuser can be written as:

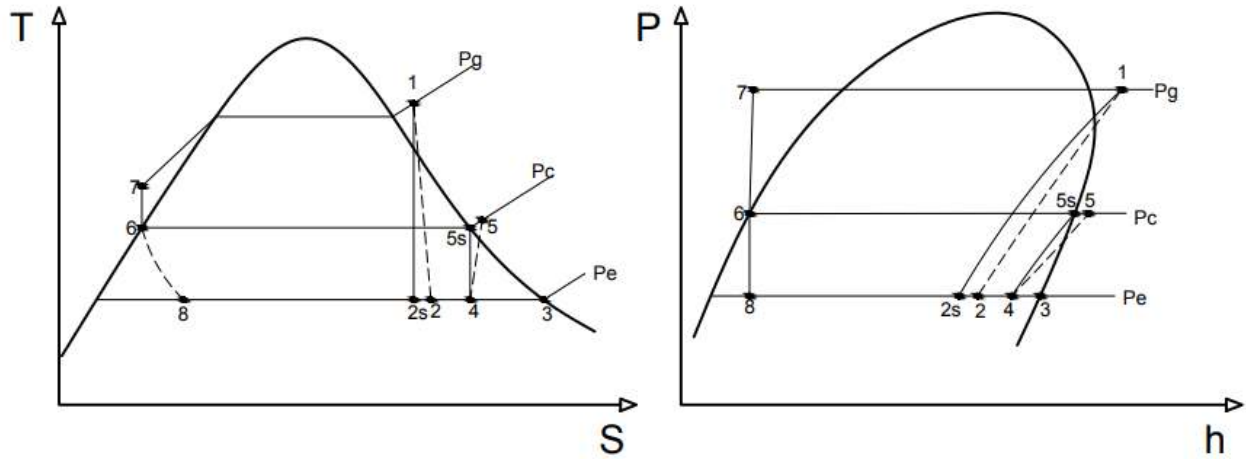
$$\frac{P_c}{P_5} = \left( \frac{\eta_d(k-1)}{2} M_5^2 + 1 \right)^{(k/(k-1))} \dots\dots\dots 2.19$$

Where  $\eta_d$  is the isentropic efficiency of the diffuser

### 2.3 VJRC theory

VJRC was described in chapter 1. The following equations and expressions are referred to Figure 2.1 That shows the schematic diagrams of VJRC and figure 2.3 a and b that show T-s and p-h diagrams for the same cycle.





a: T-s diagram of VJRC

b: p-h diagram of VJRC

Figure 2. 3: T-s and p-h diagrams of VJRC

The performance of an ejector can be defined in terms of the Entrainment ratio or mass flow ratio which is the ratio between the secondary and primary fluid mass flow rates. [9]

$$w = \frac{\dot{m}_s}{\dot{m}_p} \dots\dots\dots 2.20$$

The VJRC performance is evaluated by the coefficient of performance (COP), COP is equal the ratio between the Evaporator load  $Q_e$  to the generator load  $Q_g$  and power of the pump  $W_p$  as shown:

$$COP = \frac{Q_e}{Q_g + W_p} \dots\dots\dots 2.21$$

Where:

$$Q_e = \dot{m}_s (h_3 - h_8) \dots\dots\dots 2.22$$

$$Q_g = \dot{m}_p (h_1 - h_7) \dots\dots\dots 2.23$$

$$W_p = \dot{m}_p (h_7 - h_6) \dots\dots\dots 2.24$$

The isentropic efficiency of the primary nozzle  $\eta_n$  and the isentropic efficiency of the diffuser  $\eta_d$  can be calculated as shown:

$$\eta_n = \frac{h_{2s} - h_1}{h_2 - h_1} \dots\dots\dots 2.25$$

$$\eta_d = \frac{h_{5s} - h_4}{h_5 - h_4} \dots\dots\dots 2.26$$

The energy balance at point 4 can be calculated as

$$\dot{m}_s * h_3 + \dot{m}_p * h_2 = \dot{m}_c * h_4 \dots\dots\dots 2.27$$

For combined power and refrigeration cycle, the COP of the Carnot cycle under the same conditions can be calculated as

$$\text{COP}_{\text{carnot}} = \frac{T_e}{T_c - T_e} * \frac{T_g - T_c}{T_g} \dots\dots\dots 2.28$$

The condenser load  $Q_c$  of the cycle can be calculated as:

$$Q_c = \dot{m}_c (h_5 - h_6) \dots\dots\dots 2.29$$

Where  $\dot{m}_c$  is the condenser flow rate and equal the summation of primary and secondary flow rate as shown:

$$\dot{m}_c = \dot{m}_p + \dot{m}_s \dots\dots\dots 2.30$$

The overall performance of the solar cooling system is

$$\text{COP}_o = \text{COP} * \eta_{sc} \dots\dots\dots 2.31$$

Where  $\eta_{sc}$  is the solar collector efficiency

## 2.4 Solar collector theory

The solar thermal collector is the major component of any solar thermal system. This is a device which collects the incoming solar radiation from the sun, converts it into a heat, and transfers this heat to a heat transfer fluid that usually water, molten salt or oil, that flow through the collector. The solar energy which was collected is carried by a circulated heat transfer fluid to use directly or to store it in a thermal energy storage tank which can be utilized later at night and/or cloudy days [21]. There are mainly two types of stationary solar collectors: Flat plate collector (FPC) and Evacuated tube collector (ETC), the operating temperatures of these collectors are listed in table 2.1. ETC have wide range of operating temperatures more than Flat plate collector which make it a more suitable collector for the solar thermal systems with moderate operating temperature.

Table 2. 1: Typical operating temperature of different solar collectors

Type of collector	Typical operating temperature [°C]	Reference
FPC	≤70	[22]
High efficiency FPT	60-120	
ETC	50-200	[21]

The useful energy extracted by the collector ( $Q_{coll}$ ) is

$$Q_{coll} = \eta_{sc} G A_{coll} = \dot{m}_f c_p (T_o - T_i) \dots\dots\dots 2.32$$

Where

$G$  is the solar radiation

$\eta_{sc}$  is solar collector efficiency

$A_{coll}$  is collector area

$T_i$  and  $T_o$  are the inlet and outlet collector temperature respectively.

$\dot{m}_f$  and  $c_p$  are mass flow rate and specific heat of the circulation fluid.

The solar collector efficiency  $\eta_{sc}$  is calculated by the Hottel–Whillier–Bliss equation as follow:

$$\eta_{sc} = \eta_0 - a_1 \frac{T_m - T_a}{G} - a_2 \frac{(T_m - T_a)^2}{G} \dots\dots\dots 2.33$$

Where

$\eta_0$  is Maximum efficiency

$a_1$  is 1st order heat loss coefficient, depend on the collector type

$a_2$  is 2nd order heat loss coefficient, depend on the collector type

$T_m$  and  $T_a$  are the mean collector fluid temperature and ambient air temperature respectively

The data for ETC and FPC are listed in table 2.2 according to the manufacturer [23] and the corresponding efficiencies are plotted in figure 2.4 as function of temperature difference between collector fluid and ambient air assuming a solar radiation of 1000 W/m<sup>2</sup>.

Table 2. 2: Parameters of the evacuated tube and flat plate collectors [23]

Collector type	$\eta_0$ [-]	$a_1$ [W/(K·m <sup>2</sup> )]	$a_2$ [W/(K <sup>2</sup> ·m <sup>2</sup> )]
ETC	80	1.5	0.005
FPC	80	4	0.1

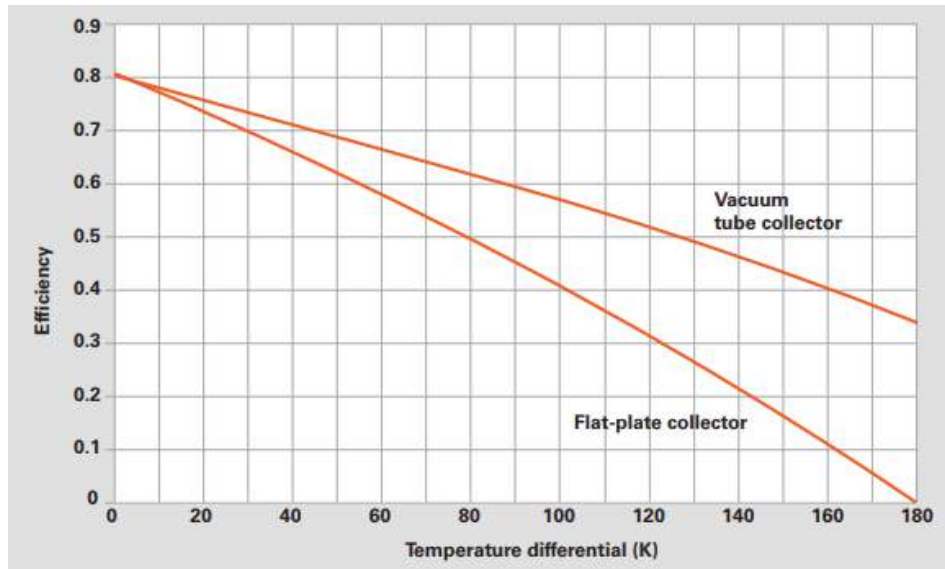


Figure 2. 4: Efficiency of the evacuated tube and flat plate collectors [23]

## 2.5 Incident solar radiation theory

The solar radiation, reaching the earth's surface can be classified into three main components: direct beam radiation, diffuse radiation and reflected radiation. Direct beam radiation is the solar radiation passing through the atmosphere to the receiver in a straight line. Diffuse radiation is a dispersed radiation caused by atmospheric molecules and aerosols, while the reflected radiation that has bounced off the ground or other surface in front of the collector [24], Figure 2.5 shows the Solar radiation striking a collector and figure 2.6 shows the solar angles, where it illustrating the collector azimuth angle  $\phi_C$  and tilt angle  $\Sigma$  along with the solar azimuth angle  $\phi_S$  and altitude angle  $\beta$  [24].

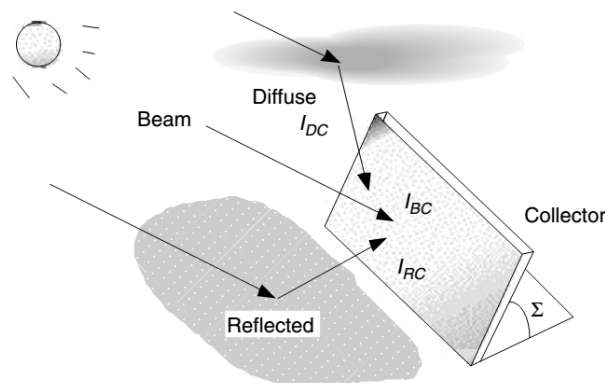


Figure 2. 5: Solar radiation striking a collector [24]

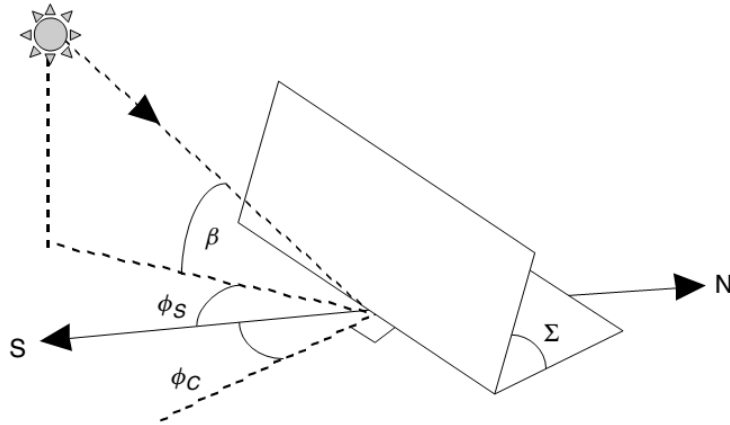


Figure 2. 6: Solar angels [24]

To estimate the suitable collector tilt angle in the period of study Clear Sky Direct-Beam Radiation theory were used, where the beam portion of the radiation reaching the earth's surface  $I_B$  can be calculated as the following [24]:

$$I_B = Ae^{-km} \dots\dots\dots 2.34$$

Where

A: is an “apparent” extraterrestrial flux.

$$A=1160 + 75\sin \left[ \frac{360}{365} (n - 275) \right] \dots\dots\dots 2.35$$

k :is a dimensionless factor called the optical depth.

$$k=0.174 + 0.035\sin \left[ \frac{360}{365} (n - 100) \right] \dots\dots\dots 2.36$$

n :day number

m :The air mass ratio

$$m=1/\sin \beta \dots\dots\dots 2.37$$

The direct solar flux striking a surface is denoted by  $I_{BC}$  and can be calculated as the following:

$$I_{BC} = I_B \cos \phi \dots\dots\dots 2.38$$

Where the  $\cos \phi$  is the cosine of the incidence angle between the normal to the collector face and the incoming solar beam radiation and can be calculated as the following:

$$\cos \phi = \cos \beta \cos (\phi_s - \phi_c) \sin \Sigma + \sin \beta \cos \Sigma \dots\dots\dots 2.39$$

The diffuse radiation on a collector is much more difficult to estimate accurately than it is for the beam. It can be assumed that the diffuse insolation on a horizontal surface  $I_{DH}$  is proportional to the direct beam radiation  $I_B$  no matter where in the sky the sun happens to be:

$$I_{DH} = C I_B \dots\dots\dots 2.40$$

Where C: is a sky diffuse factor

$$C = 0.095 + 0.04 \sin \left[ \frac{360}{365} (n - 100) \right] \dots\dots\dots 2.41$$

The following expression for diffuse radiation on the collector,  $I_{DC}$ , is used when the diffuse radiation is idealized in this way:

$$I_{DC} = I_{DH} \left[ \frac{1 + \cos \Sigma}{2} \right] = C I_B \left[ \frac{1 + \cos \Sigma}{2} \right] \dots\dots\dots 2.42$$

The final component of insolation striking a collector results from radiation that is reflected by surfaces in front of the panel  $I_{RC}$ .

$$I_{RC} = \rho I_B (\sin \beta + C) \left[ \frac{1 - \cos \Sigma}{2} \right] \dots\dots\dots 2.43$$

Where  $\rho$  is the ground reflectance between (0.1-0.8)

The total insolation on the collector is therefore

$$I_C = I_{BC} + I_{DC} + I_{RC} \dots\dots\dots 2.44$$

## CHAPTER 3

### Climate and Building Descriptions

#### 3.1 Introduction

The reference building model in this study is called typical movable house (TMH) and it is selected for two locations Hebron and Jericho cities in Palestine, the aim of this chapter is to demonstrate and study the characteristic of the TMH in terms of location and climate conditions ; solar radiation and ambient air temperature of the selected locations. Also for the building constructions, internal heat gains and air exchange. In order to simulate the TMH cooling load demand by using TRNSYS software.

#### 3.2 Location and Climate

The building cooling demand are mainly influenced by the outdoor ambient air temperature and global solar radiation around it. In this study, the TMH cooling demand calculations depends on the selected locations climates of Hebron and Jericho cities in West Bank at Palestine.

The Hebron city is located south of west bank at latitude  $31.32^{\circ}\text{N}$  and longitude  $35.06^{\circ}\text{E}$  It's a mountain view. Hebron enjoys relatively medium mean temperatures .The meteorological station is 1005 meters above sea level and the mean temperature is estimated  $17.36^{\circ}\text{C}$  in 2015 according the Palestinian Meteorology (PAL MET) in Palestine [25]. Jericho city is located east of west bank at latitude  $31.51^{\circ}\text{N}$  and longitude  $35.27^{\circ}\text{E}$ . It is located in the high mean temperature regions. This city is characterized by very hot weather in summer; summer temperatures rise up to  $45^{\circ}\text{C}$ . The meteorological station is 260 meters below sea level and the mean temperature is estimated  $24.77^{\circ}\text{C}$  in 2015 [25]

The files of the meteorological data for two locations were received in Excel-format from the PAL MET. The data files contains measurement data in 15 minute intervals for the year 2015. It includes, the global horizontal solar radiation, ambient air temperature and relative humidity. This file was converted into Energy plus Weather (EPW) format with hourly intervals.

Figure 3.1 Shows the distribution of the ambient temperatures in the two cities, where the maximum ambient temperature in Hebron and Jericho cities reached to 38.7 °C and 45 °C respectively.

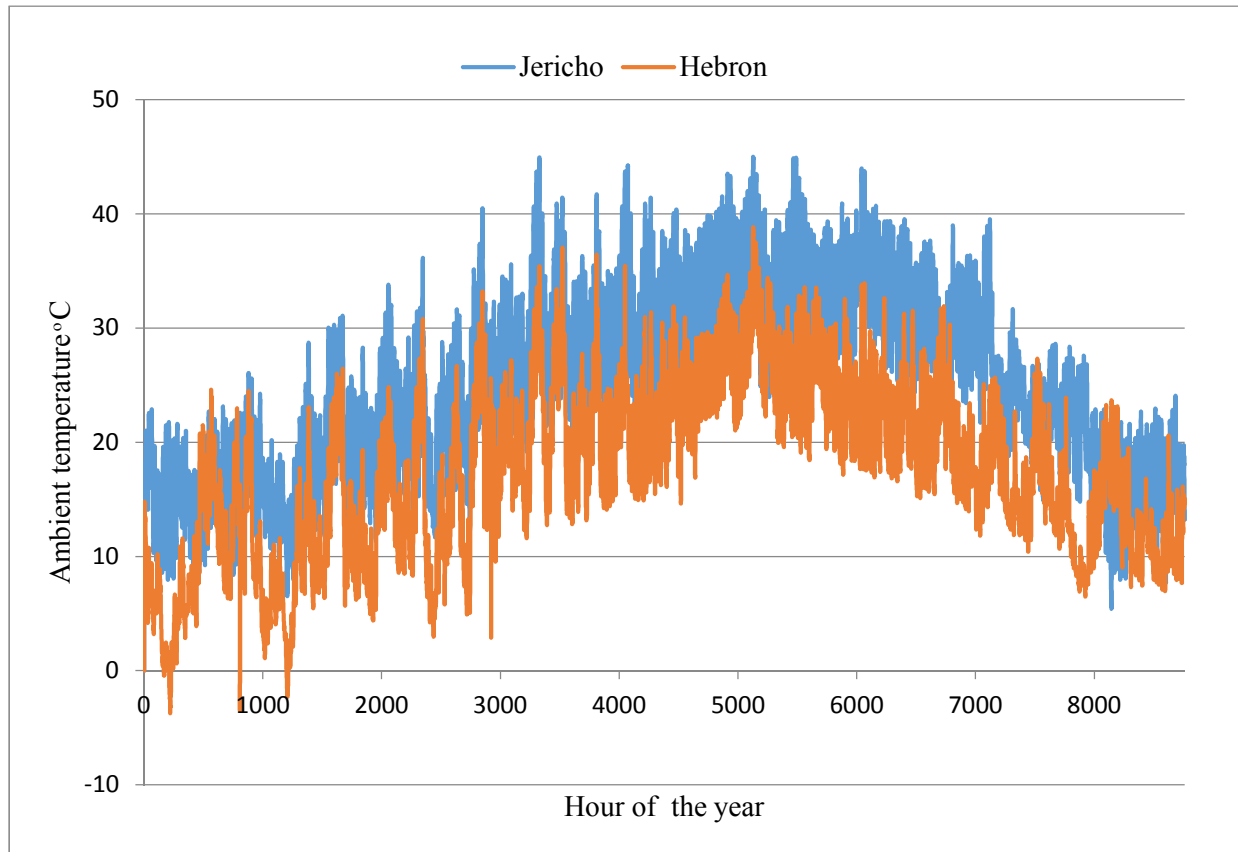


Figure 3. 1: Annual distribution of ambient temperatures for Hebron and Jericho cities.

Figure 3.2 shows the distribution of the global horizontal solar radiation for the two cities, where the maximum hourly global horizontal solar radiation in Hebron city is 1157 W/m<sup>2</sup>, and the maximum hourly global horizontal solar radiation in Jericho city is 1180 W/m<sup>2</sup>.



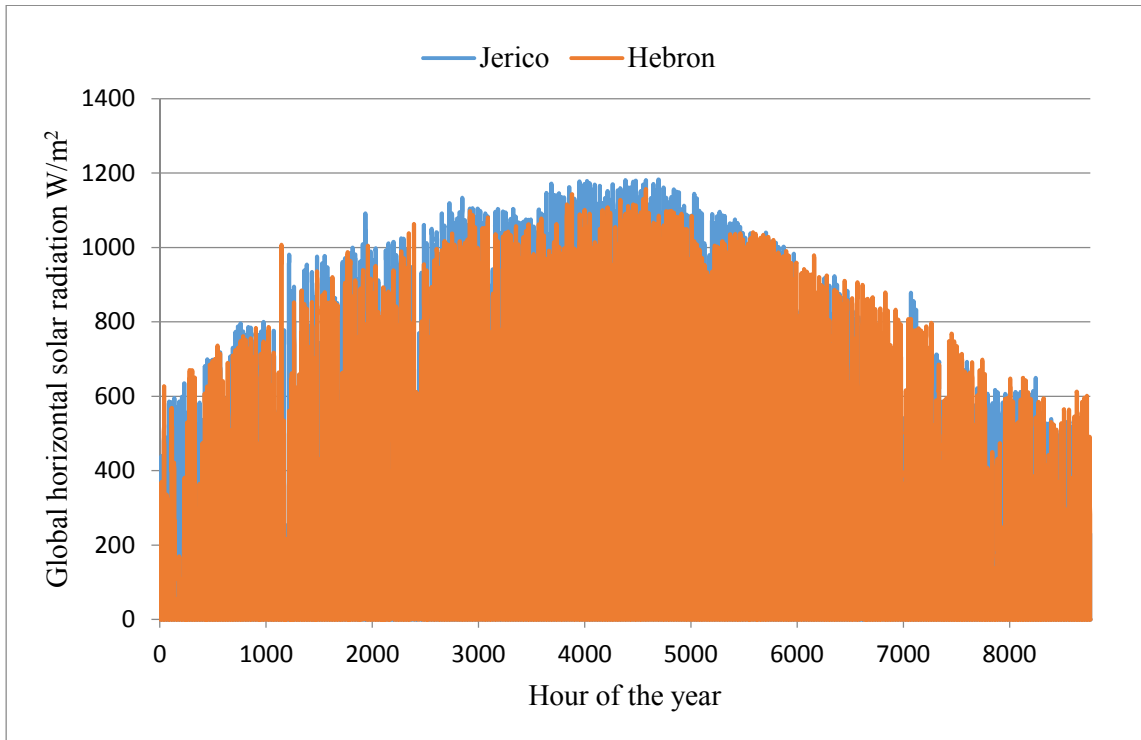


Figure 3. 2: Annual distribution of global horizontal solar radiation for Hebron and Jericho cities  $W/m^2$

Figures 3.3 and 3.4 show the mean monthly distributions for ambient temperatures and number of hours for one sun of horizontal global solar radiation in  $kWh/m^2.day$  for the two cities.

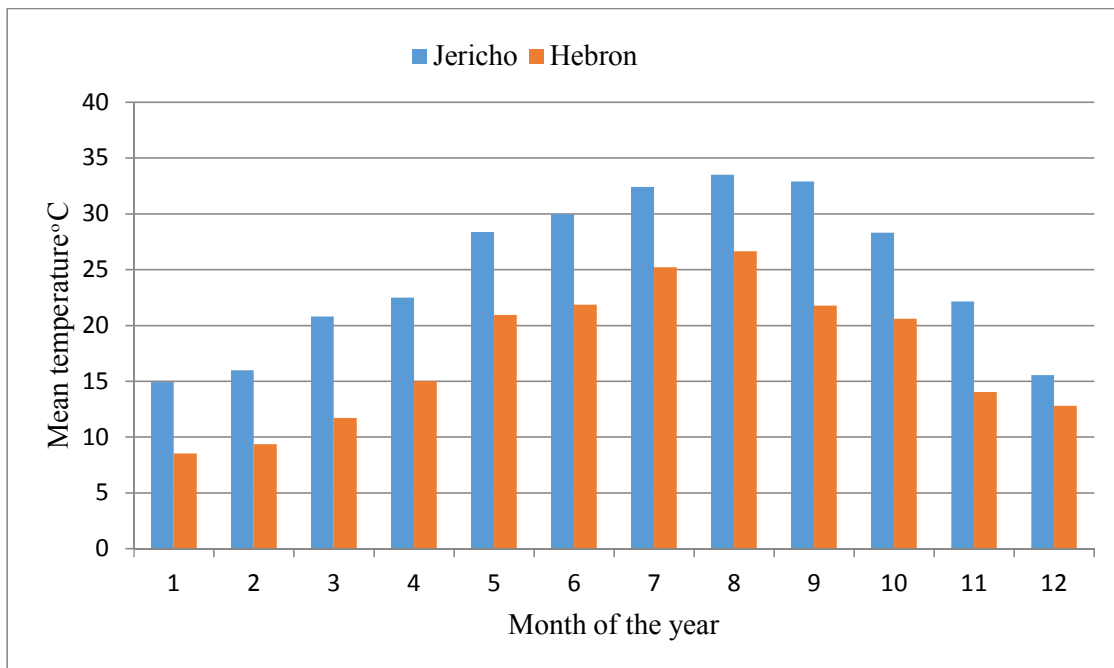


Figure 3. 3: Mean monthly distributions for ambient temperatures for Hebron and Jericho cities  $^{\circ}C$ .

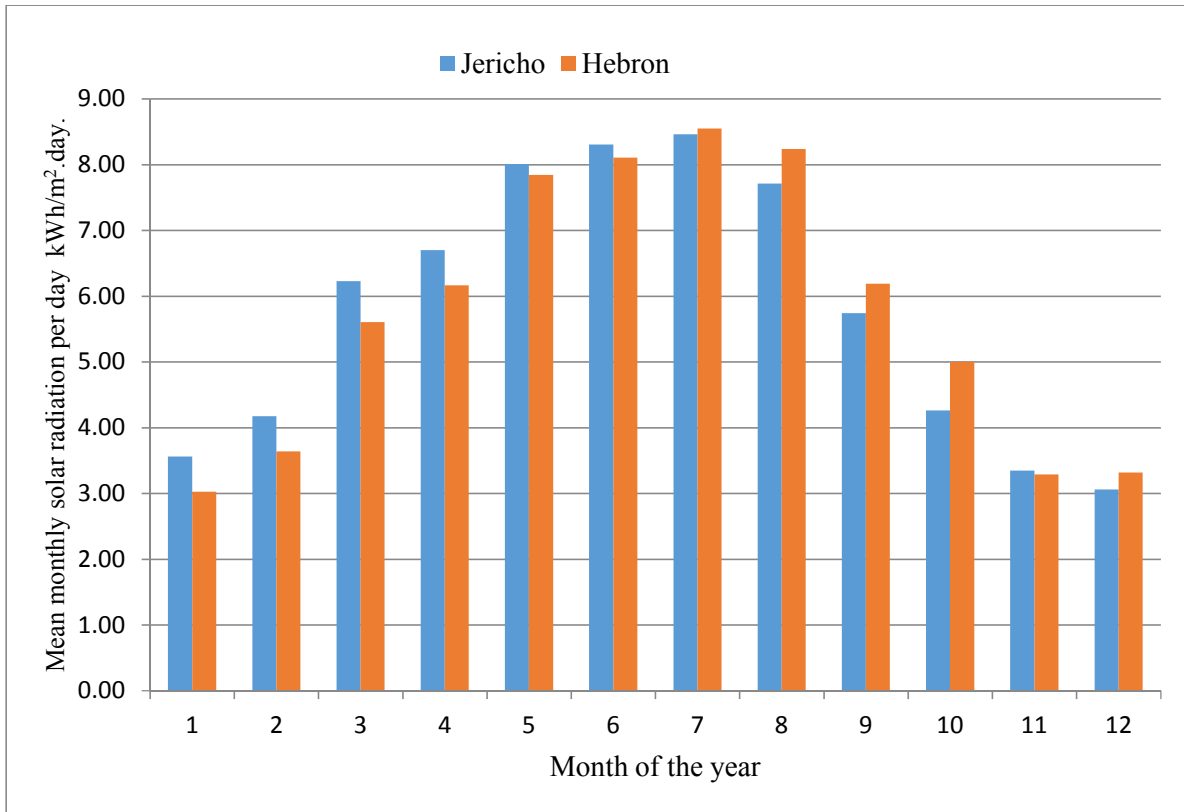


Figure 3. 4: Mean monthly distributions for one sun of horizontal global solar radiation per day for Hebron and Jericho cities kWh/m<sup>2</sup>.day.

Figure 3.2 to 3.4 show that the annual total solar radiation are mostly the same for the tow city where the total solar radiation for Hebron is 2068 kWh/.m<sup>2</sup>.y and for Jericho is 2086 kWh/.m<sup>2</sup>.y because the solar radiation depends of the latitude value of the location on the earth and the two locations have relatively the same values of latitude as mentioned above. But on the other hand the average ambient temperature for Jericho city is greater than Hebron city by 42% ,this is because of the deference of the land level from the sea level where Jericho have a valley weather and Hebron have mountain weather and this is the main deference between the two cities.

### 3.3 Building Description

The reference TMH which has been selected in this study is produced by Alamour Company for industrial and trading in Bedyá-Jeneen [26]. This section defines the TMH and the definition include architecture design and orientation, constriction building elements descriptions (walls, roof, floor and windows), internal heat gain, air change conditions and the cooling set point. This

building data must be determined in order to simulate the thermal cooling demand for the building by using TRNBuild in TRNSYS software.

The TMH is rectangular shape 8m\*3m, and ceiling height is 2.6 m. It consists of two bedrooms, Kitchen and bathroom. Number of occupants is 3 persons. The sketch of TMH in Figure 3.5 Shows the architecture design, orientation and the zones dimensions. This architecture design of the TMH was considered for the two climate locations, Hebron and Jericho cites.

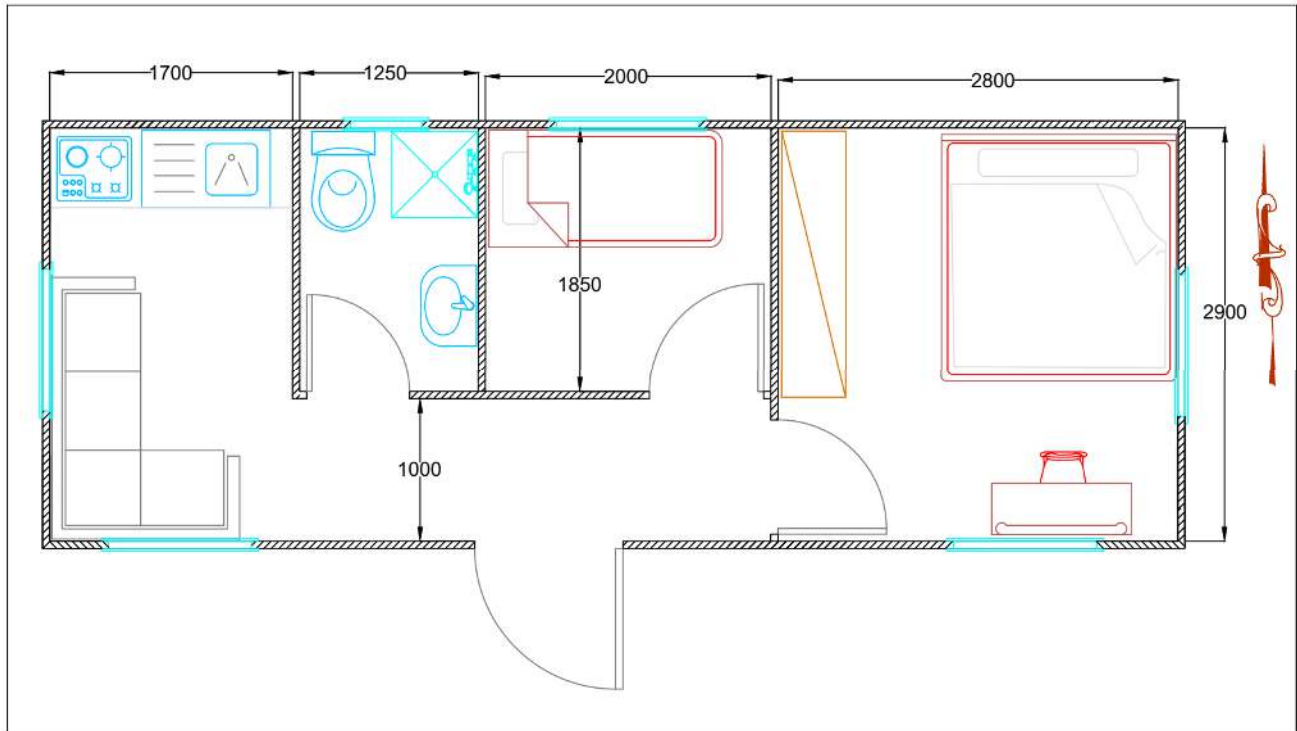


Figure 3. 5: Architecture design of the TMH

The constructions of the TMH walls, roof, door and ground are consists of typical sandwich panel with over all heat transfer coefficient (U-value) of  $0.587 \text{ W/m}^2 \text{ }^\circ\text{C}$ , it consists of two metal sheets from carbon steel and between them there is a layer from polystyrene figure 3.6 a. A double glass aluminum frame window with U-value of  $2.877 \text{ W/m}^2 \text{ }^\circ\text{C}$  was selected for the TMH as one of the most popular window types in Palestine figure 3.6 b. Inside and outside convection heat transfer coefficient was considered based on ISO 6946-2007 standard [27], table 3.1 represents the Conventional surface resistances where the convection heat transfer coefficient is inverse of the resistance .

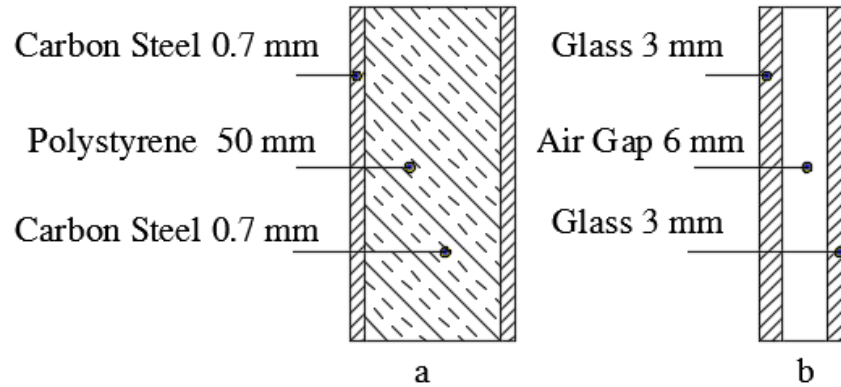


Figure 3. 6: TMH constructions, a: for walls, roof, door and floor, b: for windows

Table 3. 1: The inside and outside Conventional surface resistances [27]

Surface resistance $m^2.K/W$	Direct of heat flow		
	upwards	horizontal	downwards
$R_{inside}$	0.1	0.13	0.17
$R_{outside}$	0.04	0.04	0.04

The constructions and details of walls, roof, door, ground and windows are shown in table3.2. Where all the physical properties were taken according the Palestinian code for efficient buildings [28].

Table 3. 2: Constructional components of the TMH

assembly	layer	Thickness [mm]	Thermal conductivity [ $W/m^{\circ}C$ ]	Density [ $kg/m^3$ ]	Specific heat [ $kJ/kg^{\circ}C$ ]	U-Value [ $W/m^2^{\circ}C$ ]
External walls, roof, door, and floor	Carbon steel	0.7	60	7800	0.466	0.587
	Polystyrene	50	0.032	35	1.3	
	Carbon steel	0.7	60	7800	0.466	
windows	Glass	3	0.8	2250	0.84	2.877
	Air gap	6	0.03	1.2	1.007	
	glass	3	0.8	2250	0.84	

The rate of internal heat gain from occupants, lighting and electric equipments also contribute in cooling load. From occupants was considered based on ISO 7730-2005 standard [29] in TRNSYS data library where the number of occupants is 3 persons with 150 W/person (Seated, light work), in addition the heat gain from electrical equipment is 140 W and  $10\text{W/m}^2$  from lighting. Ventilation was considered for this building according to ANSI/ASHRAE Standard 62.1-2013, [30] where the ventilation for residential dwelling unit is 2.5 L/s.person. Infiltration was considered according cracked method [31] based on the length of the crack or the perimeter of the windows and doors under specific value of wind speed where the mean wind speed in the summer seasons in Hebron and Jericho cites are 9 and 15 km/h respectively [25].ventilation and infiltration were converted to number of air change per hour according to the house volume, where the value of ventilation is 0.5 times per hour, and the infiltration in Hebron and Jericho cites are 0.3 and 0.83 times per hour respectively for double hung metal windows and according the wind speed[31].

The indoor design conditions- temperature and relative humidity- are set according to ANSI/ASHRAE Standard 55-2013[32].where for thermal comfort purposes, the temperature could range between approximately 20 and 27 °C and the relative humidity range between approximately 40 –65%. In this study the inside temperature was chosen to be is 22 °C dry bulb and the relative humidity of 50%.

## CHAPTER 4

### Simulation and Results

#### 4.1 Introduction

As mentioned in chapter one the proposed system consist of three subsystems; VJRC subsystem, building cooling load subsystem and solar thermal subsystem.in this chapter an illustration of the simulation and results of these subsystems also an estimate of the optimum collector tilt angle is demonstrated. The work was done by utilizing different software programs and tools mentioned in previous chapters.

#### 4.2 VJRC simulation and results

##### 4.2.1 VJRC simulation

EES is a general equation - solving program that can solve thousands of non - linear and differential equations in a numerical manner. The mathematical and thermophysical property library is extensive in EES. The program offers many integrated mathematical and thermophysical properties for engineering calculations. For example, the steam tables are implemented in such a way that any thermodynamic property can be obtained in any two other properties. Similar capability is provided for most refrigerants and many other fluids [33].

The equations of ejector were programmed in the EES program. Where the properties of the steam were computed from the program built-in function in the program library. Constant-pressure mixing ejector with variable geometry that discussed by sun et al [14] is assumed. Where the operating conditions (generator, evaporator, and condenser temperature) was at saturated temperature. The efficiency of the nozzle  $\eta_n$  and diffuser  $\eta_d$  were chosen to be 0.85, and the mixing chamber efficiency  $\eta_m$  was assumed 0.98.as described by sun et al [14]. the following procedures were used for analysis and calculations the cycle parameters (as shown in figure 4.1):

- Define the design parameters and constants which includes the evaporator temperature  $T_e$  , generator temperature  $T_g$ , condenser temperature  $T_c$ , generator load  $Q_g$  , universal gas

constant  $R$ , specific heat ratio  $k$  and the efficiency of the nozzle  $\eta_n$ , diffuser  $\eta_d$ , and minimum value for the Mach number of the secondary fluid at the nozzle exit  $M_{s2}$ , where assumed to be greater than the Mach number by 10% .

- Calculate the saturation pressures of the generator  $P_g$ , condenser  $P_c$  and evaporator  $P_e$ .
- Find the enthalpy and enthalpy change of the generator, condenser and evaporator using the steam tables.
- Calculate the mass flow rate of the primary fluid  $\dot{m}_p$  using equation 2.23.
- Solve the equations from 2.11 to 2.19 find the value of the entrainment ratio  $w$ .
- Solve the equation 2.20 and equation 2.30 to find the secondary fluid flow rate  $\dot{m}_s$ , condenser mass flow rate  $\dot{m}_c$ .
- Use the steam tables, equations 2.25 to 2.27, nozzle efficiency  $\eta_n$  and diffuser efficiency  $\eta_d$  to find the enthalpy at point's  $h_2, h_{2s}, h_4, h_5, h_{5s}$  in the cycle.
- Use the equations 2.22, 2.24, 2.29, 2.21 and 2.28 to find the evaporator load  $Q_e$ , the condenser load  $Q_c$ , the pump power  $W_p$  and the coefficient of performance of the system COP and  $COP_{carnot}$ .

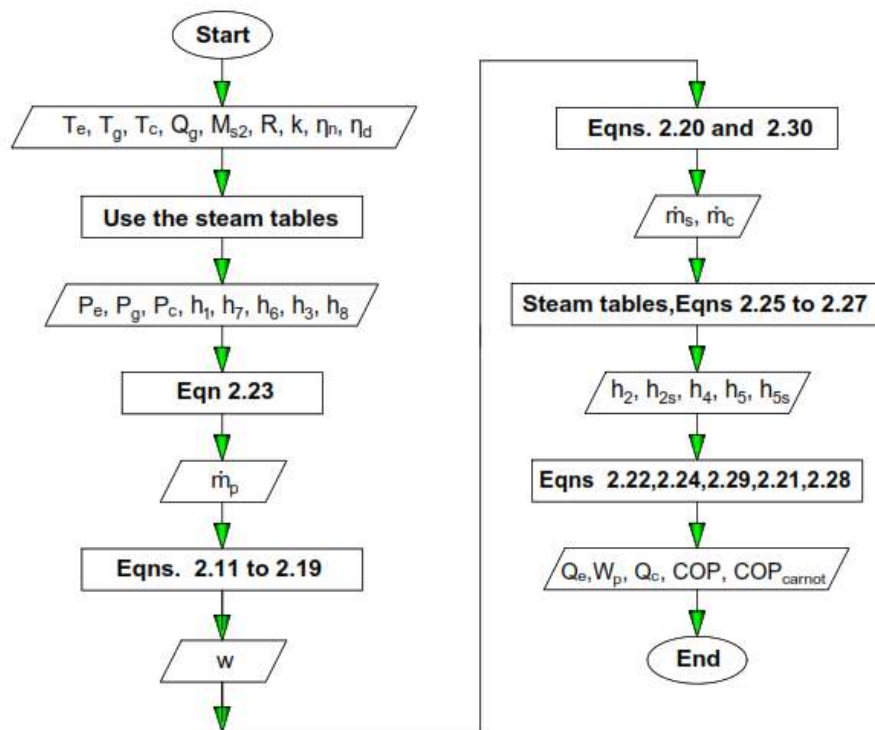


Figure 4. 1: Flowchart for analysis and calculate the VJRC parameters

## 4.2.2 VJRC results

For fixed operation conditions; generator temperature, condenser temperature, evaporator temperature is assumed to be 110°C, 35°C and 10 °C .Figure 4.2 shows and represents the cycle on the p-h diagram extracted from EES. While table 4.1 shows the cycle results.

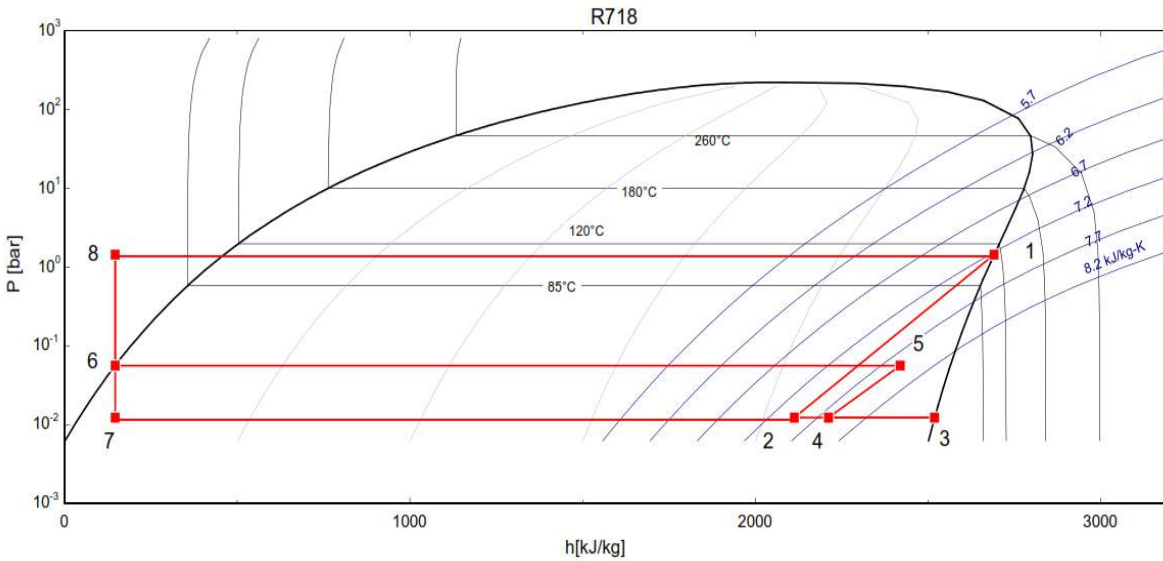


Figure 4. 2: P-h diagram for VJRC at fixed operating conditions 110 °C, 35 °C and 10°C for generator, condenser and evaporator temperature respectively.

Table 4. 1: VJRC results at fixed operating conditions 110 °C, 35 °C and 10°C for generator, condenser and evaporator temperature respectively.

Parameter	Result
$P_e$ (kpa)	1.228
$P_c$ (kpa)	5.627
$P_g$ (kpa)	143.2
$q_e$ (kJ/kg)	2372
$q_c$ (kJ/kg)	2273
$q_g$ (kJ/kg)	2545
$w_{\text{pump}}$ (kJ/kg)	0.0001197
$w$	0.32
COP	0.2984
$\text{COP}_{\text{carnot}}$	2.217



#### 4.2.2.1 Effect of the generator temperature on the cycle performance

The VJRC performance depends mainly on the operating conditions as shown in the literature review. Figure 4.3 shows the variations of cycle performance with generator temperatures at constant evaporator and condenser temperature 10 °C and 35 °C respectively. As shown in the figure the COP of the cycle increases from 0.25 to 0.34 as the generator temperature rises from 100°C to 120°C. The reason for this is that the pressure ratio of the power cycle increase and more secondary flow will be entrained from the evaporator.

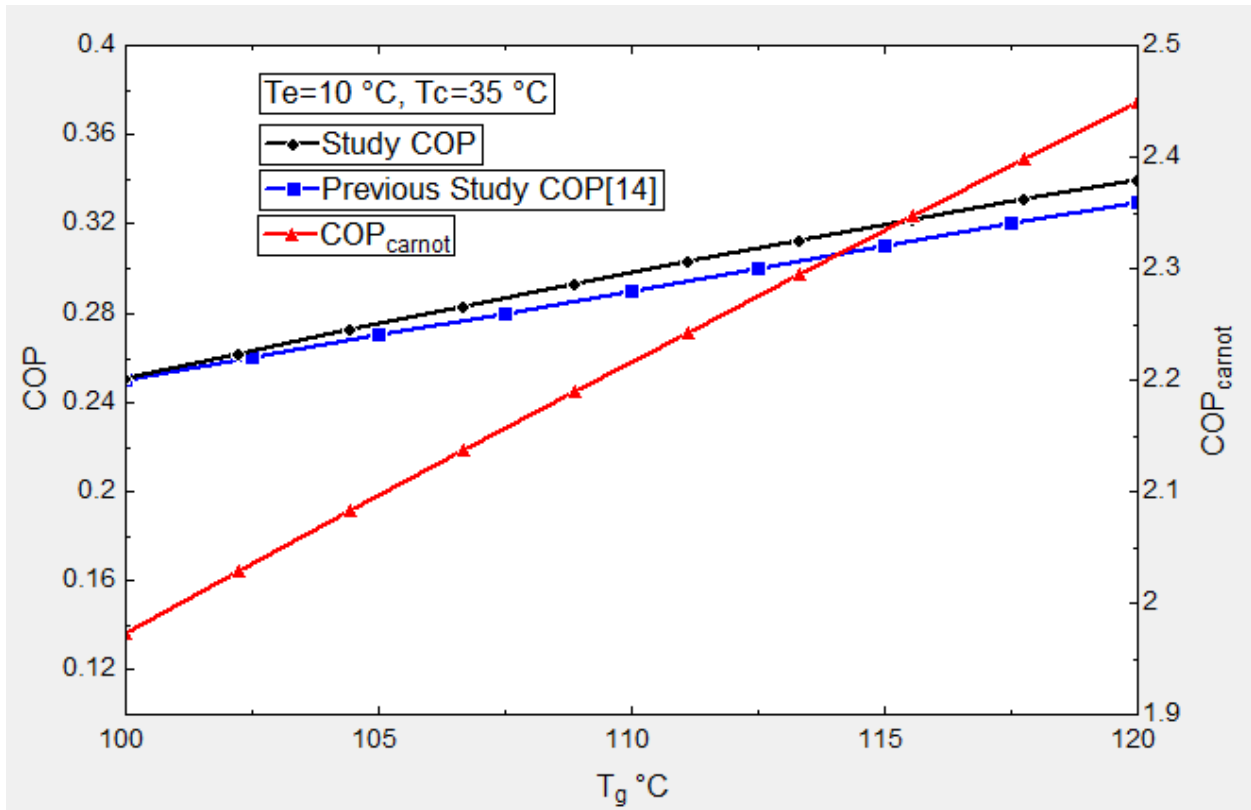


Figure 4. 3: Variations of COP with generator temperatures

#### 4.2.2.2 Effect of the evaporator temperature on the cycle performance

Figure 4.4 shows the variation of cycle performance with evaporator temperatures at constant generator and condenser temperatures 110°C and 35 °C respectively. It can be noticed that the COP increases from 0.13 to 0.55 as the evaporator temperature changes from 5°C to 15°C. This

increment is due to an increment in secondary flow which will be entrained as the evaporator temperature increases under low pressure ratio in the refrigeration cycle.

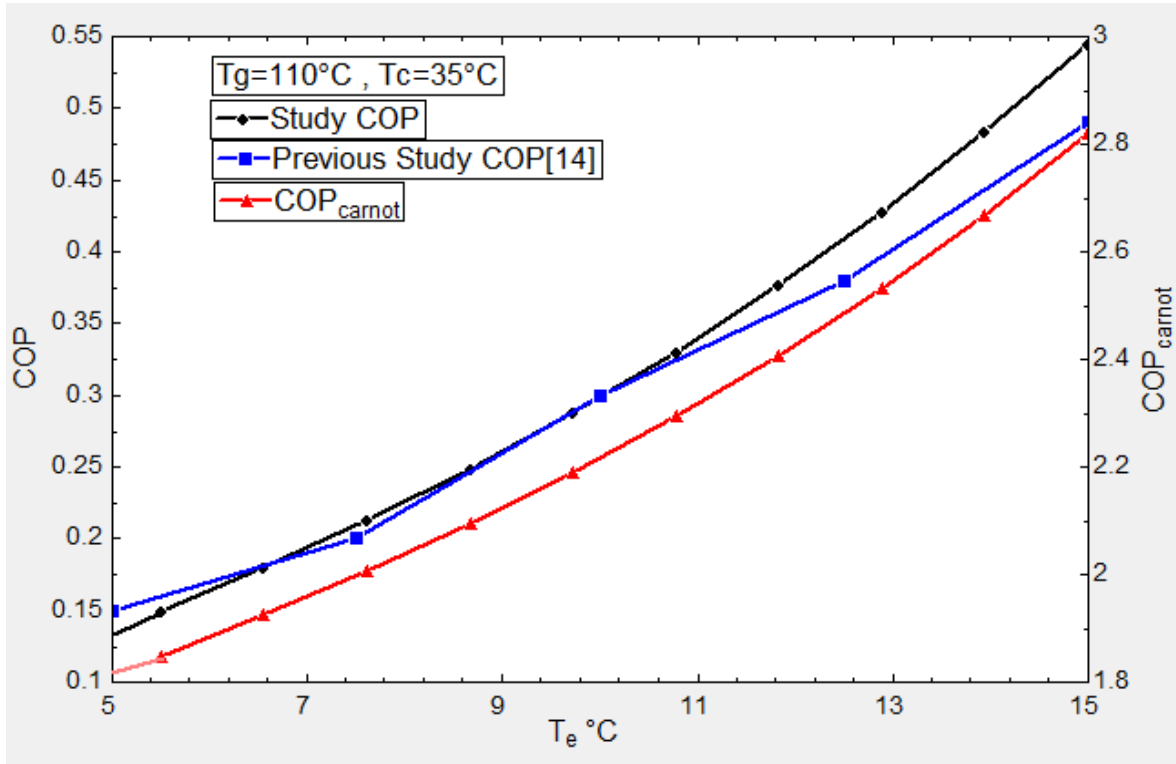


Figure 4. 4: Variations in COP with evaporator temperatures

#### 4.2.2.3 Effect of the condenser temperature on the cycle performance

Figure 4.5 shows the variations of cycle performance with respect to condenser temperature at generator temperature and evaporator temperature 110°C and 10 °C respectively. It can be seen that the COP decreased remarkably from 0.55 to 0.02 as the condenser temperature increases from 30°C to 45°C. This due to low secondary flow will be entrained as condenser temperature increases under high pressure ratio in the refrigeration cycle.

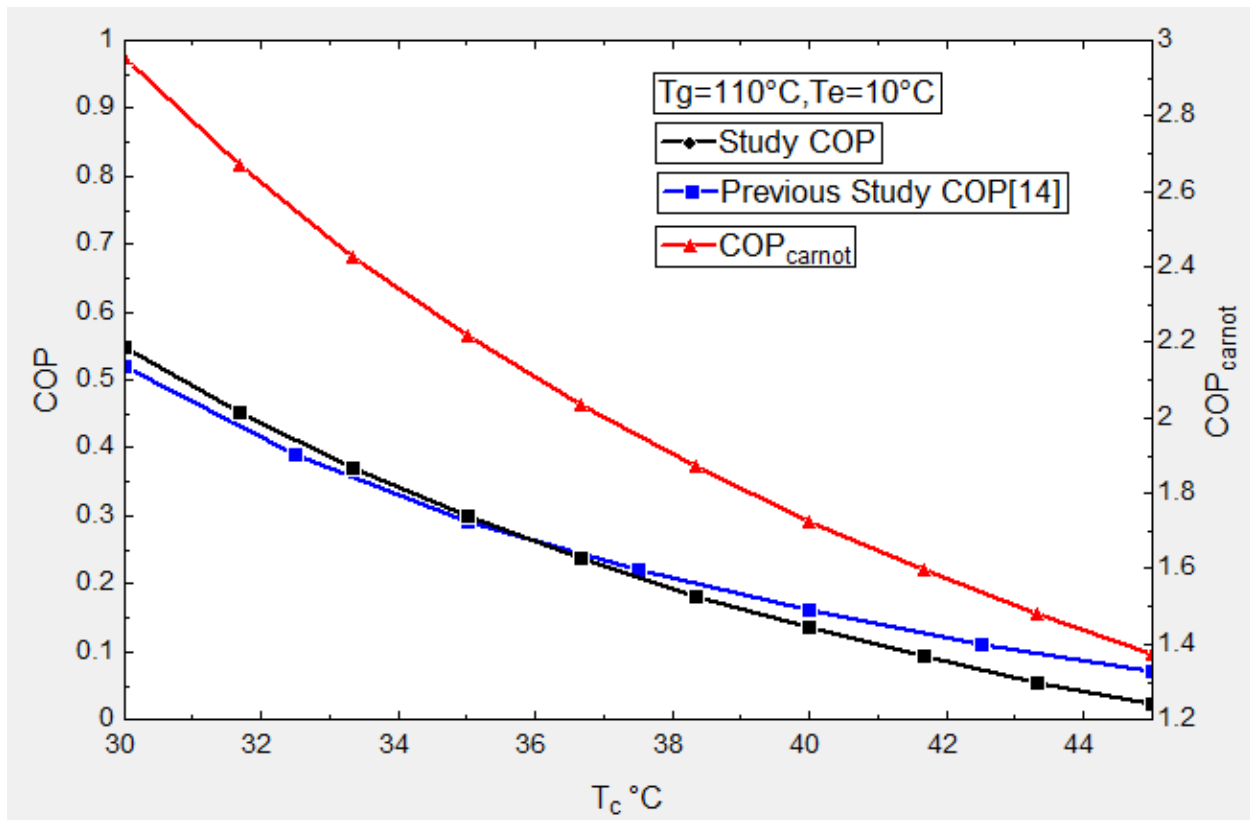


Figure 4. 5: Variations in COP with condenser temperatures

Thus, under high generator and evaporator temperature and low condenser temperature the cycle will have higher COP and cooling capacity.

In Figures 4.3 to 4.5 a three curves which represents the study results, Carnot cycle performance and the previous study COP done by sun [14] are demonstrated. as shown in the results the previous study COP and the study COP are almost identical at the same conditions and parameters. Carnot cycle performance was also calculated at the same temperature limits, as shown in the figures above, the results of this study are consistent with the concepts of the thermodynamics principle as the temperature limits are changed.

#### 4.2.2.4 VJRC characteristic curves and tables

In the proposed system the generator temperature is assumed to be variable due to the ambient temperature and the solar radiation variations. Also the condenser temperature is variable according to the ambient temperature, but the evaporator temperature was selected as affixed

value according to the desired room air temperature, the selected evaporator temperature was 10 °C to make suitable temperature difference of 12 °C between the evaporator and the room air temperature, where the room temperature was set to be 22°C . The 12 °C was chosen to accommodate the two heat exchangers in the cold side (one from the refrigerant to the circulated water and the second from the circulated water to the room air).

The characteristic curves for the cycle at the selected evaporator temperature 10°C are shown in figure 4.6 where the generator temperature changed from 80°C to 150°C and the condenser temperature changed from 25°C to 50°C.

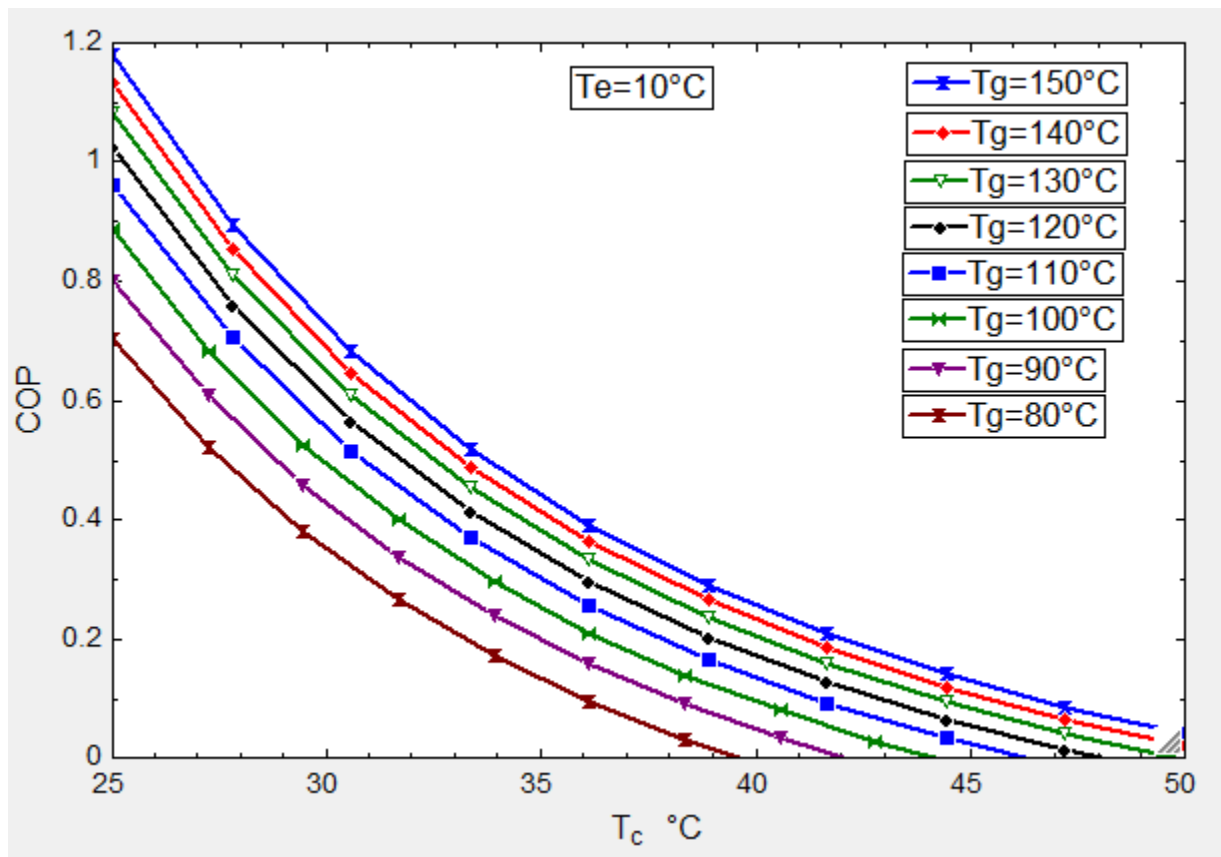


Figure 4. 6: Characteristic curves for VJRC at 10°C evaporator temperature

Characteristic tables for the cycle were created as an excel sheet table to be implemented in the TRNSYS software, where the generator and condenser temperature were varied with step of 1°C and 0.5 °C respectively, as show in appendix A1.

## **4.3 Building cooling load simulation and results**

### **4.3.1 Building cooling load simulation**

The major objective for this section is to simulate the thermal cooling load for the two locations in both Hebron and Jericho cities based the architecture and construction of the TMH.

TRNSYS software is a complete and wide simulation environment for the transient systems simulation. TRNSYS software is used by engineers and researchers around the world to validate the energy concepts especially that related by the thermal energy systems and renewable energy systems and also handle with the thermal behavior of the buildings such as cooling and heating load. TRNSYS consists of a suite of sub programs, in this study, only two of these programs have been used: TRNSYS simulation studio and Building input data visual interface (TRNBuild.exe), where TRNSYS Simulation Studio is the main visual interface. Where the users can create projects by drag-and-dropping components to the workspace, connecting them together and setting the global simulation parameters. The simulation Studio also includes an output manager from where controlling any variable are integrated, printed and/or plotted. TRNBuild is a tool used to enter input data for multizone buildings. It allows the designer to specify all the building structure details, as well as everything that is needed to simulate the thermal behavior of the building, such as windows and wall properties, infiltration and ventilation, etc.[34]

As the TRNBuild view the heat gain into the building comes from both convective heat flow to the air node and radiative heat flow to the walls and windows as shown in figure 4.7. Where the convection heat transfer comes from infiltration, ventilation, gains due to the convectonal air flow from zones, internal surface gains and internal heat gains from people, equipment, illumination, radiators, etc. while the radiation heat transfer comes from internal gains received by walls, long wave radiation exchange between this wall and all other walls and windows and solar gains through zone windows and walls. The Convective and radiative heat balance around the building are shown in Equations 4.1and 4.2 [35]

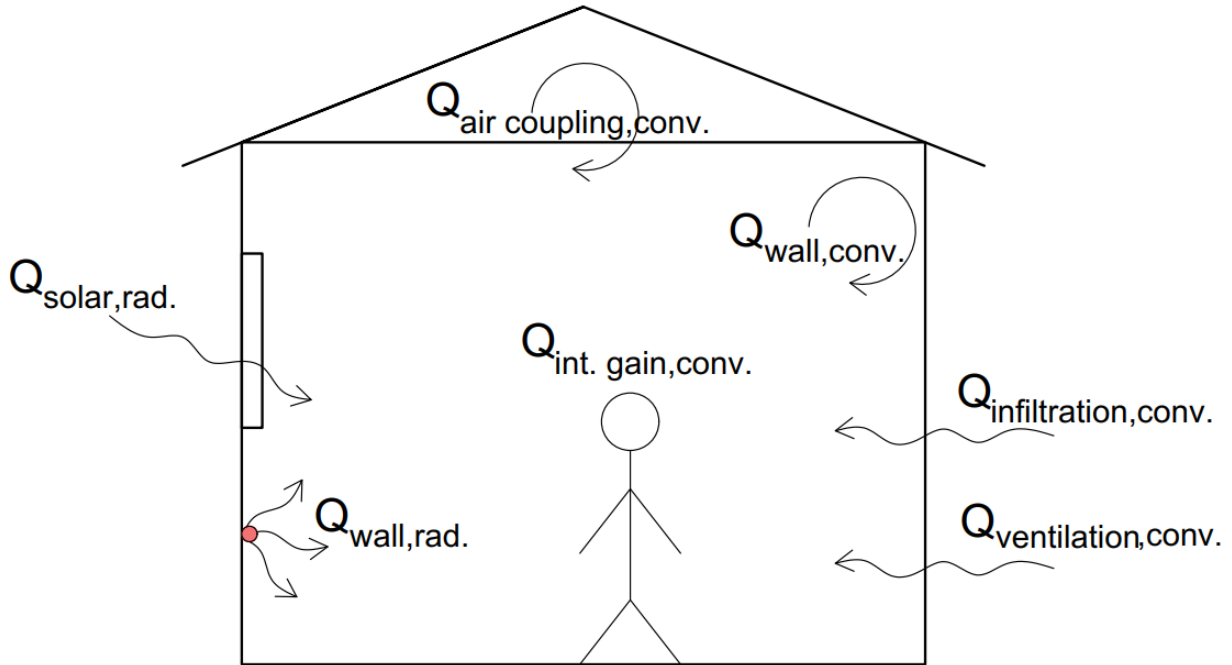


Figure 4. 7: Heat Balance on the Cooling Zone

Convective heat flow to the zone air node  $Q_{conv}$ :

$$Q_{conv} = Q_{surf} + Q_{inf} + Q_{vent} + Q_{gain} + Q_{coup} \dots\dots\dots 4.1$$

Where

$Q_{surf}$  : the internal surface gain.

$Q_{inf}$  : the infiltration gains.

$Q_{vent}$  : the ventilation gains.

$Q_{gain}$  : the internal convective gains (by people, equipment, illumination, radiators, etc.).

$Q_{coup}$  : the gains due to the convectonal air flow from zones.

Radiative heat flow to the walls and windows  $Q_{r,wi}$  :

$$Q_{r,wi} = Q_{g,r,i,wi} + Q_{sol,wi} + Q_{long,wi} \dots\dots\dots 4.2$$

Where

$Q_{g,r,i,wi}$  : the radiative zone internal gains received by walls.

$Q_{sol,wi}$  :the solar gains through zone windows and walls.

$Q_{long,wi}$  : the long wave radiation exchange between this wall and all other walls and windows.

The building model demonstrates the hourly variation of cooling load over the study period. The model is created in TRNBuild (figure 4.8 shows the TRNBuild main window) where the building parameters (constructions, materials, internal heat gain, ventilation, infiltration and cooling set point) as discussed in chapter three.

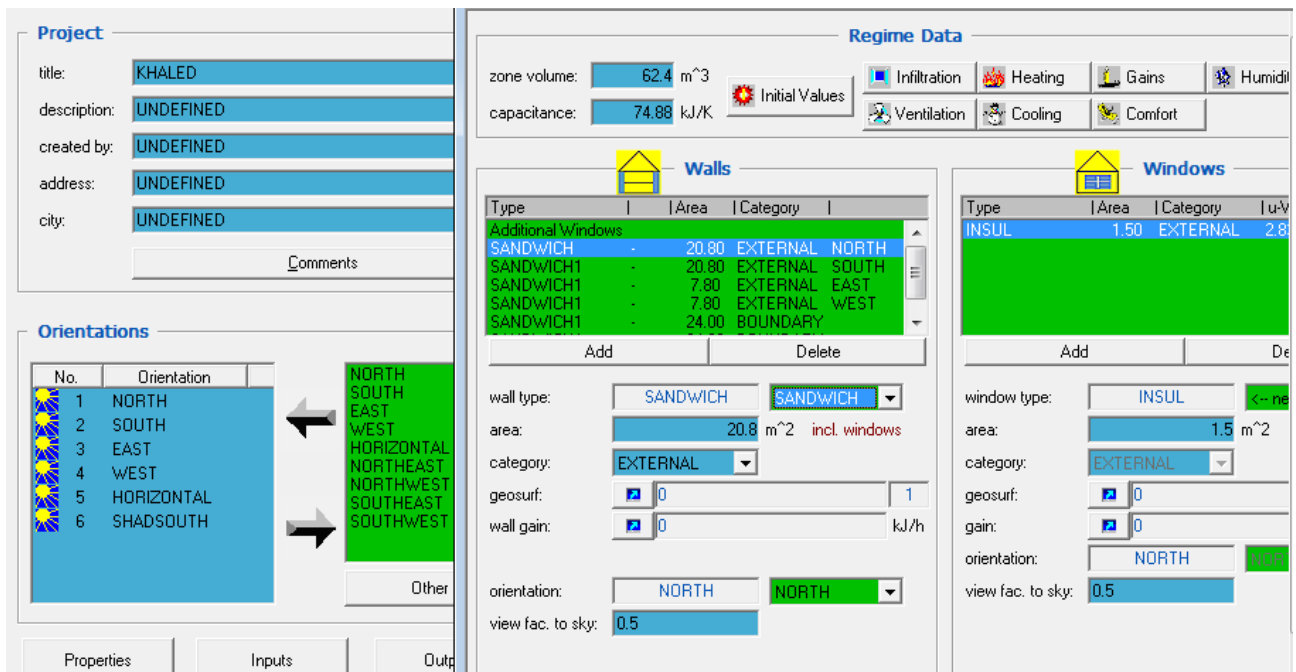


Figure 4. 8: TRNBuild main window

Then the generated TRNBuild model is executed to TRNSYS simulation Studio as an input files by type 56 (multi-zone building).Figure 4.9 shows the components of the simulation Studio window, where it consists from the inputs and outputs that is described in table 4.1 shortly.

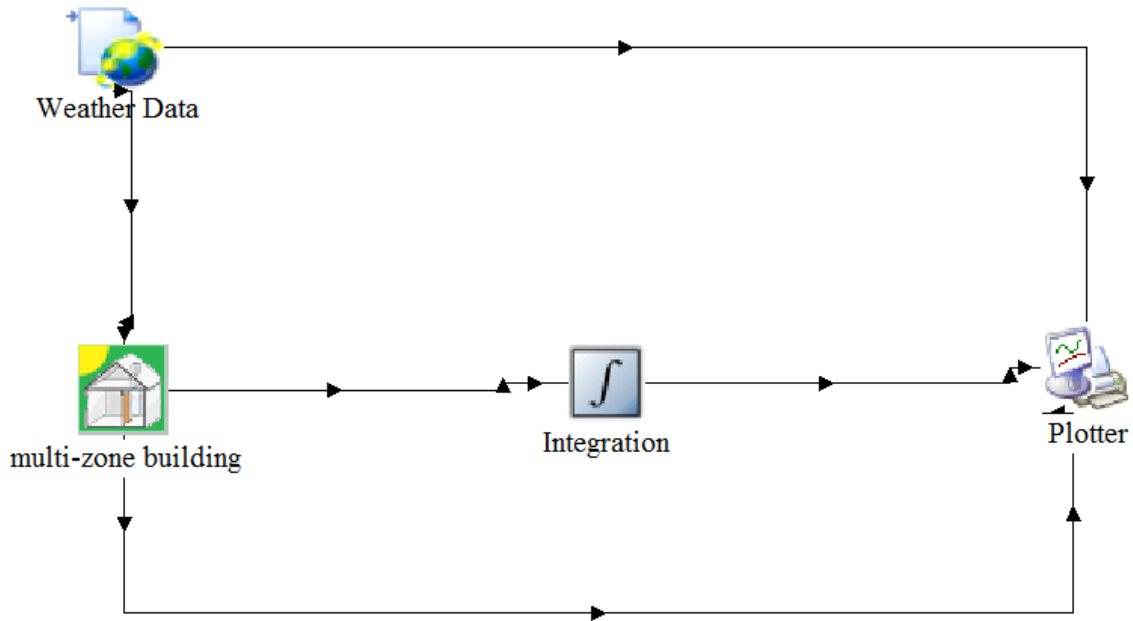


Figure 4. 9: Simulation Studio window components for building cooling load

Table 4. 2: Components of simulation Studio window and descriptions

Components	Descriptions[36]
Whether data (type15-3)	This component serves the purpose of reading data at regular time intervals from an external weather data file.
Multi-zone building (type 56)	This component models the thermal behavior of a building having up to 25 thermal zones.
Plotter (type 65a)	The online graphics component is used to display selected system variables while the simulation is progressing.
Integration (type24)	This component integrates a series of quantities over a period of time.



### 4.3.2 Building cooling load results

The cooling load demand for the TMH was hourly simulated over the study period as shown in figure 4.9 .The cooling load is synchronized with climate temperature and solar radiation where the maximum cooling load is occurring at the noon time when the solar radiation and temperature are maximum. Figure 4.10 shows the distribution of the insulations and the ambient temperatures for five days (1 to 5 July) in Hebron and Jericho cites. It can be noticed that solar insolation for the two cities is almost the same but the main difference between Jericho city and Hebron city is the ambient temperature, where there is a difference of 5-10 °C in Jericho city more than Hebron city. While figure 4.11 shows the hourly cooling load demand in this period.it can be noticed that cooling load curves for both cities follow the ambient temperature curves with a great similarity, also Hebron city has less cooling load than Jericho. This is due to the lower ambient temperatures of Hebron city. Figure 4.12 shows the monthly mean cooling energy demand and figure 4.13 shows the total seasonal cooling energy demand for Hebron and Jericho cites, in figure 4.12 and 4.13 it is clear that the monthly and seasonal cooling energy demand in Hebron city is much lower than its equivalent in Jericho city, where the total seasonal cooling energy demands in Hebron and Jericho cities 5749 kWh/year and 14864 kWh/year respectively.

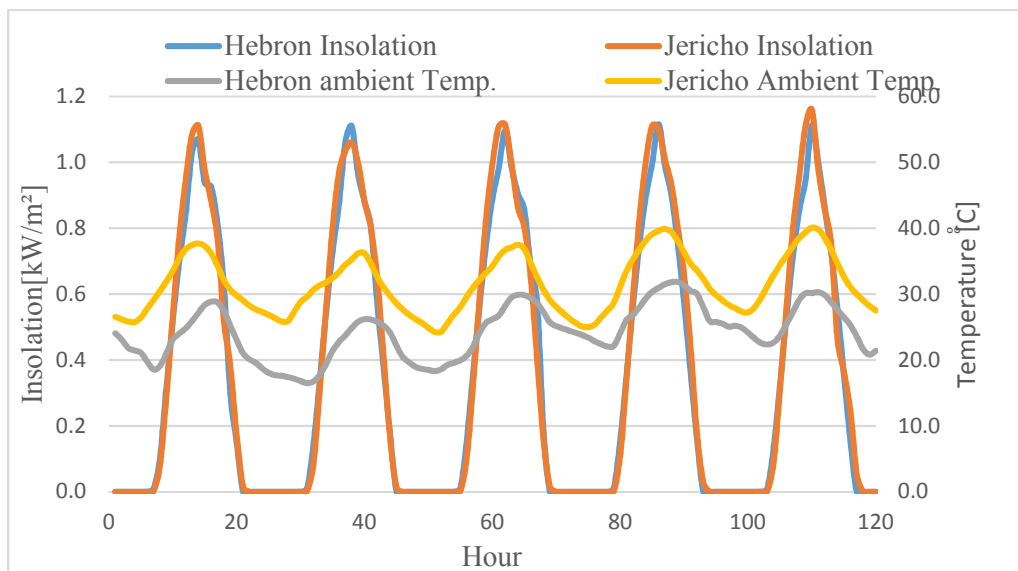


Figure 4. 10: Distribution of the insolation and ambient temperatures for five days (1 to 5 July) in Hebron and Jericho cites

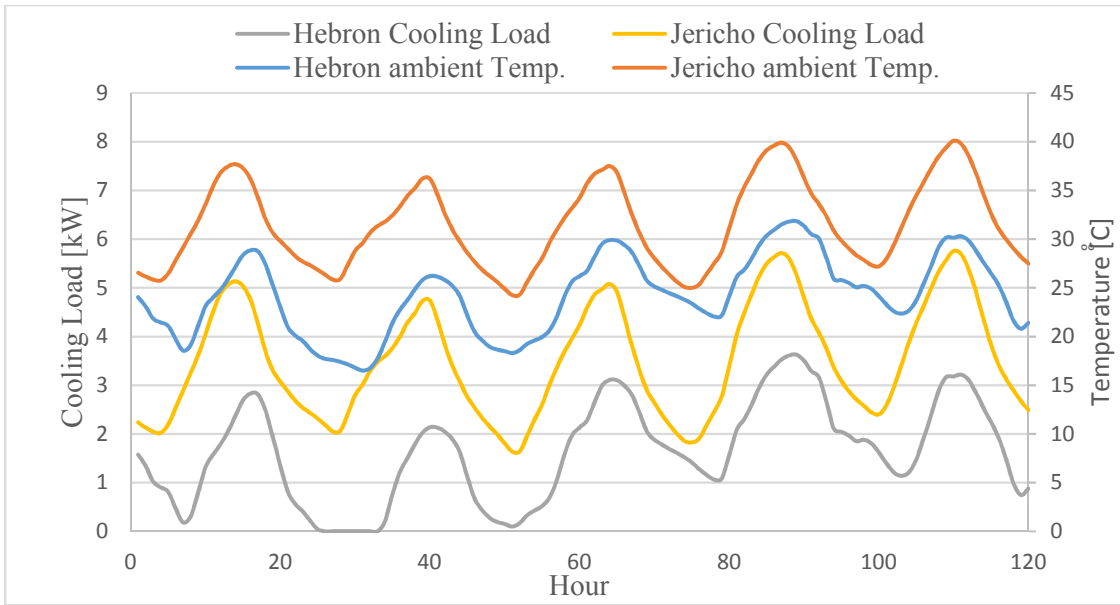


Figure 4. 11: Cooling load demand and ambient temperature for five days (1 to 5 July) in Hebron and Jericho cites

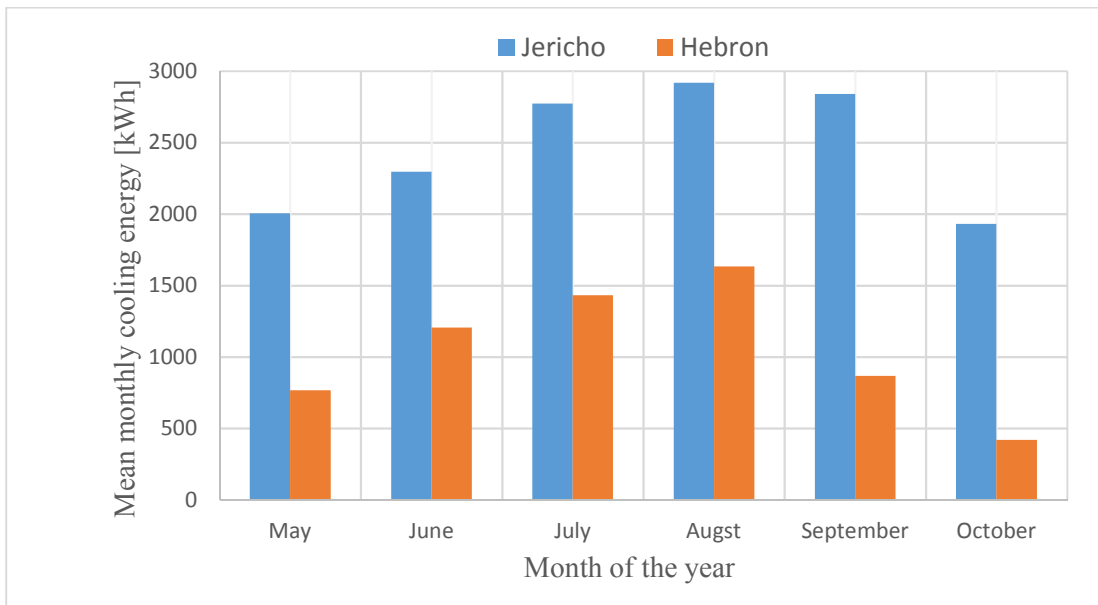


Figure 4. 12: Monthly mean cooling energy demand for study period for Hebron and Jericho cites

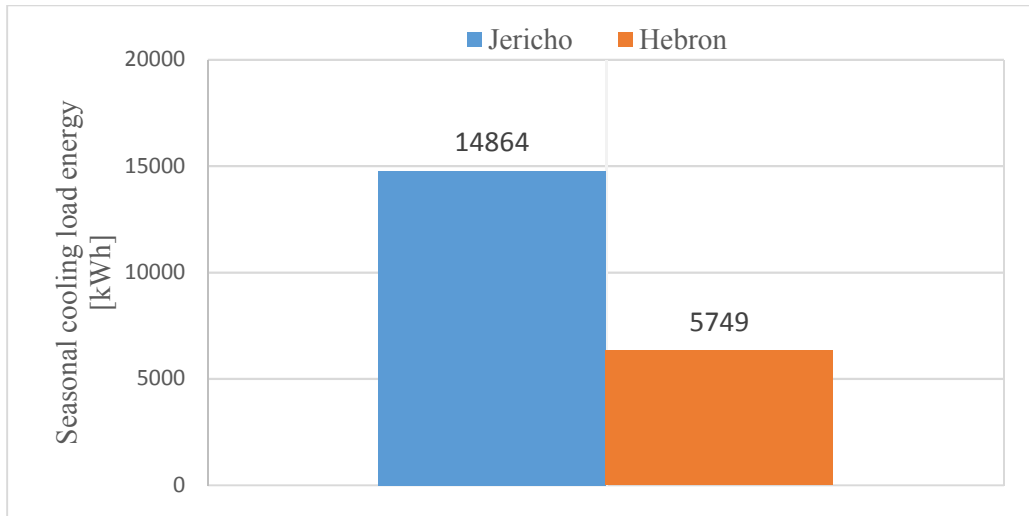


Figure 4. 13: Total seasonal cooling energy demand for Hebron and Jericho cites

From figures 4.10 to 4.13 it can be concluded that the cooling energy demand for Jericho city is much more than for Hebron city and this is because the climate in Jericho city is hotter than Hebron city.

#### 4.4 Collector tilt angle estimation

The collectors are responsible for the conversion of incident solar radiation energy into thermal energy that is later useful in the running of the VJRC to produce chilled water that is used in cooling the house. Therefore, the solar thermal collection components of the solar cooling system are such an important part that their performance must be optimized for a better performance of the whole system. One of the key parameters that can be easily changed to optimize the collector performance is the collector tilt angle. Where the tilt angle depends greatly on the collector location on the earth (latitude) and the time of the year.

Excel sheet calculations were carried out to predict the optimum tilt angles for a south facing surface for the study period, the calculations were made according to the clear sky Direct-Beam Radiation theory [24]. Where the optimum tilt was determined based on the maximum amount of total incident solar radiation for the study period, figure 4.14 shows the average daily mean insolation per month at different tilt angles for Hebron city where there is an optimum tilt angle every month according to the chart in figure 4.14. Figure 4.15 shows the total amount of insolation at different tilt angles for both Hebron and Jericho cities.

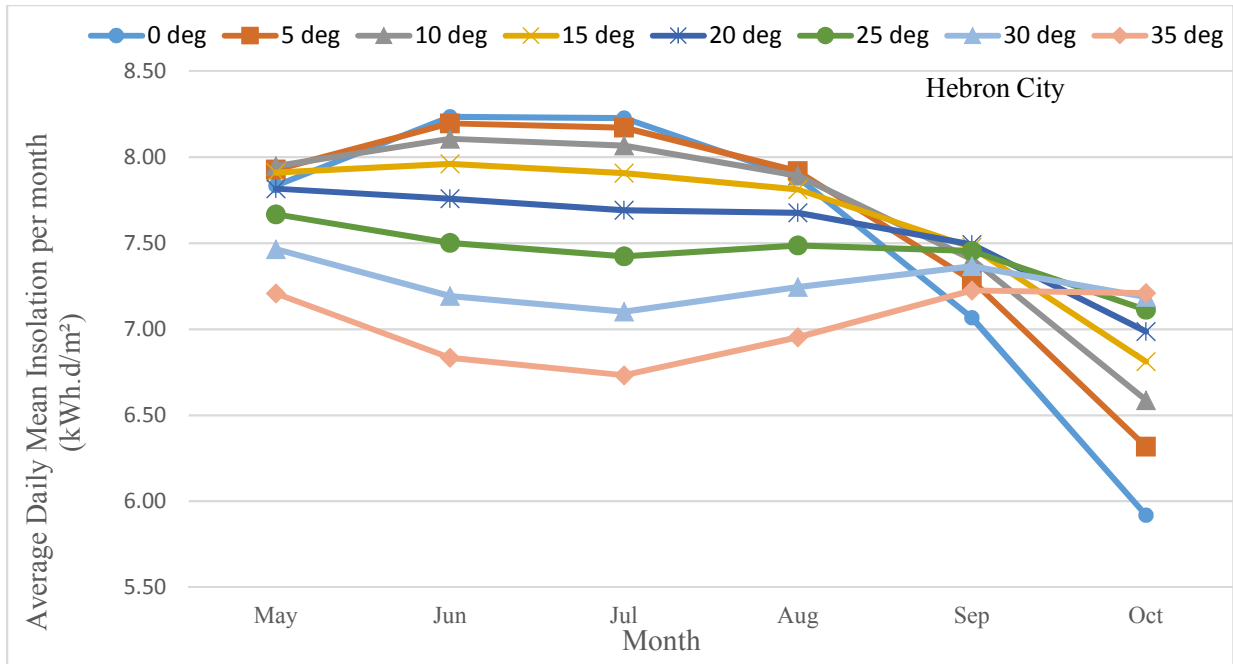


Figure 4. 14: Average daily mean insolation per month at different tilt angles for Hebron city

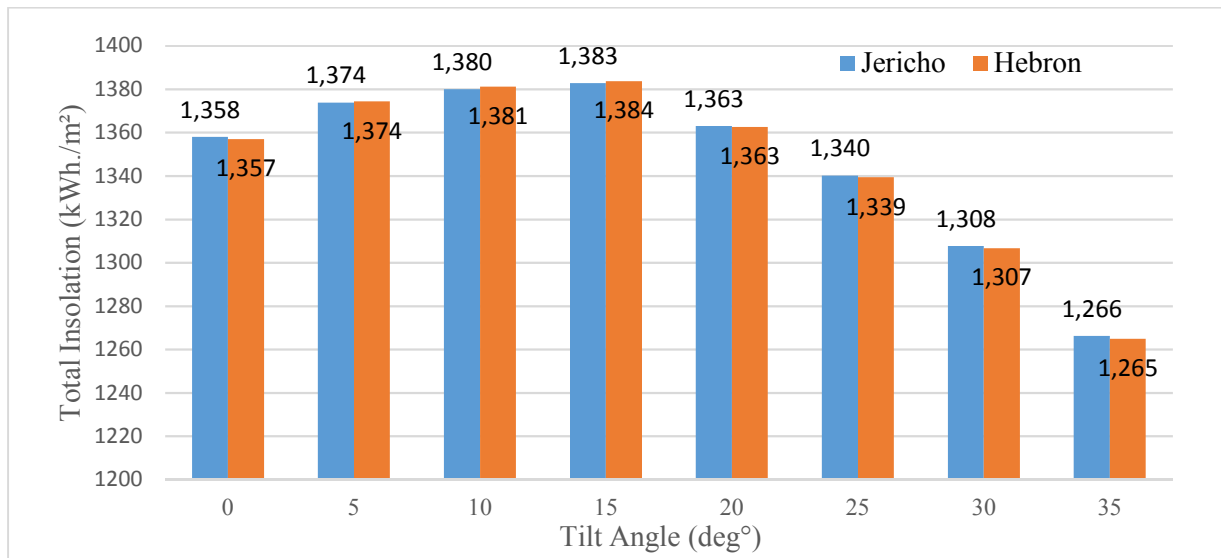


Figure 4. 15: Total amount of insolation at different tilt angles during the study period

After comparison, the total insolation at different tilt angles during the study period, it was concluded the maximum incident insolation during the study period is 1384 and 1383 kWh/m<sup>2</sup> in Hebron and Jericho cities respectively. Also, these values occurred at 15° deg for both, so the 15° deg solar collector tilt angle was selected in this study as a fixed value.

## 4.5 Overall system simulation and results

### 4.5.1 Overall system simulation

The overall TRNSYS simulation project illustrated in Figure 4.16 consists from VJRC subsystem, building cooling load subsystem and solar thermal subsystem. The VJRC subsystem was simulated previously on the EES software and the characteristic tables for the cycle were created into an Excel sheet at the evaporator temperature 10°C and the generator temperature between 80 °C to 150 °C with 1°C step and the condenser temperature between 25 °C to 50 °C with 0.5°C step as show in appendix A1. Building cooling load subsystem was also simulated previously using the TRNBuild tool in the TRNSYS software. The overall simulation project contain the solar thermal subsystem which was simulated in the TRNSYS simulation Studio with VJRC subsystem and building cooling load subsystem as shown in figure 4.16. Table 4.2 shows the inputs and outputs of the overall system and short descriptions of its elements as TRNSYS Library.

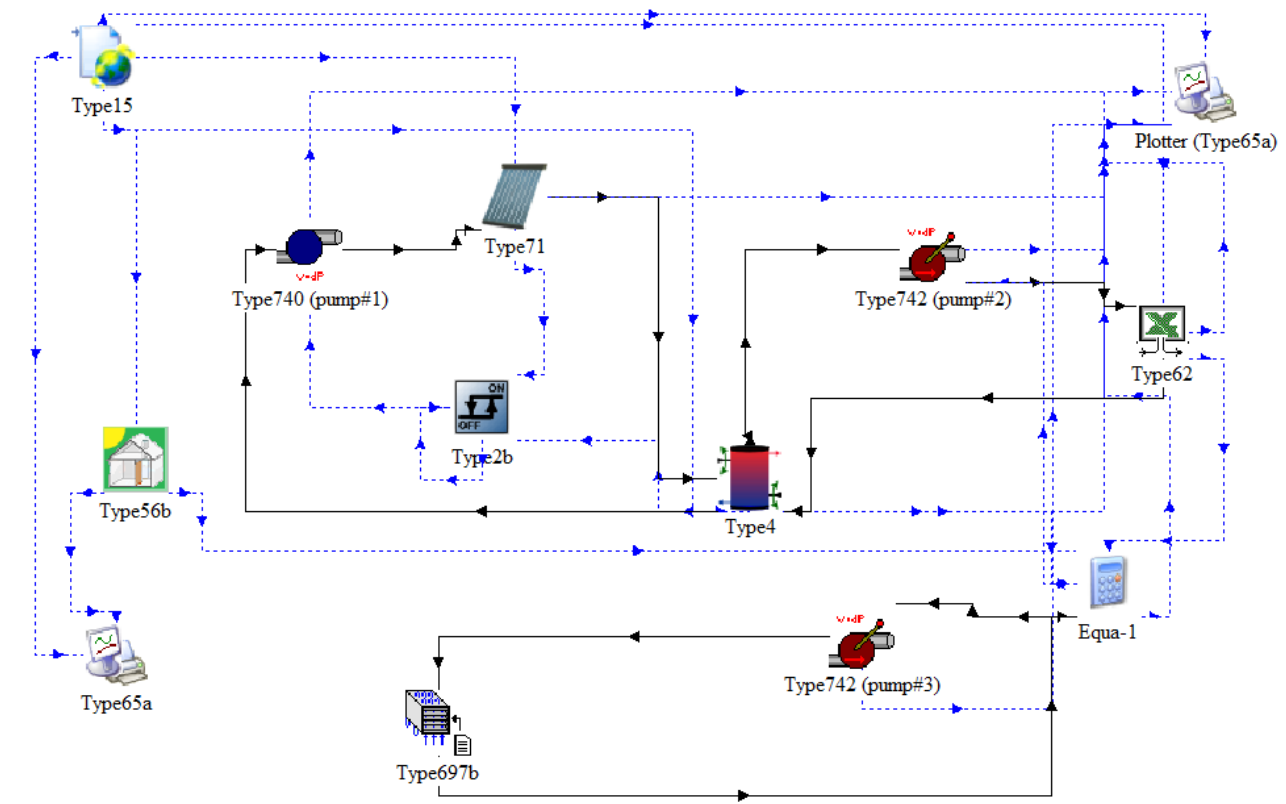


Figure 4. 16: Simulation Studio window components for overall system

Table 4. 3Components of simulation Studio window and descriptions

Components	Descriptions[36]
Whether data (type15-3)	This component serves the purpose of reading data at regular time intervals from an external weather data file.
Multi-zone building (type 56)	This component models the thermal behavior of a building having up to 25 thermal zones.
Plotter (type 65a)	The online graphics component is used to display selected system variables while the simulation is progressing
Solar Collector; Evacuated Tube (type71)	Models a single phase evacuated tube solar collector.
Storage Tank (Type4)	Models a hot storage tank.
Variable speed pump (Type742)	Models a pump that sets its fluid outlet mass flow rate equal to the user specified inlet mass flow rate.
Single speed pump (Type740)	Models a single (constant) speed pump that is able to maintain a constant fluid outlet mass flow rate.
TRNSYS / Excel Coupling (Type62)	This TRNSYS Type implements a link with Excel.
ON/OFF Differential Controller (Type2)	Generates a control function which can have a value of 1 or 0.
Cooling Coil (Type697)	Models a cooling coil where the air is cooled as it passes across a coil containing a cooler fluid (typically water).

For the TRNSYS simulation project illustrated in Figure 4.16 the black solid lines show the flow of system information, and the blue dotted lines show the flow of weather data Information, flow of control information and the flow of the output information from the simulation.

The ETC converts the incident solar radiation energy into thermal energy using heat transfer fluid (HTF) that it stores this energy in a hot storage tank at maximum temperature of 160 °C. A circulation pump (pump#1) was used to circulate the HTF between the collectors and the storage tank, the hot HTF stored in the tank, then flow due to a another variable speed circulating pump (pump#2) to the VJRC generator in the TRNSYS / Excel Coupling (Type 62) to deliver the heat to the refrigeration cycle and produce a specific amount of cooling load to cover the cooling load demand in the TMH.

In the system the setting of ETC tilt angle is 15 deg as recommended in section 4.4, and the Parameters of the ETC as shown and mentioned in table 2.2 from the manufacture ( $\eta_0 = 80\%$ ,  $a_1 = 1.5 [W/(K \cdot m^2)]$ ,  $a_2 = 0.005 [W/(K^2 \cdot m^2)]$ ), and the ambient temperature and solar radiation were delivered hourly from the weather data file to the collectors. The THERMINOL 66 HTF was

selected to deliver the heat from the collector to the storage tank where the operating temperature for the HTF is from 0 °C to 349 °C at atmospheric pressure and the average specific heat of 1.9 kJ/kg.K at 120 °C. The pump#1 flow rate was set as constant value at 0.02 kg/m<sup>2</sup> as recommended [37] and it operates according to the digital controller. The digital controller switches the pump on when the collector outlet temperature is more than the storage tank temperature by 2 °C, and switches the pump off when the collector outlet temperature and the storage tank temperature become less than 2 °C, or when the storage tank temperature is reach to the maximum desired temperature 160°C .The hot storage tank walls were assumed to be carbon steel with thickness of 2mm and thermal conductivity of 60 W/m°C. Insolated with 10cm polyurethane with thermal conductivity of 0.03 W/m°C. When the HTF temperature in the storage tank reaches 90 °C or more the pump#2 turn on pumping the HTF to the VJRC generator in TRNSYS / Excel Coupling to deliver the heat to the VJRC, then the HTF return to the tank again when their temperature is decreased by 5°C, noted that the temperature difference between the HTF and the refrigerant in the VJRC is 5°C. Also the excel sheet receives the ambient temperature from the weather data where the condenser temperature of the VJRC is above the ambient temperature by 5°C where air cooled condenser was suggested .According to the generator and condenser temperature that received in the excel sheet the performance of the VJRC is selected and the generator, condenser and evaporator load are also calculated. According to the cooling load demand from the house the amount of HTF is calculated in element “equation1” in the TRNSYS Studio window, where this element includes the needed data of the VJRC (generator temperature and COP), the building cooling load demand and all statements and equations to find the suitable amount of the HTF that needed in the cycle. The amount of the HTF that calculated is then sent to the pump#2. Finally the cooling coil delivers the evaporator cooling load in the VJRC to the house unit using another variable speed pump (pump#3) with the water as HTF. Where the temperature of the cooling coil is higher than the evaporator temperature by 5 °C. Noted that all pumps that used in this system are assumed to be worked on external power system grid or another renewable energy source.

## 4.5.2 Overall system results

### 4.5.2.1 Solar thermal subsystem results

As mentioned before the solar thermal subsystem consist of ETC, storage tank and circulation pump. This subsystem cannot operate alone without heat delivered to the VJRC, so only after connecting the systems together one can be obtain the characteristics of the solar thermal subsystem. For the proposed system the ETC outlet temperature, storage tank temperature, ambient temperature, solar insolation, and the pump flow rate are shown in figure 4.17 for the tested sample period (1 to 5 July) in Hebron city using 20 m<sup>2</sup> collector area and 1 m<sup>3</sup> storage tank, As shown in the figure the ETC outlet temperature and the storage tank temperature are greatly correlated and increased with the solar insolation and the ambient temperature increase, the circulation pump works only when the temperature of the ETC outlet temperature is more than the storage tank temperature by 2°C and switched off when the temperature of the storage tank reaches 160°C. Noted that when the circulated pump is switched off, the temperature of the ETC outlet will rise in a high rate. And this is undesirable to avoid evaporation of the HTF at high temperature. To prevent this, solar collector cover was suggested after 300°C.

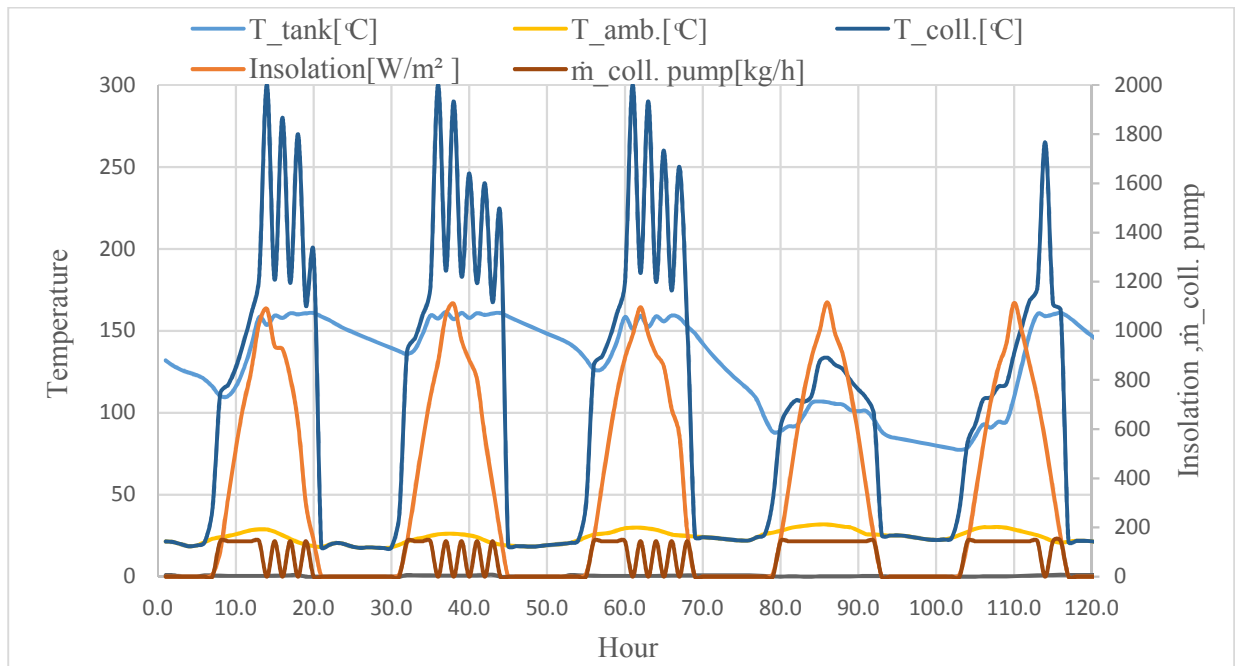


Figure 4. 17: Characteristics of the solar thermal subsystem for the tested sample period (1 to 5 July) in Hebron city using 20 m<sup>2</sup> collector area and 1 m<sup>3</sup> storage tank



#### 4.5.2.2 Overall system performance results

The efficiency of the ETC during the day is highly integrated with the solar insolation and the ambient temperature. The efficiency of the ETC increases up till noon and then decreases as illustrated in figure 4.18 for the tested sample period in Hebron city using 20 m<sup>2</sup> collector area and 1 m<sup>3</sup> storage tank. This relation is with agreement with the Hottel–Whillier–Bliss equation. i.e. the solar insolation increment leads to an increase in the collector efficiency. Figure 4.18 also shows the performance of the VJRC where the performance of the cycle is a variable related to the condenser and generator temperatures as proven and mentioned in section 4.1. The overall system efficiency equals the times of performance of the VJRC and the efficiency of the ETC and also it is a variable every time.

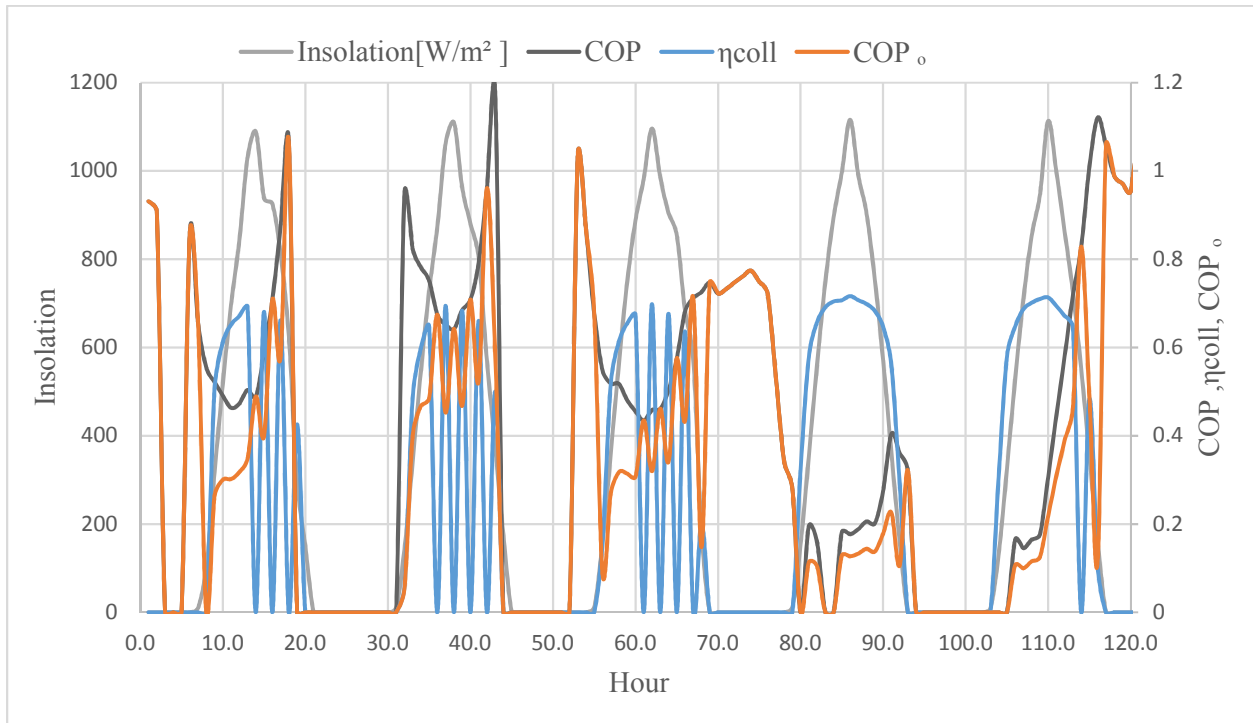


Figure 4. 18: Performance of the VJRC, and ETC efficiency according to the solar insolation for the tested sample period in Hebron city using 20 m<sup>2</sup> collector area and 1 m<sup>3</sup> storage tank

#### 4.5.2.2 Evaporator cooling load results

Figure 4.19 Shows the instantaneous cooling load demand and the available evaporator cooling load at the VJRC for the sample tested in Hebron city using 20 m<sup>2</sup> collector area and 1 m<sup>3</sup>

storage tank, it's clear from the figure that for most of the time the evaporator cooling load can cover the cooling load demand in the house unit, but in some cases when the temperature of the HTF is less than the threshold temperature of the system the cycle is failing short to cover the required cooling load demand because the cycle is switched off and there is no HTF flows to the generator to operate the refrigeration cycle. The times where the evaporator cooling load cannot cover the house cooling load demand is shown as shaded area in the figure. The cycle is failing short at the extreme conditions which occurs in a few hours per season, such as the hottest days in the season. According to the ASHRAE standards design parameters, the designed conditions can be accepted up to 95% from the extreme conditions [38], and this percentage is variable from designer to another according economic issues and location ...etc, because if one desire 100% of the cooling load demand to be covered one need a large system size which is expensive and not applicable for most applications.

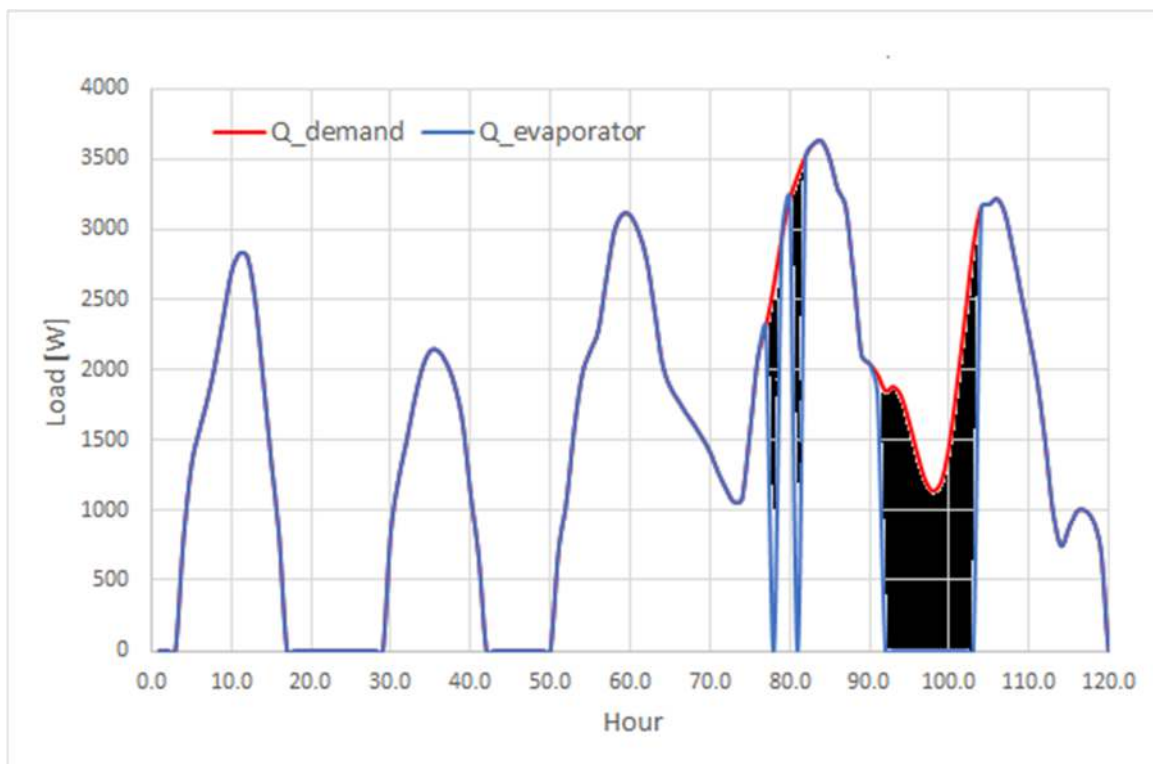


Figure 4. 19: Instantaneous cooling load demand and the evaporator cooling load for the tested sample period in Hebron city using 20 m<sup>2</sup> collector area and 1 m<sup>3</sup> storage tank

During the tested sample period shown in figure 4.19 the cooling energy demand for the house is 190.1 kWh while the evaporator cooling energy is only 163.2kWh which represent 85.8% from the cooling energy demand. So this system size cannot fulfil the human comfort requirements according to the standards during this tested period.

#### **4.5.2.3 Effect of the collector area on the evaporator cooling load and energy**

As rule of thumb the collector areas were chosen 10 m<sup>2</sup> to 60 m<sup>2</sup> with 5 m<sup>2</sup> step and the storage tank volume from 0.5 m<sup>3</sup> to 2 m<sup>3</sup> with 0.5 m<sup>3</sup> step. Figure 4.20 Shows the effect of the collector area on the instantaneous evaporator cooling load for the tested period in Hebron city using 1 m<sup>3</sup> storage tank, it can be noticed that rises the evaporator cooling load increases with the increment of the solar collector area and almost equal the cooling load demand at large areas; the evaporator cooling energy availability increased from 65% to 98.5% when the collector area increased from 10 to 60 m<sup>2</sup>. While Figure 4.21 shows the effect of the collector area on the instantaneous evaporator cooling load for the tested period in Jericho city using 1 m<sup>3</sup> storage tank, it can be notice that the evaporator cooling energy availability increased from 10% to 54.3% when the collector area increased from 10 to 60 m<sup>2</sup>.

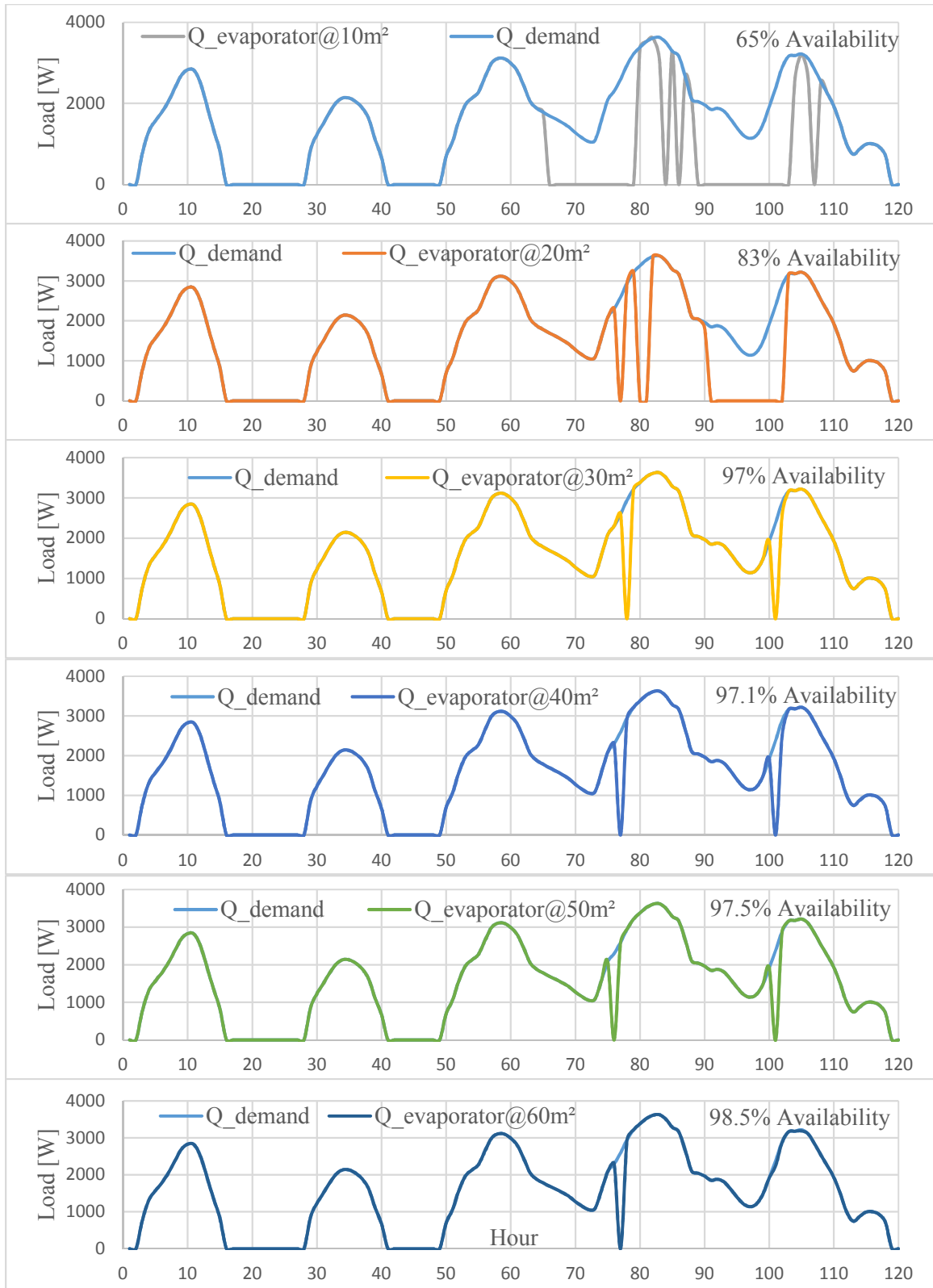


Figure 4. 20: Effect of the collector area on the instantaneous evaporator cooling load for the tested sample period in Hebron city using 1 m<sup>3</sup> storage tank

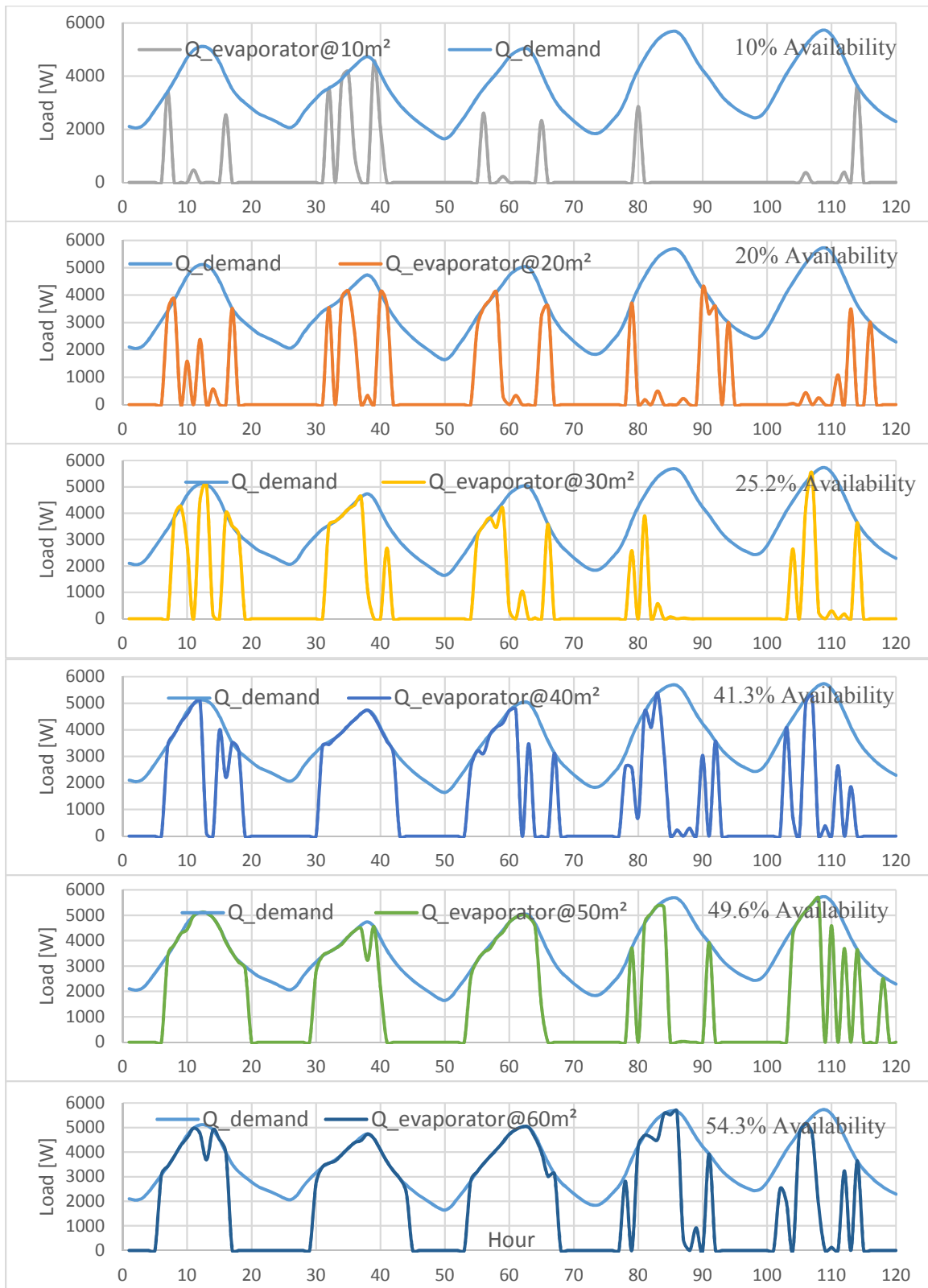


Figure 4.21: Effect of the collector area on the instantaneous evaporator cooling load for the tested sample period in Jericho city using 1 m<sup>3</sup> storage tank

Figure 4.22 Shows the effect of the collector area on the seasonal evaporator cooling energy using 1 m<sup>3</sup> storage tank in Hebron city, the effect of the collector area has a logarithmical effect on the evaporator cooling energy, where the evaporator cooling energy increased at high rate when the collector area was between 10-30 m<sup>2</sup> and increased slowly after 30 m<sup>2</sup>. The maximum evaporator cooling energy available was 5672 kWh at 60 m<sup>2</sup> collector area and representing 98.7% from the cooling energy demand.

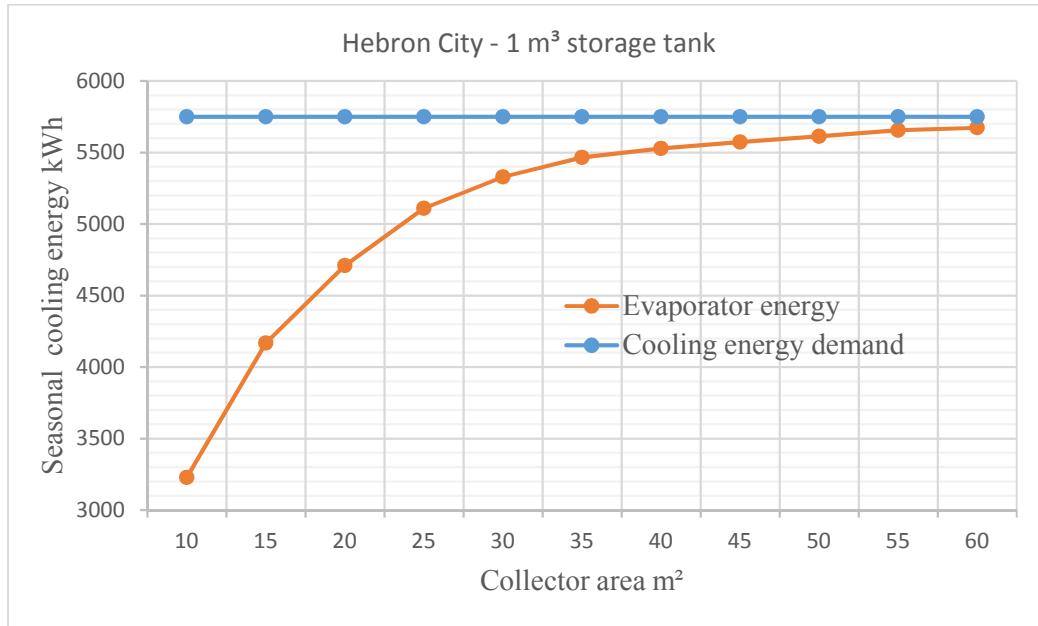


Figure 4. 212: Effect of the collector area on the seasonal evaporator cooling energy using 1 m<sup>3</sup> storage tank in Hebron city

#### 4.5.2.4 Effect of the storage tank volume on the evaporator cooling load and energy

The storage tank volume has a high impact on the system capacity and evaporator cooling load and energy. Figure 4.23 shows the effect of the storage tank volume on the instantaneous evaporator cooling load for the tested sample period in Hebron city using 10 m<sup>2</sup> collector area. The relation between storage tank volume and the evaporator cooling load availability is proportional logarithmic at high collector areas and inversely proportional at low collector area, justification of the decrement in the evaporator cooling load availability with the increasing of the storage tank volume for low collector area because the COP of the VJRC has a high relation

with temperature of the storage tank HTF which is effected by the volume in which the resides in. although at high collector area there is enough supplied by collector to the storage tank to increase the temperature of the HTF in the storage tank. In the same figure the evaporator cooling load decreased with the increasing volume of the storage tank where the evaporator cooling energy availability decreased from 68% at 0.5 m<sup>3</sup> storage tank volume to 43% at 2 m<sup>3</sup> storage tank volume. On the contrary at high collector area the evaporator cooling load increased with the increasing the volume of the storage tank where 35 m<sup>2</sup> collector area the evaporator cooling energy availability increased from 87% at 0.5 m<sup>3</sup> storage tank volume to 100% at 2 m<sup>3</sup> storage tank volume as shown in figure 4.24. For Jericho city figure 4.25 shows the effect of the storage tank volume on the instantaneous evaporator cooling load for the tested sample period in Jericho city using 10 m<sup>2</sup> collector area, it can be notice that the evaporator cooling energy availability changed very little between 9% and 12 % at various storage tank volume. While figure 4.26 shows the increment of evaporator cooling energy availability at high collector area at 100m<sup>2</sup> from 55.4% at 0.5 m<sup>3</sup> storage tank volume to 75.6% at 2 m<sup>3</sup> storage tank volume.

Figures from 4.20 to 4.26 illustrate that the percentage of the evaporator cooling load that produced in Jericho city are much lower than the percentage of the evaporator cooling load that produced in Hebron city, this is because the amount of cooling load in Jericho is much more than in Hebron city also the performance of the VJRC is low when the ambient temperature is high.

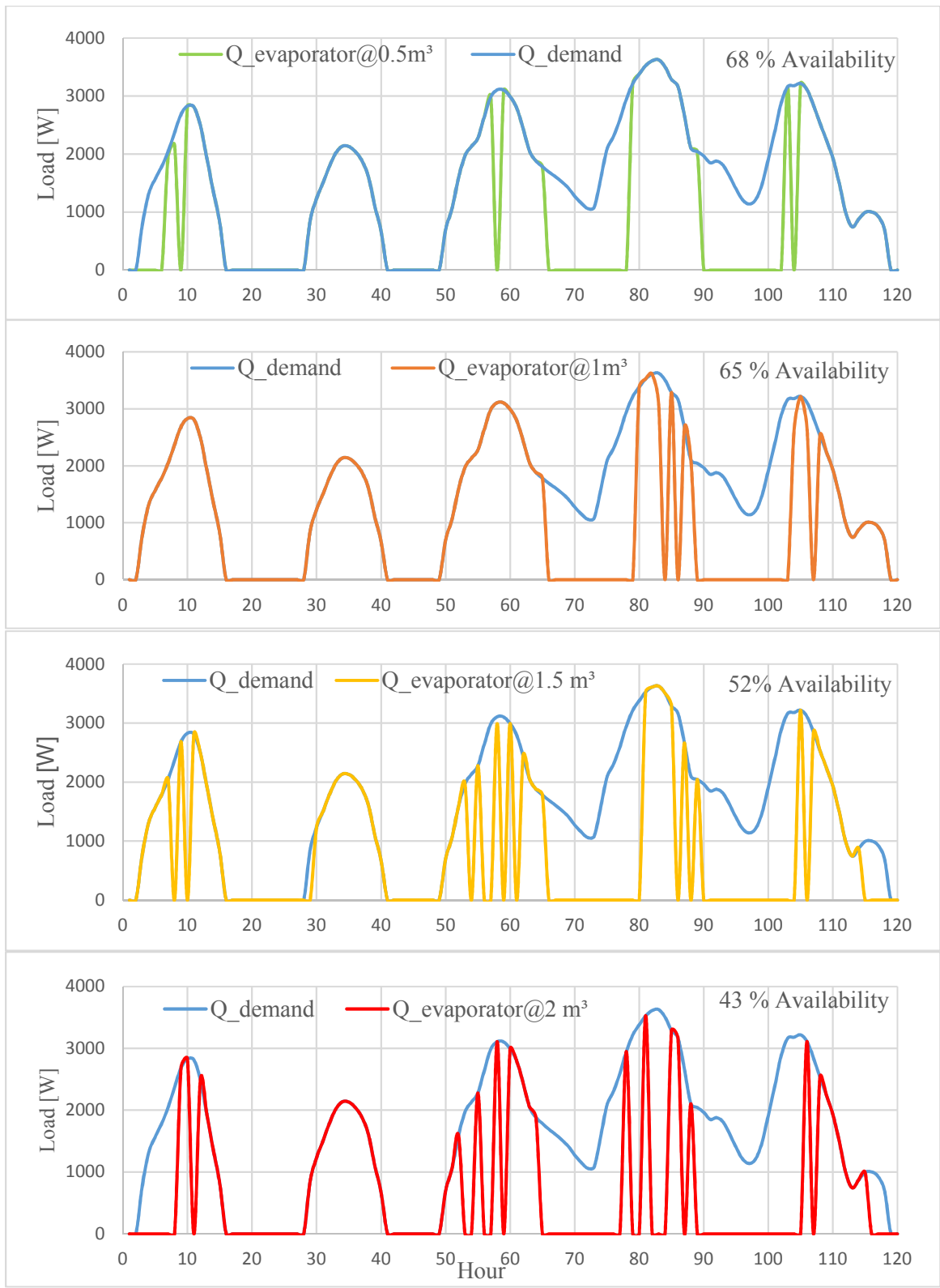


Figure 4.23: Effect of the storage tank on the evaporator cooling load for the tested sample period in Hebron city using 10 m<sup>2</sup> collector area



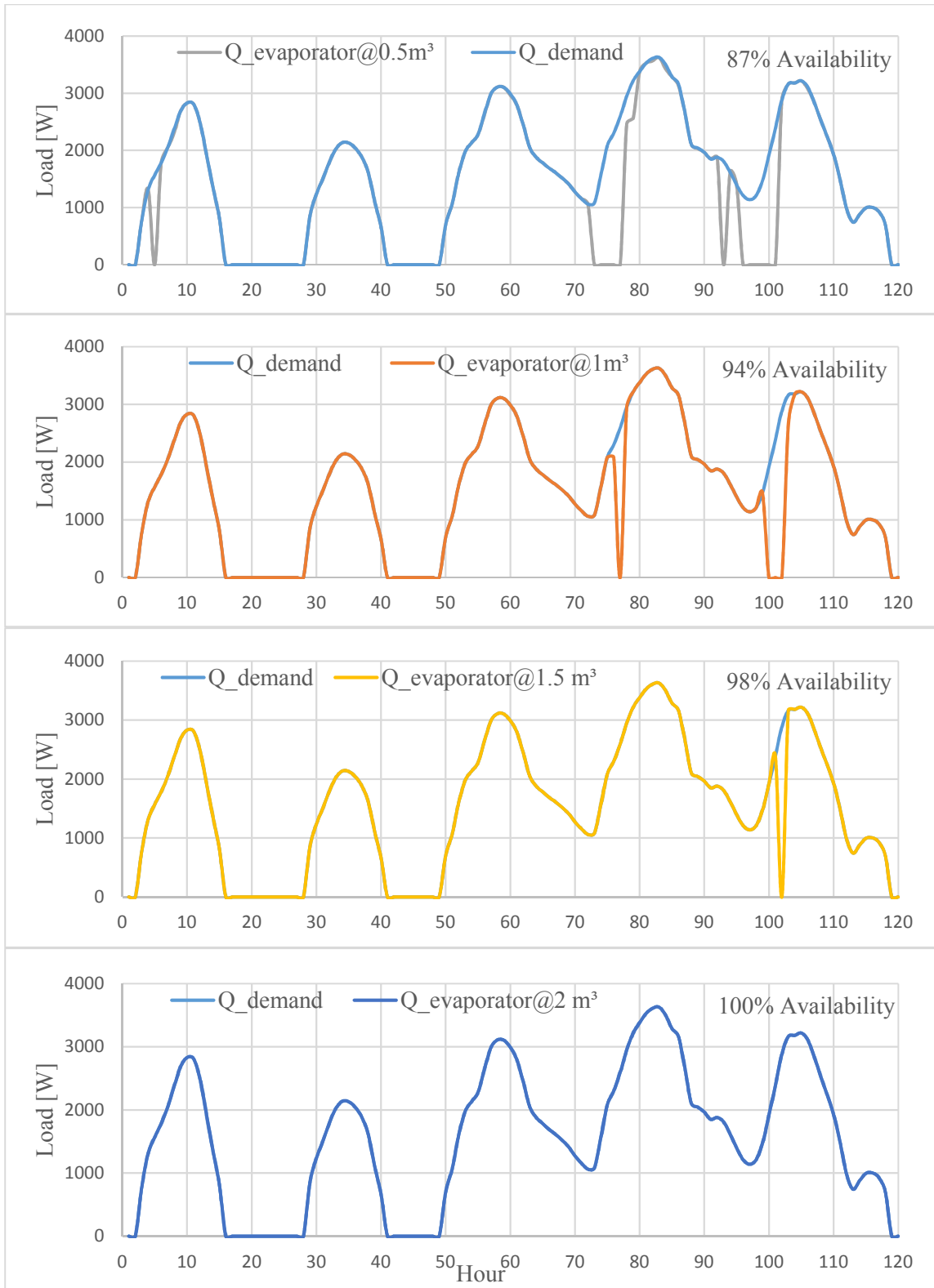


Figure 4.24: Effect of the storage tank on the evaporator cooling load for the tested sample period in Hebron city using 35 m<sup>2</sup> collector area

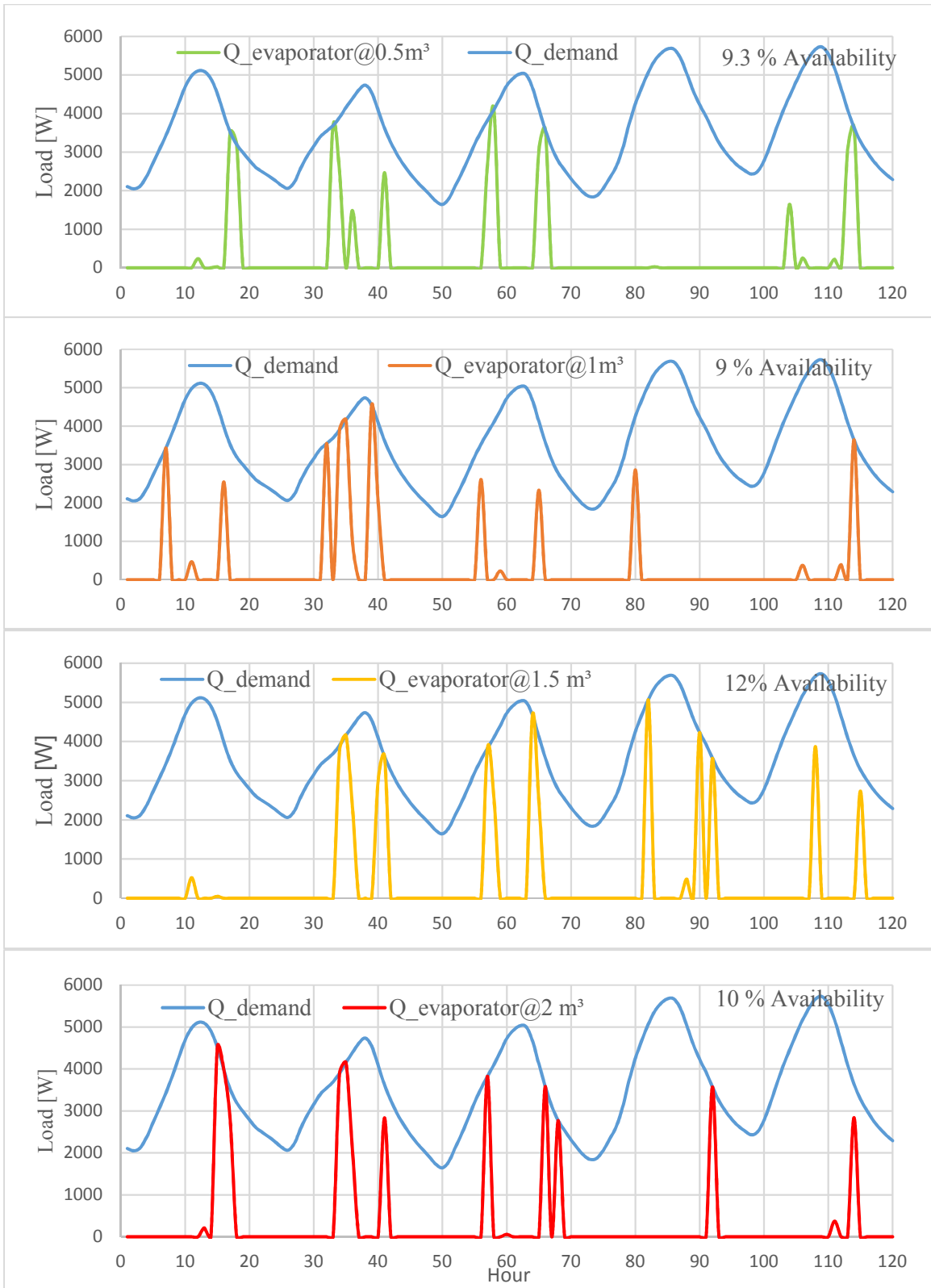


Figure 4.25: Effect of the storage tank on the evaporator cooling load for the tested sample period in Jericho city using 10 m<sup>2</sup> collector area

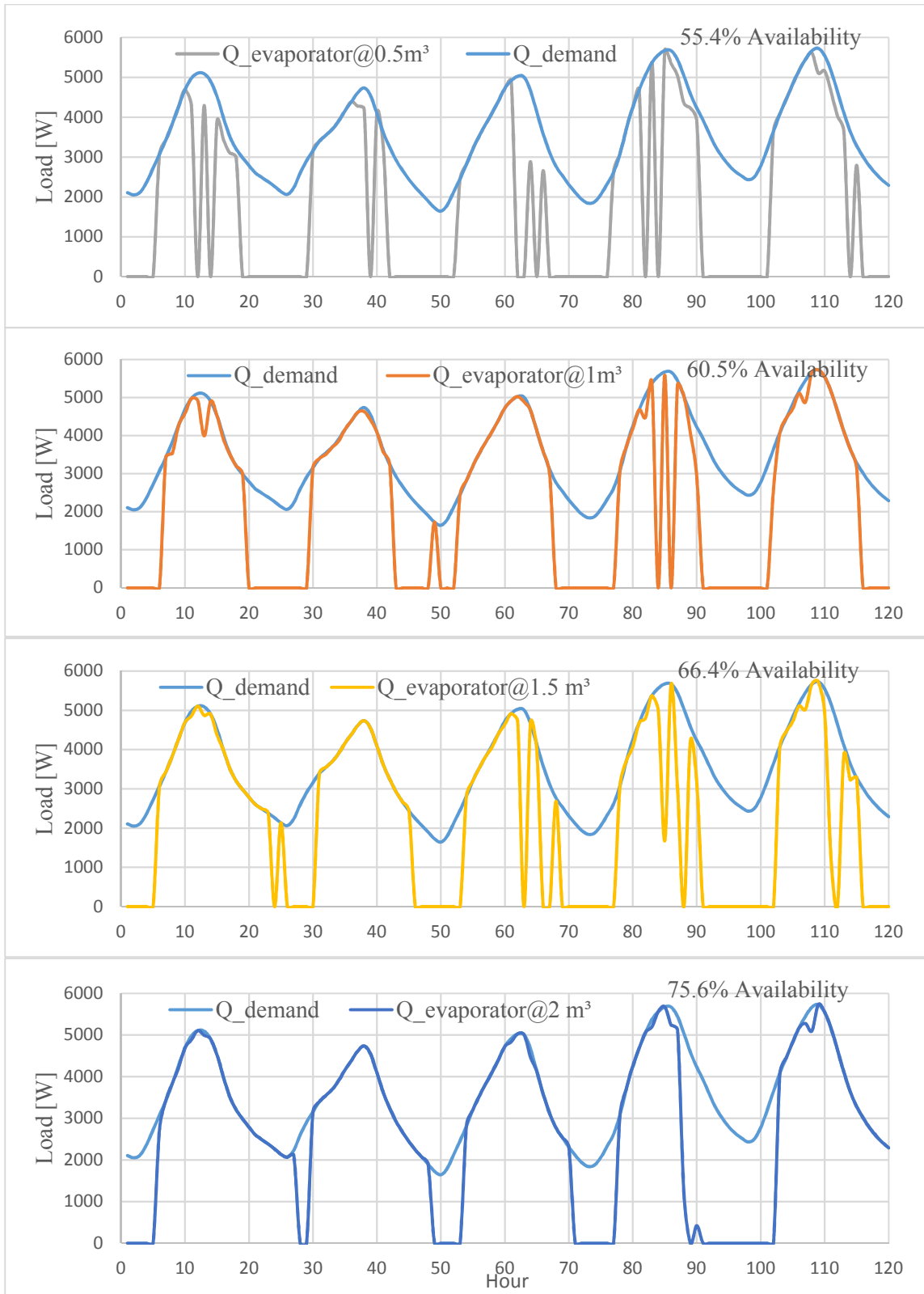


Figure 4.26: Effect of the storage tank on the evaporator cooling load for the tested sample period in Jericho city using 100 m<sup>2</sup> collector area

#### 4.5.2.5 Effect of the collector area and the storage tank volume on the evaporator cooling energy

The optimal values of the collector area and the storage tank volume can be selected according to the suitable evaporator cooling energy availability during the study period, also depends on the philosophy of the designer, economics issues and the related standards. Figure 4.27 shows the seasonal evaporator cooling energy as a percentage from the cooling energy demand for Hebron city at different collector area and storage tank volume.

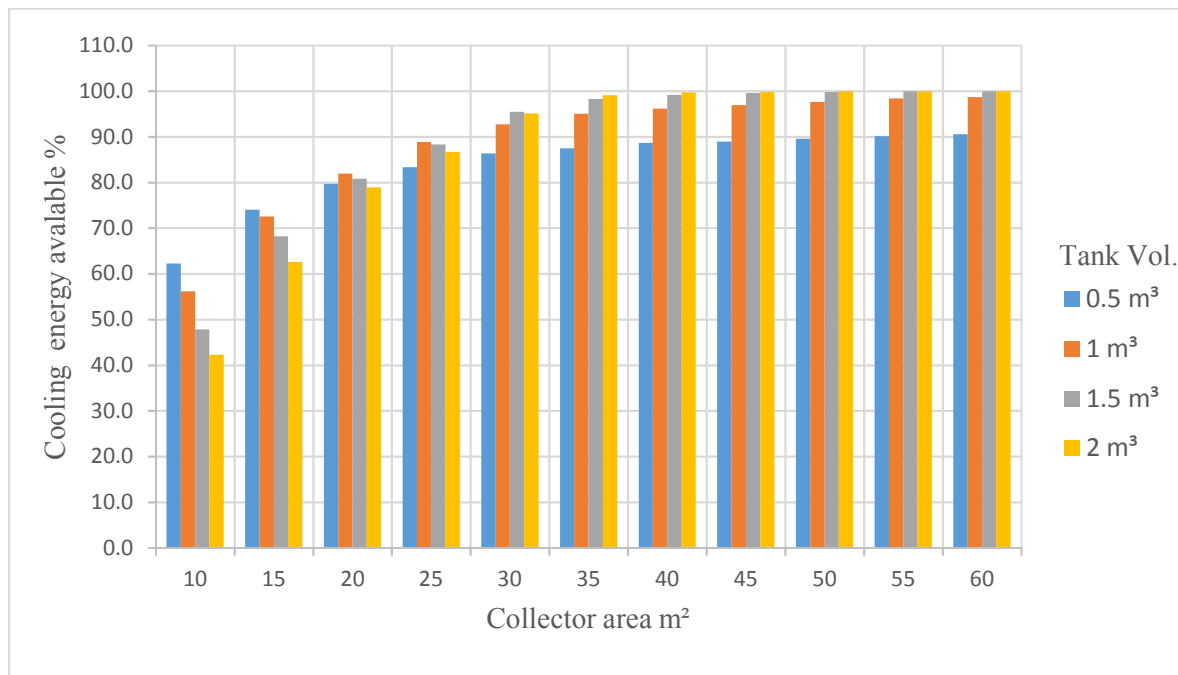


Figure 4. 22: Percentage of seasonal evaporator cooling energy from the cooling energy demand for Hebron city at different collector area and storage tank volume

From the chart there are more than one case can be selected for the system according to the evaporator cooling energy availability which can be classified as follow:

1. Minimum cooling energy availability 95% and above
  - a. 30 m<sup>2</sup> collector area & 1.5m<sup>3</sup> storage tank, the cooling energy available represent is 95.4%.
  - b. 30 m<sup>2</sup> collector area & 2m<sup>3</sup> storage tank, the cooling energy available represent is 95.1%.
  - c. 35 m<sup>2</sup> collector area & 1m<sup>3</sup> storage tank, the cooling energy available represent is 95.1%.
  - d. 35 m<sup>2</sup> collector area & 1.5m<sup>3</sup> storage tank, the cooling energy available represent is 98.2%.
  - e. 35 m<sup>2</sup> collector area & 2m<sup>3</sup> storage tank, the cooling energy available represent is 99.1%.
  - f. 40-60 m<sup>2</sup> collector area with 1, 1.5 and 2 m<sup>3</sup> storage tank.

2. Minimum cooling energy availability 90-95%
  - a. 30 m<sup>2</sup> collector area & 1m<sup>3</sup> storage tank, the cooling energy available represent is 92.7%.
  - b. 50 m<sup>2</sup> collector area & 0.5m<sup>3</sup> storage tank, the cooling energy available represent is 90%.
  
3. Minimum cooling load availability 85-90%
  - a. 25 m<sup>2</sup> collector area & 1m<sup>3</sup> storage tank, the cooling energy available represent is 89%.
  - b. 25 m<sup>2</sup> collector area & 1.5m<sup>3</sup> storage tank, the cooling energy available represent is 88%.
  - c. 25 m<sup>2</sup> collector area & 2m<sup>3</sup> storage tank, the cooling energy available represent is 86.7%.
  - d. 30 m<sup>2</sup> collector area & 0.5m<sup>3</sup> storage tank, the cooling energy available represent is 86.4%.
  - e. 35 m<sup>2</sup> collector area & 0.5m<sup>3</sup> storage tank, the cooling energy available represent is 87.5%.
  - f. 40 m<sup>2</sup> collector area & 0.5m<sup>3</sup> storage tank, the cooling energy available represent is 88.6%.
  - g. 45 m<sup>2</sup> collector area & 0.5m<sup>3</sup> storage tank, the cooling energy available represent is 89%.
  
4. Minimum cooling load availability 80-85%
  - a. 20 m<sup>2</sup> collector area & 1m<sup>3</sup> storage tank, the cooling energy available represent is 82.4%.
  - b. 20 m<sup>2</sup> collector area & 1.5m<sup>3</sup> storage tank, the cooling energy available represent is 81.1%.
  - c. 25 m<sup>2</sup> collector area & 0.5m<sup>3</sup> storage tank, the cooling energy available represent is 82.8%.

The optimal design size for the system is related to the philosophy of the designer, economics issues and the related standards as mentioned above. three cases can be suggested to be the optimal design for the system which satisfy the standards and the human comfort consideration, a high satisfactory percentage of the cooling energy availability (more than 92.7%), which one as following:

Case1: 30 m<sup>2</sup> collector area & 1m<sup>3</sup> storage tank, where the cooling energy available represent is 92.7 %.

Case2: 30 m<sup>2</sup> collector area & 1.5m<sup>3</sup> storage tank, where the cooling energy available represent is 95.4%.

Case3: 35 m<sup>2</sup> collector area & 1m<sup>3</sup> storage tank, where the cooling energy available represent is 95.1%.

As mentioned previously all pumps that used in this system are working on external power system grid or another renewable energy source which represent a small amount of energy consumption, where the total energy needed for the best three options above were simulated during the study period and the results were taken from the TRNSYS program as a summation of hourly power of all pumps during the study period as following:

Case1: For 97.2 % availability, energy consumption is 51 kWh

Case2: For 95.4 % availability, energy consumption is 53.7 kWh

Case3: For 95.1 % availability, energy consumption is 52.5kWh

The same procedures were made for Jericho city where the collector areas were chosen from 10 m<sup>2</sup> to 150 m<sup>2</sup> with 10 m<sup>2</sup> step and the storage tank from 0.5 m<sup>3</sup> to 2 m<sup>3</sup> with 0.5 m<sup>3</sup> step. In Jericho the performance of the system was very low because the condenser temperature in the VJRC is high according figure 4.6, also the cooling energy demand is high as shown in figure4.13, this causes a very high extreme conditions that cannot be satisfied by the evaporator cooling energy produced at these conditions. Figure 4.28 shows the effect of the collector area and the storage tank volume on the seasonal evaporator cooling energy, where the maximum cooling energy available at maximum system size (150m<sup>2</sup> collector area and 2m<sup>3</sup> storage tank volume) reached 72.4 % from the cooling energy demand of the TMH, and this percentage do not satisfy the human comfort according to the standards, also the system is over size and can not to build.

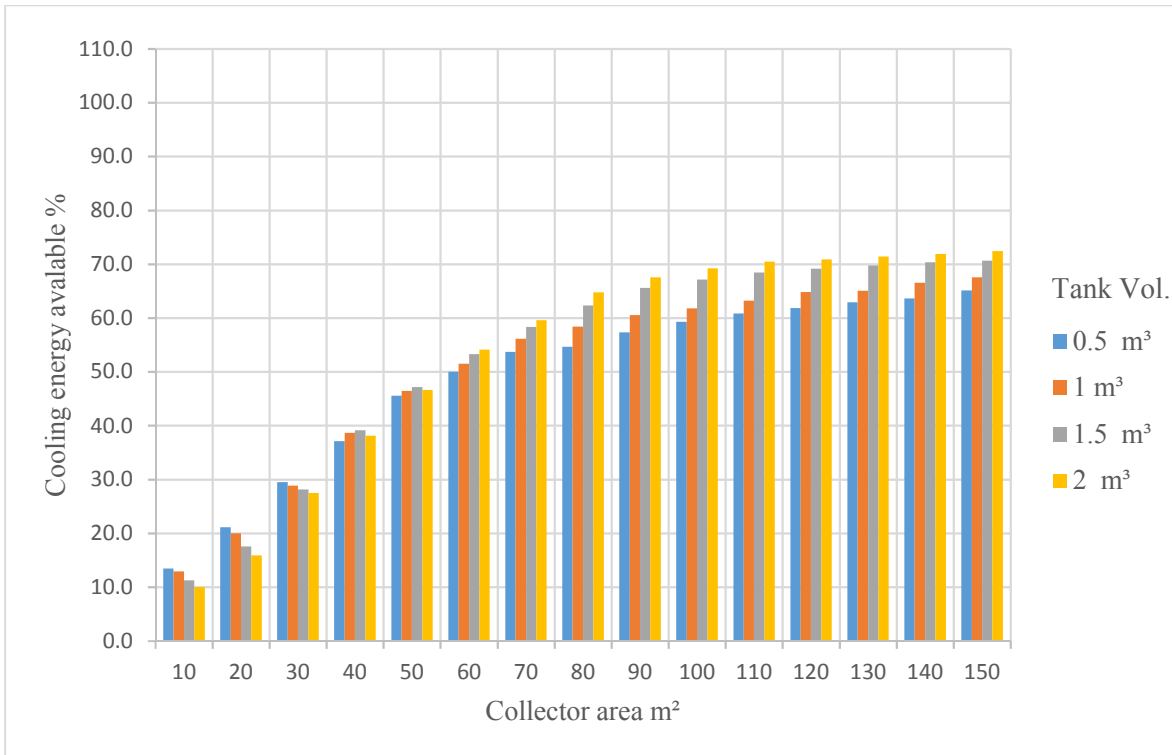


Figure 4. 23: Percentage of seasonal evaporator cooling energy from the cooling energy demand for Jericho city at different collector area and storage tank volume

## CHAPTER 5

### Economical Study

An economic feasibility study was made for two cases of Hebron and Jericho cities at the same system size (30m<sup>2</sup> collector area and 0.5 m<sup>3</sup> storage tank) where the evaporator cooling load availability 87% and 29% in Hebron and Jericho cities respectively. Three methods of economical calculations were made; payback period, net present value and internal rate of return as follow [24].

#### 1. Bayback period method

$$\text{Payback Period} = \frac{\text{Total Capital Cost}}{\text{Total Annual Saving}} \dots\dots\dots 5.1$$

$$\text{Total Capital Cost} = \frac{\text{Total Annual Cost}}{\text{CRF}} \dots\dots\dots 5.2$$

$$\text{Total Annual Cost} = \text{Anuul cost} + \text{Operating \& Maintenance Cost} \dots\dots\dots 5.3$$

$$\text{Anuul cost} = \text{Initial Cost} \times \text{CRF} \dots\dots\dots 5.4$$

Where CRF is the Constant Rate Factor, can be calculated as shown

$$\text{CRF}(5\%, 25 \text{ yr}) = \frac{i(i+1)^n}{(i+1)^n - 1} \dots\dots\dots 5.5$$

Where i is the Loan interest 5% and n is the project life 25 year

To find the total annual saving. The annual electrical energy saving must be calculated, vapor compression refrigeration cycle was assumed to cover the cooling load demand instead of VJRC.

Where the average COP of the vapor compression refrigeration cycle is 3. The annual electrical energy saving for the proposed system can be calculated as:

$$E_{\text{anunual}} = \frac{\text{Evaporator cooling load}}{\text{COP}}$$

The annual saving can be calculated as shown

$$\text{Annual Saving} = E_{\text{Annual}} \times \text{price of kWh} \dots\dots\dots 5.6$$

Where the price of kWh in Palestine is 0.165 \$/kWh

Table 5.1 shows the summary of the payback period calculations, where the operating and maintenance O&M are assumed 5% from the annual cost.



Table 5.1 payback period calculations summary of the three cases

		Hebron city	Jericho city
Initial cost \$	Solar collector	1500	1500
	Storage tank	400	400
	VJRC	500	500
	HTF	500	500
	Installation cost	500	500
	Total equipment cost	3400	3400
CRF /yr		0.071	0.071
Annual Cost \$		241.4	241.4
O&M Cost \$		12.07	12.07
Total Annual Cost \$		253.47	253.47
Total Capital Cost \$		3570	3570
Eannual cooling kWh/yr		5001.63	4310.56
Eannual Electrical		1667.21	1436.853
Annual Saving \$/yr		275.0897	237.0808
Payback period/yr		12.97759	15.05816

From table 5.1 we can notice that the payback period of the proposed system in Hebron city is less than in Jericho city where it is 12.97 year in Hebron while it is 15 year in Jericho. Also must be noticed that the percentage of the evaporator cooling load availability in Hebron is 87% while in Jericho is only 29% from the cooling load demand.

## 2. Net present value method

Net Present Value also used to determine the present value of an investment by the discounted sum of all cash flows received from the project. The formula for the discounted sum of all cash flows can be rewritten as:

$$NPV = -C_0 + \sum_{i=1}^T \frac{C_i}{(1+r)^i} \dots\dots\dots 5.7$$

Where

-C<sub>0</sub> is the initial investment.

$C_i$  is the cash flow

$r$  is the discount rate

$T$  is the time per year

Figure 5.1 shows the flow chart of the cash flow for Hebron and Jericho cities where the net present value are 3475\$ and 2525\$ respectively assuming that zero discount rate value. Also it is noticed that payback period of the proposed system is about 12.5 year in Hebron city and 14.4 year in Jericho city.

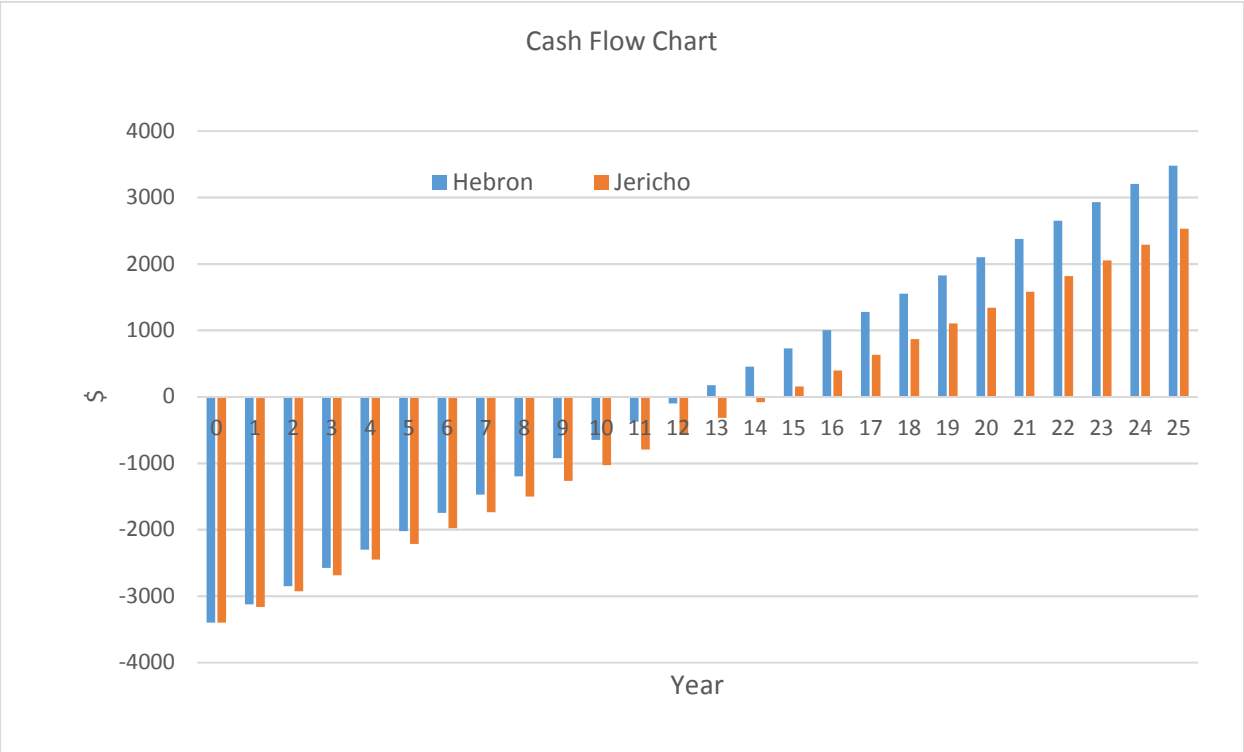


Figure 5.1 cash flow chart for the proposed system in Hebron and Jericho

3. Internal rate of return method

The Internal Rate of Return is the discount rate that makes the net present value of a project zero to estimate the success of potential investments, this value cannot be calculated analytically, software programs are used to solve it or also through trial-and-error, the internal rate of return can be calculated as the following equation [24]

$$IRR = NPV = \sum_{i=1}^T \frac{C_i}{(1+r)^i} - C_0 = 0 \dots\dots\dots 5.8$$

By applying equation 5.8 on the cases of Hebron and Jericho cities that illustrate in table 5.1, and by using excel software program, the results showed that the internal rate of return is equal 6.4% and 4.8% for Hebron and Jericho cities respectively.

From the three methods above to estimate the economical investment of the proposed system in Hebron and Jericho cities, it can be noticed that the proposed system in Hebron city is more economically than in Jericho city, furthermore the proposed system in Jericho city cover only 29% from the cooling load demand of the house unit, while in Hebron city this percentage reached to 87%.

## CHAPTER 6

### Conclusions and Recommendations

#### 6.1 Introduction

In this study we studied and evaluated the thermal behavior of the VJRC driven by solar thermal energy to cover the cooling load demand for a TMH in Hebron and Jericho cities at Palestine by using software programs, also an economically study was done for the proposed system to estimate and calculate the success of this investment, in this section we write the conclusions and Recommendations for this study.

#### 6.2 Conclusions

From this study it can be concluded that:

1. VJRC has the benefit of being simple, uses environmental friendly refrigerants, and can be to operate with a low temperature heat source such as solar heat or waste heat from industrial applications.
2. The performance of the VJRC depends strongly on the operating conditions, where the cycle COP increases with generator and evaporating temperature, but decreases by increasing condensing temperatures. By that the condensing temperature should therefore be kept as low as possible to maintaining the good performance by the ejector and increasing the system performance.
3. The characteristics of the cooling load demand for the house is different at various times and locations for the same building specifications and construction. Where the cooling load demand during the study period for Hebron and Jericho cities were: 5.35 kW and 7.02 kW respectively; and the seasonal cooling energy demands were: 5749 kWh/year and 14864 kWh/year respectively
4. The performance of the overall system depends on both of the cooling subsystem performance and solar thermal subsystem efficiency. Also the solar collector area and the storage tank volume that used in the solar thermal subsystem have a strong effect on the performance of the VJRC and the evaporator cooling load at various locations and time.

5. Using VJRC driven by solar thermal energy in Hebron city is thermally efficient in contrast to Jericho city where the proposed system showed a lack of cooling energy produced because a high condenser temperature.
6. Economically, the proposed system demonstrates that Hebron city has a good investment opportunity more than Jericho city, where the payback period of the system in Hebron city is less than Jericho, besides Hebron has a high percentage of the human comfort more than Jericho.

### **6.3 Recommendations**

This simulation studied the two main parameters of the system (solar collector area and the storage tank volume) but in fact there are a lot of parameters that effect on the cycle performance and cooling capacity, and I recommend to study the following parameters in any future works besides making an experimental device for the cycle.

1. Study of using a water cooled condenser instead of the air cooled condenser especially in Jericho to increase the performance of the VJRC.
2. Study of using a HTF with high specific heat or use the water under high pressure or use phase change material to increase the amount of energy stored in the system and to decrease the storage tank size.
3. Study of varying the HTF flow rate.
4. Study of varying the working fluid of the VJRC.
5. Study of using a backup generator or an external heat source such as biomass to compensate the shortage for the stream conditions.

## References

- [1] Pérez-Lombard, L., Ortiz, J. and Pout, C., 2008. A review on buildings energy consumption information. *Energy and buildings*, 40(3), pp.394-398.
- [2] Besagni, G., Mereu, R. and Inzoli, F., 2016. Ejector refrigeration: a comprehensive review. *Renewable and Sustainable Energy Reviews*, 53, pp.373-407.
- [3] Tashtoush, B., Alshare, A. and Al-Rifai, S., 2015. Performance study of ejector cooling cycle at critical mode under superheated primary flow. *Energy Conversion and Management*, 94, pp.300-310.
- [4] Dincer, I., 2017. *Refrigeration systems and applications*. John Wiley & Sons.
- [5] Meyer, A.J., Harms, T.M. and Dobson, R.T., 2009. Steam jet ejector cooling powered by waste or solar heat. *Renewable Energy*, 34(1), pp.297-306.
- [6] Keenan, J.H., 1950. An investigation of ejector design by analysis and experiment. *Journal of Applied Mechanics*, 17, p.299.
- [7] Al-Khalidy, N.A.H., 1997. Performance of solar refrigerant ejector refrigerating machine (No. CONF-9702141-). American Society of Heating, Refrigerating and Air-Conditioning Engineers, Inc., Atlanta, GA (United States).
- [8] Rani, S. and Sachdeva, G., 2015. Theoretical Performance Analysis of Vapour Jet Ejector for R 134a. *International Journal of Engineering, Management & Sciences*, 2, pp.300-310.
- [9] Eames, I.W., Aphornratana, S. and Haider, H., 1995. A theoretical and experimental study of a small-scale steam jet refrigerator. *International journal of refrigeration*, 18(6), pp.378-386.
- [10] Chunnanond, K. and Aphornratana, S., 2004. An experimental investigation of a steam ejector refrigerator: the analysis of the pressure profile along the ejector. *Applied Thermal Engineering*, 24(2-3), pp.311-322.
- [11] Ruangtrakoon, N., Aphornratana, S. and Sriveerakul, T., 2011. Experimental studies of a steam jet refrigeration cycle: effect of the primary nozzle geometries to system performance. *Experimental Thermal and Fluid Science*, 35(4), pp.676-683.
- [12] Ma, X., Zhang, W., Omer, S.A. and Riffat, S.B., 2010. Experimental investigation of a novel steam ejector refrigerator suitable for solar energy applications. *Applied Thermal Engineering*, 30(11-12), pp.1320-1325.
- [13] Selvaraju, A. and Mani, A., 2004. Analysis of an ejector with environment friendly refrigerants. *Applied Thermal Engineering*, 24(5-6), pp.827-838.
- [14] Sun, D.W., 1996. Variable geometry ejectors and their applications in ejector refrigeration systems. *Energy*, 21(10), pp.919-929.

- [15] Alexis, G.K. and Karayiannis, E.K., 2005. A solar ejector cooling system using refrigerant R134a in the Athens area. *Renewable Energy*, 30(9), pp.1457-1469.
- [16] Ersoy, H.K., Yalcin, S., Yapici, R. and Ozgoren, M., 2007. Performance of a solar ejector cooling-system in the southern region of Turkey. *Applied Energy*, 84(9), pp.971-983.
- [17] Tashtoush, B., Alshare, A. and Al-Rifai, S., 2015. Hourly dynamic simulation of solar ejector cooling system using TRNSYS for Jordanian climate. *Energy conversion and management*, 100, pp.288-299.
- [18] Pridasawas, W. and Lundqvist, P., 2007. A year-round dynamic simulation of a solar-driven ejector refrigeration system with iso-butane as a refrigerant. *International Journal of Refrigeration*, 30(5), pp.840-850.
- [19] AHMED, M.H., MONTAGNINO, F., AMIN, A. and HASSAN, R., Modelling of Solar Absorption Cooling System under Egypt Climate Using TRNSYS. *Environment and Financial Science*, ISBN: 978-1-61804-361-0.
- [20] Asim, M., Dewsbury, J. and Kanan, S., 2016. TRNSYS simulation of a solar cooling system for the hot climate of Pakistan. *Energy Procedia*, 91, pp.702-706.
- [21] Kalogirou, S.A., 2004. Solar thermal collectors and applications. *Progress in energy and combustion science*, 30(3), pp.231-295.
- [22] Rona, N., 2004. Solar air-conditioning systems-Focus on components and their working principles. Chalmers University of Technology. ISSN 1652-6007.
- [23] Viessmann co., Technical guide-Solar thermal systems 2009. <https://www.viessmann.com>.
- [24] Masters, G.M., 2013. Renewable and efficient electric power systems. John Wiley & Sons.
- [25] Palestinian Meteorology (PAL MET) in Palestine. <http://www.pmd.ps>.
- [26] Alamour Company for industrial and trading. <http://www.alamourco.ps>.
- [27] Iso, E., 2007. Building components and building elements-thermal resistance and thermal transmittance-calculation method. 6946: 2007. Brussel: European Standard.
- [28] Palestinian authority, Ministry of local government.2004. Energy Efficient Building Code. .
- [29] International Organization for Standardization, 2005. Ergonomics of the thermal environment: analytical determination and interpretation of thermal comfort using calculation of the PMV and PPD indices and local thermal comfort criteria. 7730: 2005. International Organization for Standardization.
- [30] ANSI/ASHRAE Standard 62.1-2013. Ventilation for Acceptable Indoor Air Quality. ASHRAE.2013.
- [31] Alsaad, M. and Hammad, M., 2007. Heating and air conditioning for residential buildings. National Library department.

- [32] ANSI/ASHRAE Standard 55-2013. Thermal Environmental Conditions for Human Occupancy. ASHRAE.2013.
- [33] S.A. Klein, Engineering Equation Solver manual for Commercial and Professional Versions, <http://www.fchart.com>.
- [34] Klein, S.A., 2004. TRNSYS 16—A TRaNsient SYstem Simulation program, User Manual. Volume 1: Getting Started. Solar Energy Laboratory, University of Wisconsin-Madison.
- [35] Klein, S.A., Beckman, W.A., Mitchell, J.W., Duffie, J.A., Duffie, N.A., Freeman, T.L., Mitchell, J.C., Braun, J.E., Evans, B.L. and Kummer, J.P., 2004. Trnsys 16—Volume 6 Multizone Building Modeling with Type 56 and Trnbuild. Solar Energy Laboratory, University of Wisconsin: Madison, WI, USA.
- [36] Klein, S.A., Beckman, W.A., Mitchell, J.W., Duffie, J.A., Duffie, N.A., Freeman, T.L., Mitchell, J.C., Braun, J.E., Evans, B.L. and Kummer, J.P., 2005. Trnsys 16—Volume 3 Standard Component Library Overview. Solar Energy Laboratory, University of Wisconsin: Madison, WI, USA, p.92.
- [37] Daniel Trier, 2012. Solar district heating guidelines. [www.solar-district-heating.eu](http://www.solar-district-heating.eu).
- [38] Handbook, A.F., 2009. American society of heating, refrigerating and air-conditioning engineers. Inc.: Atlanta, GA, USA.



# Appendixes

Appendix A: Characteristic tables for VJRC at 10°C evaporator temperature.

	Generator temperature [°C]												
	80	81	82	83	84	85	86	87	88	89	90	91	92
25.0	0.703	0.713	0.724	0.734	0.744	0.754	0.764	0.773	0.783	0.792	0.801	0.810	0.819
25.5	0.658	0.668	0.678	0.688	0.698	0.708	0.717	0.726	0.736	0.745	0.754	0.762	0.771
26.0	0.615	0.625	0.635	0.645	0.654	0.664	0.673	0.682	0.691	0.700	0.708	0.717	0.725
26.5	0.575	0.585	0.594	0.604	0.613	0.622	0.631	0.640	0.649	0.657	0.666	0.674	0.682
27.0	0.537	0.547	0.556	0.565	0.574	0.583	0.592	0.601	0.609	0.617	0.626	0.634	0.642
27.5	0.501	0.510	0.520	0.529	0.537	0.546	0.555	0.563	0.571	0.580	0.588	0.596	0.603
28.0	0.467	0.476	0.485	0.494	0.503	0.511	0.519	0.528	0.536	0.544	0.552	0.559	0.567
28.5	0.435	0.444	0.453	0.461	0.469	0.478	0.486	0.494	0.502	0.510	0.517	0.525	0.532
29.0	0.404	0.413	0.422	0.430	0.438	0.446	0.454	0.462	0.470	0.477	0.485	0.492	0.500
29.5	0.375	0.384	0.392	0.400	0.408	0.416	0.424	0.432	0.439	0.447	0.454	0.461	0.468
30.0	0.348	0.356	0.364	0.372	0.380	0.388	0.395	0.403	0.410	0.418	0.425	0.432	0.439
30.5	0.321	0.329	0.337	0.345	0.353	0.360	0.368	0.375	0.383	0.390	0.397	0.404	0.411
31.0	0.296	0.304	0.312	0.320	0.327	0.335	0.342	0.349	0.356	0.363	0.370	0.377	0.384
31.5	0.272	0.280	0.288	0.295	0.303	0.310	0.317	0.324	0.331	0.338	0.345	0.351	0.358
32.0	0.249	0.257	0.264	0.272	0.279	0.286	0.293	0.300	0.307	0.314	0.321	0.327	0.334
32.5	0.227	0.235	0.242	0.250	0.257	0.264	0.271	0.278	0.284	0.291	0.297	0.304	0.310
33.0	0.206	0.214	0.221	0.228	0.235	0.242	0.249	0.256	0.262	0.269	0.275	0.282	0.288
33.5	0.186	0.194	0.201	0.208	0.215	0.222	0.228	0.235	0.241	0.248	0.254	0.260	0.266
34.0	0.167	0.174	0.181	0.188	0.195	0.202	0.208	0.215	0.221	0.228	0.234	0.240	0.246
34.5	0.149	0.156	0.163	0.170	0.176	0.183	0.189	0.196	0.202	0.208	0.214	0.220	0.226
35.0	0.131	0.138	0.145	0.152	0.158	0.165	0.171	0.177	0.184	0.190	0.196	0.202	0.207
35.5	0.115	0.121	0.128	0.135	0.141	0.147	0.154	0.160	0.166	0.172	0.178	0.184	0.189
36.0	0.098	0.105	0.112	0.118	0.124	0.131	0.137	0.143	0.149	0.155	0.161	0.166	0.172
36.5	0.083	0.089	0.096	0.102	0.109	0.115	0.121	0.127	0.133	0.138	0.144	0.150	0.155
37.0	0.068	0.074	0.081	0.087	0.093	0.099	0.105	0.111	0.117	0.123	0.128	0.134	0.139
37.5	0.054	0.060	0.066	0.072	0.079	0.085	0.090	0.096	0.102	0.108	0.113	0.119	0.124
38.0	0.040	0.046	0.052	0.058	0.064	0.070	0.076	0.082	0.088	0.093	0.099	0.104	0.109
38.5	0.026	0.033	0.039	0.045	0.051	0.057	0.062	0.068	0.074	0.079	0.084	0.090	0.095
39.0	0.014	0.020	0.026	0.032	0.038	0.043	0.049	0.055	0.060	0.066	0.071	0.076	0.081
39.5	0.001	0.007	0.013	0.019	0.025	0.031	0.036	0.042	0.047	0.053	0.058	0.063	0.068
40.0	0.000	0.000	0.001	0.007	0.013	0.019	0.024	0.030	0.035	0.040	0.045	0.050	0.056
40.5	0.000	0.000	0.000	0.000	0.001	0.007	0.012	0.018	0.023	0.028	0.033	0.038	0.043
41.0	0.000	0.000	0.000	0.000	0.000	0.000	0.001	0.006	0.011	0.017	0.022	0.027	0.032
41.5	0.000	0.000	0.000	0.000	0.000	0.000	0.000	0.000	0.000	0.005	0.010	0.015	0.020
42.0	0.000	0.000	0.000	0.000	0.000	0.000	0.000	0.000	0.000	0.000	0.000	0.004	0.009
42.5	0.000	0.000	0.000	0.000	0.000	0.000	0.000	0.000	0.000	0.000	0.000	0.000	0.000
43.0	0.000	0.000	0.000	0.000	0.000	0.000	0.000	0.000	0.000	0.000	0.000	0.000	0.000
43.5	0.000	0.000	0.000	0.000	0.000	0.000	0.000	0.000	0.000	0.000	0.000	0.000	0.000
44.0	0.000	0.000	0.000	0.000	0.000	0.000	0.000	0.000	0.000	0.000	0.000	0.000	0.000
44.5	0.000	0.000	0.000	0.000	0.000	0.000	0.000	0.000	0.000	0.000	0.000	0.000	0.000
45.0	0.000	0.000	0.000	0.000	0.000	0.000	0.000	0.000	0.000	0.000	0.000	0.000	0.000
45.5	0.000	0.000	0.000	0.000	0.000	0.000	0.000	0.000	0.000	0.000	0.000	0.000	0.000
46.0	0.000	0.000	0.000	0.000	0.000	0.000	0.000	0.000	0.000	0.000	0.000	0.000	0.000
46.5	0.000	0.000	0.000	0.000	0.000	0.000	0.000	0.000	0.000	0.000	0.000	0.000	0.000
47.0	0.000	0.000	0.000	0.000	0.000	0.000	0.000	0.000	0.000	0.000	0.000	0.000	0.000
47.5	0.000	0.000	0.000	0.000	0.000	0.000	0.000	0.000	0.000	0.000	0.000	0.000	0.000
48.0	0.000	0.000	0.000	0.000	0.000	0.000	0.000	0.000	0.000	0.000	0.000	0.000	0.000
48.5	0.000	0.000	0.000	0.000	0.000	0.000	0.000	0.000	0.000	0.000	0.000	0.000	0.000
49.0	0.000	0.000	0.000	0.000	0.000	0.000	0.000	0.000	0.000	0.000	0.000	0.000	0.000
49.5	0.000	0.000	0.000	0.000	0.000	0.000	0.000	0.000	0.000	0.000	0.000	0.000	0.000
50.0	0.000	0.000	0.000	0.000	0.000	0.000	0.000	0.000	0.000	0.000	0.000	0.000	0.000

	Generator temperature [°C] Cont.												
	93	94	95	96	97	98	99	100	101	102	103	104	100
25.0	0.828	0.837	0.845	0.854	0.862	0.870	0.878	0.886	0.894	0.902	0.909	0.917	0.924
25.5	0.780	0.788	0.796	0.804	0.812	0.820	0.828	0.836	0.844	0.851	0.859	0.866	0.873
26.0	0.734	0.742	0.750	0.758	0.766	0.774	0.781	0.789	0.796	0.803	0.811	0.818	0.825
26.5	0.691	0.698	0.706	0.714	0.722	0.729	0.737	0.744	0.751	0.758	0.765	0.772	0.779
27.0	0.650	0.657	0.665	0.673	0.680	0.687	0.695	0.702	0.709	0.716	0.723	0.729	0.736
27.5	0.611	0.619	0.626	0.633	0.641	0.648	0.655	0.662	0.669	0.676	0.682	0.689	0.695
28.0	0.574	0.582	0.589	0.596	0.603	0.610	0.617	0.624	0.631	0.637	0.644	0.650	0.657
28.5	0.540	0.547	0.554	0.561	0.568	0.575	0.582	0.588	0.595	0.601	0.608	0.614	0.620
29.0	0.507	0.514	0.521	0.528	0.534	0.541	0.548	0.554	0.561	0.567	0.573	0.579	0.585
29.5	0.475	0.482	0.489	0.496	0.503	0.509	0.515	0.522	0.528	0.534	0.540	0.546	0.552
30.0	0.446	0.452	0.459	0.466	0.472	0.479	0.485	0.491	0.497	0.503	0.509	0.515	0.521
30.5	0.417	0.424	0.430	0.437	0.443	0.449	0.456	0.462	0.468	0.474	0.479	0.485	0.491
31.0	0.390	0.397	0.403	0.409	0.416	0.422	0.428	0.434	0.440	0.445	0.451	0.457	0.462
31.5	0.364	0.371	0.377	0.383	0.389	0.395	0.401	0.407	0.413	0.419	0.424	0.430	0.435
32.0	0.340	0.346	0.352	0.358	0.364	0.370	0.376	0.382	0.387	0.393	0.398	0.404	0.409
32.5	0.316	0.322	0.328	0.334	0.340	0.346	0.352	0.357	0.363	0.368	0.374	0.379	0.384
33.0	0.294	0.300	0.306	0.312	0.317	0.323	0.329	0.334	0.340	0.345	0.350	0.355	0.361
33.5	0.272	0.278	0.284	0.290	0.295	0.301	0.307	0.312	0.317	0.323	0.328	0.333	0.338
34.0	0.252	0.258	0.263	0.269	0.274	0.280	0.285	0.291	0.296	0.301	0.306	0.311	0.316
34.5	0.232	0.238	0.243	0.249	0.254	0.260	0.265	0.270	0.275	0.281	0.286	0.290	0.295
35.0	0.213	0.219	0.224	0.230	0.235	0.240	0.246	0.251	0.256	0.261	0.266	0.271	0.275
35.5	0.195	0.200	0.206	0.211	0.217	0.222	0.227	0.232	0.237	0.242	0.247	0.252	0.256
36.0	0.178	0.183	0.188	0.194	0.199	0.204	0.209	0.214	0.219	0.224	0.229	0.233	0.238
36.5	0.161	0.166	0.171	0.177	0.182	0.187	0.192	0.197	0.202	0.206	0.211	0.216	0.220
37.0	0.145	0.150	0.155	0.160	0.165	0.170	0.175	0.180	0.185	0.190	0.194	0.199	0.203
37.5	0.129	0.135	0.140	0.145	0.150	0.155	0.159	0.164	0.169	0.174	0.178	0.183	0.187
38.0	0.114	0.120	0.125	0.130	0.135	0.139	0.144	0.149	0.154	0.158	0.163	0.167	0.171
38.5	0.100	0.105	0.110	0.115	0.120	0.125	0.130	0.134	0.139	0.143	0.148	0.152	0.156
39.0	0.086	0.091	0.096	0.101	0.106	0.111	0.115	0.120	0.124	0.129	0.133	0.138	0.142
39.5	0.073	0.078	0.083	0.088	0.093	0.097	0.102	0.106	0.111	0.115	0.119	0.124	0.128
40.0	0.060	0.065	0.070	0.075	0.080	0.084	0.089	0.093	0.098	0.102	0.106	0.110	0.115
40.5	0.048	0.053	0.058	0.062	0.067	0.072	0.076	0.080	0.085	0.089	0.093	0.097	0.102
41.0	0.036	0.041	0.046	0.050	0.055	0.059	0.064	0.068	0.073	0.077	0.081	0.085	0.089
41.5	0.025	0.030	0.034	0.039	0.043	0.048	0.052	0.056	0.061	0.065	0.069	0.073	0.077
42.0	0.014	0.019	0.023	0.028	0.032	0.037	0.041	0.045	0.049	0.053	0.057	0.061	0.065
42.5	0.003	0.008	0.012	0.017	0.021	0.026	0.030	0.034	0.038	0.042	0.046	0.050	0.054
43.0	0.000	0.000	0.002	0.007	0.011	0.015	0.019	0.024	0.028	0.032	0.036	0.040	0.043
43.5	0.000	0.000	0.000	0.000	0.001	0.005	0.009	0.013	0.017	0.021	0.025	0.029	0.033
44.0	0.000	0.000	0.000	0.000	0.000	0.000	0.000	0.003	0.007	0.011	0.015	0.019	0.023
44.5	0.000	0.000	0.000	0.000	0.000	0.000	0.000	0.000	0.000	0.002	0.006	0.009	0.013
45.0	0.000	0.000	0.000	0.000	0.000	0.000	0.000	0.000	0.000	0.000	0.000	0.000	0.004
45.5	0.000	0.000	0.000	0.000	0.000	0.000	0.000	0.000	0.000	0.000	0.000	0.000	0.000
46.0	0.000	0.000	0.000	0.000	0.000	0.000	0.000	0.000	0.000	0.000	0.000	0.000	0.000
46.5	0.000	0.000	0.000	0.000	0.000	0.000	0.000	0.000	0.000	0.000	0.000	0.000	0.000
47.0	0.000	0.000	0.000	0.000	0.000	0.000	0.000	0.000	0.000	0.000	0.000	0.000	0.000
47.5	0.000	0.000	0.000	0.000	0.000	0.000	0.000	0.000	0.000	0.000	0.000	0.000	0.000
48.0	0.000	0.000	0.000	0.000	0.000	0.000	0.000	0.000	0.000	0.000	0.000	0.000	0.000
48.5	0.000	0.000	0.000	0.000	0.000	0.000	0.000	0.000	0.000	0.000	0.000	0.000	0.000
49.0	0.000	0.000	0.000	0.000	0.000	0.000	0.000	0.000	0.000	0.000	0.000	0.000	0.000
49.5	0.000	0.000	0.000	0.000	0.000	0.000	0.000	0.000	0.000	0.000	0.000	0.000	0.000
50.0	0.000	0.000	0.000	0.000	0.000	0.000	0.000	0.000	0.000	0.000	0.000	0.000	0.000

	Generator temperature [°C] Cont.												
	101	102	103	104	105	106	107	108	109	110	111	112	113
25.0	0.894	0.902	0.909	0.917	0.924	0.932	0.939	0.946	0.953	0.960	0.967	0.974	0.980
25.5	0.844	0.851	0.859	0.866	0.873	0.880	0.887	0.894	0.901	0.908	0.914	0.921	0.927
26.0	0.796	0.803	0.811	0.818	0.825	0.832	0.838	0.845	0.852	0.858	0.865	0.871	0.878
26.5	0.751	0.758	0.765	0.772	0.779	0.786	0.792	0.799	0.806	0.812	0.818	0.824	0.831
27.0	0.709	0.716	0.723	0.729	0.736	0.743	0.749	0.755	0.762	0.768	0.774	0.780	0.786
27.5	0.669	0.676	0.682	0.689	0.695	0.702	0.708	0.714	0.720	0.726	0.732	0.738	0.744
28.0	0.631	0.637	0.644	0.650	0.657	0.663	0.669	0.675	0.681	0.687	0.693	0.699	0.704
28.5	0.595	0.601	0.608	0.614	0.620	0.626	0.632	0.638	0.644	0.650	0.655	0.661	0.667
29.0	0.561	0.567	0.573	0.579	0.585	0.591	0.597	0.603	0.609	0.614	0.620	0.625	0.631
29.5	0.528	0.534	0.540	0.546	0.552	0.558	0.564	0.569	0.575	0.581	0.586	0.591	0.597
30.0	0.497	0.503	0.509	0.515	0.521	0.526	0.532	0.538	0.543	0.549	0.554	0.559	0.564
30.5	0.468	0.474	0.479	0.485	0.491	0.496	0.502	0.507	0.513	0.518	0.523	0.528	0.533
31.0	0.440	0.445	0.451	0.457	0.462	0.468	0.473	0.479	0.484	0.489	0.494	0.499	0.504
31.5	0.413	0.419	0.424	0.430	0.435	0.440	0.446	0.451	0.456	0.461	0.466	0.471	0.476
32.0	0.387	0.393	0.398	0.404	0.409	0.414	0.420	0.425	0.430	0.435	0.440	0.445	0.449
32.5	0.363	0.368	0.374	0.379	0.384	0.389	0.395	0.400	0.405	0.409	0.414	0.419	0.424
33.0	0.340	0.345	0.350	0.355	0.361	0.366	0.371	0.376	0.380	0.385	0.390	0.395	0.399
33.5	0.317	0.323	0.328	0.333	0.338	0.343	0.348	0.353	0.357	0.362	0.367	0.371	0.376
34.0	0.296	0.301	0.306	0.311	0.316	0.321	0.326	0.331	0.335	0.340	0.345	0.349	0.353
34.5	0.275	0.281	0.286	0.290	0.295	0.300	0.305	0.310	0.314	0.319	0.323	0.328	0.332
35.0	0.256	0.261	0.266	0.271	0.275	0.280	0.285	0.289	0.294	0.298	0.303	0.307	0.311
35.5	0.237	0.242	0.247	0.252	0.256	0.261	0.266	0.270	0.275	0.279	0.283	0.288	0.292
36.0	0.219	0.224	0.229	0.233	0.238	0.243	0.247	0.251	0.256	0.260	0.264	0.269	0.273
36.5	0.202	0.206	0.211	0.216	0.220	0.225	0.229	0.234	0.238	0.242	0.246	0.251	0.255
37.0	0.185	0.190	0.194	0.199	0.203	0.208	0.212	0.217	0.221	0.225	0.229	0.233	0.237
37.5	0.169	0.174	0.178	0.183	0.187	0.191	0.196	0.200	0.204	0.208	0.212	0.217	0.220
38.0	0.154	0.158	0.163	0.167	0.171	0.176	0.180	0.184	0.188	0.192	0.196	0.200	0.204
38.5	0.139	0.143	0.148	0.152	0.156	0.161	0.165	0.169	0.173	0.177	0.181	0.185	0.189
39.0	0.124	0.129	0.133	0.138	0.142	0.146	0.150	0.154	0.158	0.162	0.166	0.170	0.174
39.5	0.111	0.115	0.119	0.124	0.128	0.132	0.136	0.140	0.144	0.148	0.152	0.156	0.160
40.0	0.098	0.102	0.106	0.110	0.115	0.119	0.123	0.127	0.131	0.134	0.138	0.142	0.146
40.5	0.085	0.089	0.093	0.097	0.102	0.106	0.110	0.114	0.117	0.121	0.125	0.129	0.132
41.0	0.073	0.077	0.081	0.085	0.089	0.093	0.097	0.101	0.105	0.109	0.112	0.116	0.120
41.5	0.061	0.065	0.069	0.073	0.077	0.081	0.085	0.089	0.092	0.096	0.100	0.104	0.107
42.0	0.049	0.053	0.057	0.061	0.065	0.069	0.073	0.077	0.081	0.084	0.088	0.092	0.095
42.5	0.038	0.042	0.046	0.050	0.054	0.058	0.062	0.066	0.069	0.073	0.077	0.080	0.084
43.0	0.028	0.032	0.036	0.040	0.043	0.047	0.051	0.055	0.058	0.062	0.066	0.069	0.073
43.5	0.017	0.021	0.025	0.029	0.033	0.037	0.041	0.044	0.048	0.051	0.055	0.058	0.062
44.0	0.007	0.011	0.015	0.019	0.023	0.027	0.030	0.034	0.038	0.041	0.045	0.048	0.051
44.5	0.000	0.002	0.006	0.009	0.013	0.017	0.021	0.024	0.028	0.031	0.035	0.038	0.041
45.0	0.000	0.000	0.000	0.000	0.004	0.007	0.011	0.015	0.018	0.022	0.025	0.028	0.032
45.5	0.000	0.000	0.000	0.000	0.000	0.000	0.002	0.005	0.009	0.012	0.016	0.019	0.022
46.0	0.000	0.000	0.000	0.000	0.000	0.000	0.000	0.000	0.000	0.003	0.007	0.010	0.013
46.5	0.000	0.000	0.000	0.000	0.000	0.000	0.000	0.000	0.000	0.000	0.000	0.001	0.004
47.0	0.000	0.000	0.000	0.000	0.000	0.000	0.000	0.000	0.000	0.000	0.000	0.000	0.000
47.5	0.000	0.000	0.000	0.000	0.000	0.000	0.000	0.000	0.000	0.000	0.000	0.000	0.000
48.0	0.000	0.000	0.000	0.000	0.000	0.000	0.000	0.000	0.000	0.000	0.000	0.000	0.000
48.5	0.000	0.000	0.000	0.000	0.000	0.000	0.000	0.000	0.000	0.000	0.000	0.000	0.000
49.0	0.000	0.000	0.000	0.000	0.000	0.000	0.000	0.000	0.000	0.000	0.000	0.000	0.000
49.5	0.000	0.000	0.000	0.000	0.000	0.000	0.000	0.000	0.000	0.000	0.000	0.000	0.000
50.0	0.000	0.000	0.000	0.000	0.000	0.000	0.000	0.000	0.000	0.000	0.000	0.000	0.000

	Generator temperature [°C] Cont.												
	114	115	116	117	118	119	120	121	122	123	124	125	126
25.0	0.987	0.993	1.000	1.006	1.012	1.019	1.025	1.031	1.037	1.043	1.049	1.054	1.060
25.5	0.934	0.940	0.946	0.953	0.959	0.965	0.971	0.977	0.982	0.988	0.994	0.999	1.005
26.0	0.884	0.890	0.896	0.902	0.908	0.914	0.920	0.925	0.931	0.937	0.942	0.948	0.953
26.5	0.837	0.843	0.849	0.854	0.860	0.866	0.872	0.877	0.883	0.888	0.893	0.899	0.904
27.0	0.792	0.798	0.804	0.809	0.815	0.821	0.826	0.831	0.837	0.842	0.847	0.853	0.858
27.5	0.750	0.756	0.761	0.767	0.772	0.778	0.783	0.788	0.794	0.799	0.804	0.809	0.814
28.0	0.710	0.716	0.721	0.726	0.732	0.737	0.742	0.747	0.753	0.758	0.763	0.767	0.772
28.5	0.672	0.678	0.683	0.688	0.693	0.699	0.704	0.709	0.714	0.719	0.723	0.728	0.733
29.0	0.636	0.641	0.647	0.652	0.657	0.662	0.667	0.672	0.677	0.682	0.686	0.691	0.696
29.5	0.602	0.607	0.612	0.617	0.622	0.627	0.632	0.637	0.642	0.646	0.651	0.656	0.660
30.0	0.569	0.575	0.580	0.584	0.589	0.594	0.599	0.604	0.608	0.613	0.617	0.622	0.626
30.5	0.539	0.543	0.548	0.553	0.558	0.563	0.567	0.572	0.576	0.581	0.585	0.590	0.594
31.0	0.509	0.514	0.519	0.523	0.528	0.533	0.537	0.542	0.546	0.551	0.555	0.559	0.563
31.5	0.481	0.486	0.490	0.495	0.500	0.504	0.509	0.513	0.517	0.522	0.526	0.530	0.534
32.0	0.454	0.459	0.463	0.468	0.472	0.477	0.481	0.485	0.490	0.494	0.498	0.502	0.506
32.5	0.428	0.433	0.437	0.442	0.446	0.451	0.455	0.459	0.463	0.468	0.472	0.476	0.480
33.0	0.404	0.408	0.413	0.417	0.421	0.426	0.430	0.434	0.438	0.442	0.446	0.450	0.454
33.5	0.380	0.385	0.389	0.393	0.398	0.402	0.406	0.410	0.414	0.418	0.422	0.426	0.430
34.0	0.358	0.362	0.366	0.371	0.375	0.379	0.383	0.387	0.391	0.395	0.399	0.403	0.406
34.5	0.336	0.341	0.345	0.349	0.353	0.357	0.361	0.365	0.369	0.373	0.377	0.380	0.384
35.0	0.316	0.320	0.324	0.328	0.332	0.336	0.340	0.344	0.348	0.352	0.355	0.359	0.363
35.5	0.296	0.300	0.304	0.308	0.312	0.316	0.320	0.324	0.327	0.331	0.335	0.338	0.342
36.0	0.277	0.281	0.285	0.289	0.293	0.297	0.301	0.304	0.308	0.312	0.315	0.319	0.322
36.5	0.259	0.263	0.267	0.271	0.274	0.278	0.282	0.286	0.289	0.293	0.296	0.300	0.303
37.0	0.241	0.245	0.249	0.253	0.257	0.260	0.264	0.268	0.271	0.275	0.278	0.282	0.285
37.5	0.224	0.228	0.232	0.236	0.240	0.243	0.247	0.251	0.254	0.258	0.261	0.264	0.268
38.0	0.208	0.212	0.216	0.220	0.223	0.227	0.230	0.234	0.237	0.241	0.244	0.248	0.251
38.5	0.193	0.196	0.200	0.204	0.207	0.211	0.215	0.218	0.221	0.225	0.228	0.232	0.235
39.0	0.178	0.181	0.185	0.189	0.192	0.196	0.199	0.203	0.206	0.209	0.213	0.216	0.219
39.5	0.163	0.167	0.171	0.174	0.178	0.181	0.185	0.188	0.191	0.195	0.198	0.201	0.204
40.0	0.149	0.153	0.157	0.160	0.164	0.167	0.170	0.174	0.177	0.180	0.184	0.187	0.190
40.5	0.136	0.140	0.143	0.147	0.150	0.153	0.157	0.160	0.163	0.167	0.170	0.173	0.176
41.0	0.123	0.127	0.130	0.134	0.137	0.140	0.144	0.147	0.150	0.153	0.156	0.160	0.163
41.5	0.111	0.114	0.118	0.121	0.124	0.128	0.131	0.134	0.137	0.140	0.144	0.147	0.150
42.0	0.099	0.102	0.106	0.109	0.112	0.115	0.119	0.122	0.125	0.128	0.131	0.134	0.137
42.5	0.087	0.090	0.094	0.097	0.100	0.104	0.107	0.110	0.113	0.116	0.119	0.122	0.125
43.0	0.076	0.079	0.083	0.086	0.089	0.092	0.095	0.099	0.102	0.105	0.108	0.111	0.114
43.5	0.065	0.068	0.072	0.075	0.078	0.081	0.084	0.088	0.091	0.094	0.097	0.099	0.102
44.0	0.055	0.058	0.061	0.064	0.068	0.071	0.074	0.077	0.080	0.083	0.086	0.089	0.092
44.5	0.045	0.048	0.051	0.054	0.057	0.061	0.064	0.067	0.070	0.073	0.075	0.078	0.081
45.0	0.035	0.038	0.041	0.044	0.048	0.051	0.054	0.057	0.060	0.062	0.065	0.068	0.071
45.5	0.026	0.029	0.032	0.035	0.038	0.041	0.044	0.047	0.050	0.053	0.056	0.058	0.061
46.0	0.016	0.020	0.023	0.026	0.029	0.032	0.035	0.038	0.041	0.043	0.046	0.049	0.052
46.5	0.008	0.011	0.014	0.017	0.020	0.023	0.026	0.029	0.032	0.034	0.037	0.040	0.043
47.0	0.000	0.002	0.005	0.008	0.011	0.014	0.017	0.020	0.023	0.026	0.028	0.031	0.034
47.5	0.000	0.000	0.000	0.000	0.003	0.006	0.009	0.012	0.014	0.017	0.020	0.023	0.025
48.0	0.000	0.000	0.000	0.000	0.000	0.000	0.001	0.004	0.006	0.009	0.012	0.014	0.017
48.5	0.000	0.000	0.000	0.000	0.000	0.000	0.000	0.000	0.000	0.001	0.004	0.006	0.009
49.0	0.000	0.000	0.000	0.000	0.000	0.000	0.000	0.000	0.000	0.000	0.000	0.000	0.001
49.5	0.000	0.000	0.000	0.000	0.000	0.000	0.000	0.000	0.000	0.000	0.000	0.000	0.000
50.0	0.000	0.000	0.000	0.000	0.000	0.000	0.000	0.000	0.000	0.000	0.000	0.000	0.000

	Generator temperature [°C] Cont.												
	127	128	129	130	131	132	133	134	135	136	137	138	139
25.0	1.066	1.071	1.077	1.082	1.088	1.093	1.098	1.103	1.109	1.114	1.119	1.124	1.129
25.5	1.010	1.016	1.021	1.026	1.032	1.037	1.042	1.047	1.052	1.057	1.062	1.067	1.072
26.0	0.958	0.964	0.969	0.974	0.979	0.984	0.989	0.994	0.999	1.004	1.008	1.013	1.018
26.5	0.909	0.914	0.919	0.924	0.929	0.934	0.939	0.944	0.949	0.953	0.958	0.962	0.967
27.0	0.863	0.868	0.873	0.877	0.882	0.887	0.892	0.896	0.901	0.906	0.910	0.915	0.919
27.5	0.819	0.824	0.828	0.833	0.838	0.842	0.847	0.852	0.856	0.861	0.865	0.869	0.874
28.0	0.777	0.782	0.787	0.791	0.796	0.800	0.805	0.809	0.814	0.818	0.822	0.826	0.831
28.5	0.738	0.742	0.747	0.751	0.756	0.760	0.765	0.769	0.773	0.777	0.782	0.786	0.790
29.0	0.700	0.705	0.709	0.714	0.718	0.722	0.726	0.731	0.735	0.739	0.743	0.747	0.751
29.5	0.665	0.669	0.673	0.678	0.682	0.686	0.690	0.694	0.698	0.702	0.706	0.710	0.714
30.0	0.631	0.635	0.639	0.643	0.648	0.652	0.656	0.660	0.664	0.668	0.672	0.676	0.679
30.5	0.598	0.603	0.607	0.611	0.615	0.619	0.623	0.627	0.631	0.635	0.639	0.642	0.646
31.0	0.568	0.572	0.576	0.580	0.584	0.588	0.592	0.596	0.599	0.603	0.607	0.611	0.614
31.5	0.538	0.542	0.546	0.550	0.554	0.558	0.562	0.566	0.569	0.573	0.577	0.580	0.584
32.0	0.510	0.514	0.518	0.522	0.526	0.530	0.533	0.537	0.541	0.544	0.548	0.552	0.555
32.5	0.484	0.487	0.491	0.495	0.499	0.503	0.506	0.510	0.513	0.517	0.521	0.524	0.527
33.0	0.458	0.462	0.466	0.469	0.473	0.477	0.480	0.484	0.487	0.491	0.494	0.498	0.501
33.5	0.434	0.437	0.441	0.445	0.448	0.452	0.455	0.459	0.462	0.466	0.469	0.472	0.476
34.0	0.410	0.414	0.417	0.421	0.425	0.428	0.432	0.435	0.438	0.442	0.445	0.448	0.452
34.5	0.388	0.391	0.395	0.398	0.402	0.405	0.409	0.412	0.416	0.419	0.422	0.425	0.428
35.0	0.366	0.370	0.373	0.377	0.380	0.384	0.387	0.390	0.394	0.397	0.400	0.403	0.406
35.5	0.346	0.349	0.353	0.356	0.359	0.363	0.366	0.369	0.372	0.376	0.379	0.382	0.385
36.0	0.326	0.329	0.333	0.336	0.339	0.343	0.346	0.349	0.352	0.355	0.358	0.362	0.365
36.5	0.307	0.310	0.314	0.317	0.320	0.323	0.327	0.330	0.333	0.336	0.339	0.342	0.345
37.0	0.289	0.292	0.295	0.299	0.302	0.305	0.308	0.311	0.314	0.317	0.320	0.323	0.326
37.5	0.271	0.274	0.278	0.281	0.284	0.287	0.290	0.293	0.296	0.299	0.302	0.305	0.308
38.0	0.254	0.257	0.261	0.264	0.267	0.270	0.273	0.276	0.279	0.282	0.285	0.288	0.291
38.5	0.238	0.241	0.244	0.247	0.251	0.254	0.257	0.260	0.263	0.265	0.268	0.271	0.274
39.0	0.222	0.226	0.229	0.232	0.235	0.238	0.241	0.244	0.247	0.249	0.252	0.255	0.258
39.5	0.207	0.211	0.214	0.217	0.220	0.223	0.225	0.228	0.231	0.234	0.237	0.240	0.242
40.0	0.193	0.196	0.199	0.202	0.205	0.208	0.211	0.214	0.216	0.219	0.222	0.225	0.227
40.5	0.179	0.182	0.185	0.188	0.191	0.194	0.197	0.199	0.202	0.205	0.208	0.210	0.213
41.0	0.166	0.169	0.172	0.174	0.177	0.180	0.183	0.186	0.188	0.191	0.194	0.197	0.199
41.5	0.153	0.156	0.158	0.161	0.164	0.167	0.170	0.173	0.175	0.178	0.181	0.183	0.186
42.0	0.140	0.143	0.146	0.149	0.152	0.154	0.157	0.160	0.162	0.165	0.168	0.170	0.173
42.5	0.128	0.131	0.134	0.137	0.139	0.142	0.145	0.148	0.150	0.153	0.155	0.158	0.160
43.0	0.116	0.119	0.122	0.125	0.128	0.130	0.133	0.136	0.138	0.141	0.143	0.146	0.148
43.5	0.105	0.108	0.111	0.114	0.116	0.119	0.122	0.124	0.127	0.129	0.132	0.134	0.137
44.0	0.094	0.097	0.100	0.103	0.105	0.108	0.111	0.113	0.116	0.118	0.121	0.123	0.126
44.5	0.084	0.087	0.089	0.092	0.095	0.097	0.100	0.103	0.105	0.108	0.110	0.112	0.115
45.0	0.074	0.076	0.079	0.082	0.084	0.087	0.090	0.092	0.095	0.097	0.100	0.102	0.104
45.5	0.064	0.067	0.069	0.072	0.075	0.077	0.080	0.082	0.085	0.087	0.090	0.092	0.094
46.0	0.055	0.057	0.060	0.062	0.065	0.068	0.070	0.073	0.075	0.077	0.080	0.082	0.084
46.5	0.045	0.048	0.051	0.053	0.056	0.058	0.061	0.063	0.066	0.068	0.070	0.073	0.075
47.0	0.037	0.039	0.042	0.044	0.047	0.049	0.052	0.054	0.057	0.059	0.061	0.064	0.066
47.5	0.028	0.031	0.033	0.036	0.038	0.041	0.043	0.045	0.048	0.050	0.053	0.055	0.057
48.0	0.020	0.022	0.025	0.027	0.030	0.032	0.035	0.037	0.039	0.042	0.044	0.046	0.049
48.5	0.012	0.014	0.017	0.019	0.022	0.024	0.026	0.029	0.031	0.033	0.036	0.038	0.040
49.0	0.004	0.006	0.009	0.011	0.014	0.016	0.019	0.021	0.023	0.026	0.028	0.030	0.032
49.5	0.000	0.000	0.001	0.004	0.006	0.009	0.011	0.013	0.016	0.018	0.020	0.022	0.024
50.0	0.000	0.000	0.000	0.000	0.000	0.001	0.004	0.006	0.008	0.010	0.013	0.015	0.017

	Generator temperature [°C] Cont.												
	140	141	142	143	144	145	146	147	148	149	150		
25.0	1.134	1.138	1.143	1.148	1.153	1.157	1.162	1.167	1.171	1.176	1.180		
25.5	1.076	1.081	1.086	1.090	1.095	1.099	1.104	1.108	1.113	1.117	1.121		
26.0	1.022	1.027	1.031	1.036	1.040	1.045	1.049	1.053	1.058	1.062	1.066		
26.5	0.971	0.976	0.980	0.985	0.989	0.993	0.997	1.002	1.006	1.010	1.014		
27.0	0.923	0.928	0.932	0.936	0.940	0.945	0.949	0.953	0.957	0.961	0.965		
27.5	0.878	0.882	0.886	0.890	0.894	0.899	0.903	0.906	0.910	0.914	0.918		
28.0	0.835	0.839	0.843	0.847	0.851	0.855	0.859	0.863	0.866	0.870	0.874		
28.5	0.794	0.798	0.802	0.806	0.810	0.813	0.817	0.821	0.825	0.828	0.832		
29.0	0.755	0.759	0.763	0.767	0.770	0.774	0.778	0.782	0.785	0.789	0.792		
29.5	0.718	0.722	0.726	0.730	0.733	0.737	0.741	0.744	0.748	0.751	0.755		
30.0	0.683	0.687	0.691	0.694	0.698	0.701	0.705	0.708	0.712	0.715	0.719		
30.5	0.650	0.653	0.657	0.661	0.664	0.668	0.671	0.674	0.678	0.681	0.685		
31.0	0.618	0.621	0.625	0.628	0.632	0.635	0.639	0.642	0.645	0.649	0.652		
31.5	0.588	0.591	0.594	0.598	0.601	0.605	0.608	0.611	0.614	0.618	0.621		
32.0	0.559	0.562	0.565	0.569	0.572	0.575	0.579	0.582	0.585	0.588	0.591		
32.5	0.531	0.534	0.538	0.541	0.544	0.547	0.550	0.554	0.557	0.560	0.563		
33.0	0.504	0.508	0.511	0.514	0.517	0.520	0.524	0.527	0.530	0.533	0.536		
33.5	0.479	0.482	0.485	0.489	0.492	0.495	0.498	0.501	0.504	0.507	0.510		
34.0	0.455	0.458	0.461	0.464	0.467	0.470	0.473	0.476	0.479	0.482	0.485		
34.5	0.432	0.435	0.438	0.441	0.444	0.447	0.450	0.453	0.456	0.458	0.461		
35.0	0.409	0.412	0.415	0.418	0.421	0.424	0.427	0.430	0.433	0.436	0.439		
35.5	0.388	0.391	0.394	0.397	0.400	0.403	0.406	0.408	0.411	0.414	0.417		
36.0	0.368	0.371	0.373	0.376	0.379	0.382	0.385	0.388	0.390	0.393	0.396		
36.5	0.348	0.351	0.354	0.357	0.359	0.362	0.365	0.368	0.370	0.373	0.376		
37.0	0.329	0.332	0.335	0.338	0.340	0.343	0.346	0.348	0.351	0.354	0.356		
37.5	0.311	0.314	0.317	0.319	0.322	0.325	0.327	0.330	0.333	0.335	0.338		
38.0	0.293	0.296	0.299	0.302	0.304	0.307	0.310	0.312	0.315	0.317	0.320		
38.5	0.277	0.279	0.282	0.285	0.287	0.290	0.293	0.295	0.298	0.300	0.303		
39.0	0.261	0.263	0.266	0.269	0.271	0.274	0.276	0.279	0.281	0.284	0.286		
39.5	0.245	0.248	0.250	0.253	0.255	0.258	0.261	0.263	0.266	0.268	0.270		
40.0	0.230	0.233	0.235	0.238	0.240	0.243	0.245	0.248	0.250	0.253	0.255		
40.5	0.216	0.218	0.221	0.223	0.226	0.228	0.231	0.233	0.236	0.238	0.240		
41.0	0.202	0.204	0.207	0.209	0.212	0.214	0.217	0.219	0.221	0.224	0.226		
41.5	0.188	0.191	0.193	0.196	0.198	0.201	0.203	0.205	0.208	0.210	0.212		
42.0	0.175	0.178	0.180	0.183	0.185	0.188	0.190	0.192	0.195	0.197	0.199		
42.5	0.163	0.165	0.168	0.170	0.173	0.175	0.177	0.180	0.182	0.184	0.186		
43.0	0.151	0.153	0.156	0.158	0.160	0.163	0.165	0.167	0.170	0.172	0.174		
43.5	0.139	0.142	0.144	0.146	0.149	0.151	0.153	0.156	0.158	0.160	0.162		
44.0	0.128	0.130	0.133	0.135	0.137	0.140	0.142	0.144	0.146	0.149	0.151		
44.5	0.117	0.120	0.122	0.124	0.126	0.129	0.131	0.133	0.135	0.138	0.140		
45.0	0.107	0.109	0.111	0.114	0.116	0.118	0.120	0.123	0.125	0.127	0.129		
45.5	0.097	0.099	0.101	0.103	0.106	0.108	0.110	0.112	0.114	0.116	0.119		
46.0	0.087	0.089	0.091	0.094	0.096	0.098	0.100	0.102	0.104	0.106	0.109		
46.5	0.077	0.080	0.082	0.084	0.086	0.088	0.091	0.093	0.095	0.097	0.099		
47.0	0.068	0.070	0.073	0.075	0.077	0.079	0.081	0.083	0.085	0.087	0.089		
47.5	0.059	0.062	0.064	0.066	0.068	0.070	0.072	0.074	0.076	0.078	0.080		
48.0	0.051	0.053	0.055	0.057	0.059	0.062	0.064	0.066	0.068	0.070	0.072		
48.5	0.042	0.045	0.047	0.049	0.051	0.053	0.055	0.057	0.059	0.061	0.063		
49.0	0.034	0.037	0.039	0.041	0.043	0.045	0.047	0.049	0.051	0.053	0.055		
49.5	0.027	0.029	0.031	0.033	0.035	0.037	0.039	0.041	0.043	0.045	0.047		
50.0	0.019	0.021	0.023	0.025	0.027	0.029	0.031	0.033	0.035	0.037	0.039		